Long-term drainage effects on carbon fluxes of an Arctic permafrost ecosystem

Dissertation

zur Erlangungen des akademischen Grades doctor rerum naturalium

(Dr. rer. nat.)

vorgelegt dem Rat der Chemisch-Geowissenschaftlichen Fakultät der Friedrich-Schiller-Universität Jena

von Fanny Kittler, M. Sc. Geoökologie, geboren am 16. Juli 1988 in Dresden

Gutachter:

1. Prof. Dr. Sabine Attinger, Universität Potsdam
2. Prof. Dr. Martin Heimann, MPI Biogeochemie

Tag der Verteidigung: 07.08.2017

Abstract

Permafrost landscapes in the Northern high latitudes with their massive organic carbon stocks are critically important for the global carbon cycle. Still large uncertainties in the sustainability of these carbon pools under future climate conditions persist, to a large part caused by limited understanding of mechanisms and drivers dominating permafrost carbon cycling due to scarce observational databases for Arctic permafrost ecosystems.

To address these open issues, a continuous observation program was established within an Arctic permafrost ecosystem that represents a floodplain of the Kolyma river near the city of Chersky, NE Siberia, Russia. Year-round eddy-covariance measurements from a wet tussock tundra ecosystem focused on the ecosystem–atmosphere exchange fluxes of carbon (CO_2 and CH_4). Recent observations started mid-July 2013 and are still ongoing, while historic measurements are available for the period 2002–2005. Since 2004 part of the observation area has been disturbed by a circular drainage ditch, altering the soil water conditions in the surrounding area in a way that is expected for degrading of ice-rich permafrost under a warming climate. Parallel observations over a disturbed tundra ecosystem (i.e., drained) and a control tundra ecosystem aim to evaluate the disturbance effect on the carbon cycle budgets and the dominating biogeochemical mechanisms.

Regarding the impact of the drainage disturbance, systematic shifts in the tundra ecosystem carbon cycle patterns triggered by persistently drier soils are observed. By comparing CO_2 budgets from the drained and control ecosystems a systematically reduced sink strength within the drained area is found, dominated by increased respiration due to warmer near-surface soil layers. Reduced CH_4 emissions are observed under drier and more aerobic conditions resulting in half the efflux from the drained ecosystem in comparison to the control ecosystem. As a net effect of the drainage an increased source of $CO_{2,\,eq.}$ to the atmosphere is caused by a pronounced additional source of CO_2 dominating reduced CH_4

emissions. This indicates a positive effect on global warming, based on the global warming potential metrics under relevant timeframes.

In comparison to the strong reduction of fluxes immediately following the drainage disturbance in 2005, recent CO_2 exchange with the atmosphere over this disturbed part of the tundra indicate a higher carbon turnover, and a seasonal amplitude that is comparable again to that within the control section. This indicates that the local permafrost ecosystem is capable of adapting to significantly different hydrologic conditions without losing its capacity to act as a net sink for CO_2 over the growing season. The comparison of undisturbed CO_2 flux rates from 2013–2015 to the period of 2002–2004 indicates that CO_2 exchange with the atmosphere was intensified over the past decade.

For the quantifications of reliable annual budgets, it was found that the quality of eddy-covariance flux measurements during the winter season with regards to instrument heating is crucial. By accounting for active heating periods of the sonic anemometer and correcting the self-heating effect of the open-path sensor by using an approach for inclined senor mounting, high quality eddy-covariance CO_2 budgets under cold climatic conditions are estimated.

Mean annual budgets for the control ecosystem show an uptake of 44 gC m^{-2} for CO_2 and a release of 7 gC m^{-2} for CH_4. Year-round measurements emphasize the importance of the non-growing season to the annual budget, with substantial contributions during the zero-curtain period representing the re-freezing of the active layer in fall. Around 50 % of the growing-season CO_2 uptake is lost during the cold-seasons, while non-growing season CH_4 emissions account for 30 % of the annual budget. The interannual variability in net budgets for CO_2 and CH_4 is found to result mainly from variations during the growing season and year-to-year variability in temperature conditions during the late growing season are identified as the primary control for the observed interannual variability in CO_2 and CH_4 fluxes.

Zusammenfassung

Permafrost Regionen in den nördlichen Breiten sind massive Kohlenstoffspeicher und dadurch entscheidend für den globalen Kohlenstoffhaushalt. Aufgrund mangelnder Beobachtungen in arktischen Ökosystemen bestehen große Unsicherheiten in Bezug auf die Nachhaltigkeit dieses Kohlenstoffspeichers unter zukünftigen klimatischen Bedingungen und ein begrenztes Verständnis der Mechanismen und Einflussfaktoren die den Kohlenstoffkreislauf dominieren.

Um diese offenen Fragen anzugehen, wurde in einem arktischen Permafrost-Ökosystem ein kontinuierliches Beobachtungsprogramm eingerichtet, das eine Überschwemmungsfläche des Kolyma Flusses in der Nähe der Stadt Chersky (nordöstliches Sibirien) darstellt. Ganzjährige Eddy-Kovarianz Messungen geben Aufschluss über Kohlenstoffaustauschprozesse (CO_2 und CH_4) zwischen der Atmosphäre und dem Ökosystem, während zusätzliche meteorologische Messungen Einblicke über deren Einflussfaktoren geben. Fortlaufende Beobachtungen werden seit Juli 2013 durchgeführt. Ein historischer Datensatz ist für den Zeitraum 2002–2005 verfügbar. Um die Degradierung von eisreichem Permafrost unter zukünftigen klimatischen Bedingungen zu simulieren, wurde ein Teil des Beobachtungsgebiets im Herbst 2004 durch einen kreisförmigen Entwässerungsgraben gestört. Durch parallele Beobachtung einer gestörten (drainierten) Untersuchungsfläche und einer Kontroll-Fläche können die Effekte eines verringerten Wasserspiegels auf den Kohlenstoffkreislauf und dessen dominierende Einflussfaktoren untersucht werden.

In Bezug auf die Auswirkungen der Drainage-Störung werden systematische Verschiebungen in den Kohlenstoff-Austauschprozessen des Tundra Ökosystems unter trockenen Bedingungen beobachtet. Der Vergleich von CO_2 Bilanzen zwischen der drainierten und der Kontroll-Fläche zeigt eine systematische Reduzierung der Aufnahmefähigkeit der entwässerten Fläche, die durch ein starke Zunahme der Respiration aufgrund wärmerer oberflächennahen Bodenschichten dominiert wird. Reduzierte CH_4 Emissionen werden unter trockeneren und

aeroben Bedingungen beobachtet, was zur Folge hat, dass das drainierte Ökosystem nur noch die Hälfte der CH_4 Emissionen der Kontroll-Fläche aufweist. Als Folge der Drainage kommt es zu einer Zunahme in der $CO_{2,\ eq}$. Quelle, da erhöhte CO_2 Emissionen die reduzierten CH_4 Emissionen dominieren. Dies deutet auf einen positiven Effekt in Folge der globalen Erwärmung hin, basierend auf dem globalen Erwärmungspotential für relevante Zeiträume.

Im Vergleich zu den stark reduzierten CO_2 Flussraten direkt nach der Installation des Entwässerungssystems weisen die jüngsten CO_2 Austauschraten der gestörten Fläche auf eine intensivierte Kohlenstoffdynamik hin und die saisonale Amplitude ist wieder vergleichbar mit der Kontroll-Fläche. Dies deutet darauf hin, dass das Permafrost-Ökosystem in der Lage ist, sich an signifikant unterschiedliche hydrologische Bedingungen anzupassen, ohne die Fähigkeit zu verlieren, während der Vegetationsperiode als Netto-Senke für CO_2 zu fungieren. CO_2-Flussraten des ungestörten Ökosystems von 2013–2015 im Vergleich zu dem Zeitraum 2002–2004 zeigen, dass der CO_2-Austausch mit der Atmosphäre in den letzten zehn Jahren intensiviert wurde.

Für die Quantifizierung zuverlässiger Jahresbudgets wurde festgestellt, dass die Qualität der Eddy-Kovarianz Messung während der Wintersaison im Hinblick auf Geräteheizungen entscheidend ist. Unter Berücksichtigung der aktiven Heizperioden des Ultraschall-Anemometers und durch die Korrektur der Selbst-Heizung des „open-path“ Sensors unter Verwendung eines Ansatzes für geneigte Sensoren, ist es möglich qualitativ hochwertige Eddy-Kovarianz CO_2 Budgets unter extrem kalten Bedingungen abzuschätzen.

Mittlere Jahresbilanzen der Kontroll-Fläche zeigen eine Aufnahme von 44 gC m^{-2} für CO_2 und eine Freisetzung von 7 gC m^{-2} für CH_4. Ganzjährige Flussmessungen zeigen die Bedeutung der Nebensaisons für das Jahresbudget, mit erheblichen Beiträgen während der „zero-curtain“ Periode die den Zeitraum des Einfrierens der Auftauschicht im Herbst beschreibt, auf. Ungefähr 50 % der CO_2 Aufnahme des Sommers wird innerhalb der kälteren Jahreszeiten wieder abgeben. CH_4 Emissionen außerhalb der Sommersaison machen 30 % der Jahresbilanz aus. Die zwischenjährliche Variabilität in den Netto-Budgets von CO_2 und CH_4

resultiert größtenteils aus Variationen in der Vegetationsperiode und Temperaturschwankungen von Jahr zu Jahr innerhalb des Spätsommers wurde als primäre Kontrollmechanismus für die beobachtete Variabilität in den beobachteten CO_2 und CH_4 Flüssen identifiziert.

Content

List of Figures

List of Tables

List of Abbreviations, Acronyms and Symbols

C	Carbon
CH_4	Methane
CO_2	Carbon dioxide
CP	Closed-path
DOY	Day of year
EC	Eddy-covariance
F	Flux
GA	Gas analyzer
GHG	Greenhouse gas
GPP	Gross primary production
H_2O	Water
NEE	Net ecosystem exchange
OP	Open-path
PPT	Precipitation
q_c	Partial densities of CO_2
r	Pearson's correlation coefficients
r_a	Aerodynamic resistance
Reco	Ecosystem Respiration
rH	Relative humidity
Rn	Net radiation
T_a	Air temperature
T_{soil}	Soil temperature
T_s	Surface temperature
u	Horizontal wind speed
u_*	Friction velocity
ξ	Fraction
ρ_d	Partial densities of dry air

ρ_v	Partial densities of H_2O

1 INTRODUCTION

Feedback processes between global climate and terrestrial and ocean ecosystems, respectively, will be one of the factors dominating the future trajectory of the climate (Friedlingstein et al., 2006). Within this context permafrost regions play a key role in the carbon (C) budget and therefore in the climate system (Beer, 2008) because of their huge carbon reservoir and the uncertain net impact of biogeochemical and biogeophysical responses to climate change.

1.1 PERMAFROST CARBON CYCLE AND CLIMATE CHANGE

1.1.1 Permafrost definition and properties

Permafrost, defined as frozen ground for at least two consecutive years, covers nearly a quarter of the exposed land surface in the northern hemisphere (Zhang et al., 1999). Distribution and thickness of the permafrost is controlled by snow and vegetation cover, topography, water bodies, the geothermal heat flux and air temperature (Boike et al., 2013). The thickness spans a wide range, typically ranging between 350 to 650 m in continuous permafrost zones of the northern hemisphere, but reaching up to 1450 m in unglaciated areas of Siberia (Schuur et al., 2008). The upper part of the surface that thaws during the summer season and refreezes completely within winter is referred to as the “active layer”. The thickness of the active layer is determined to a large extent by the regional climate, hydrological processes, the quality of the soil organic matter, and is influenced by plant rooting depth (Schuur et al., 2008).

1.1.2 Carbon cycle

Permafrost soils are critically important for the carbon cycle of the earth system because of the large carbon storage. Northern high-latitude permafrost

landscapes contain over 1035 Pg of organic carbon in the upper 3 m of the soil (Hugelius et al., 2014), equaling approximately 50 % of the global belowground carbon storage. Siberian soils are estimated to hold 13 % of the total global amount of organic carbon (Titlyanova et al., 1998) and are therefore of global relevance. This vast amount of organic carbon has been accumulated due to the slow decomposition rates of organic matter under low temperatures and anoxic conditions during the last two glacial cycles (e.g., Holocene and Pleistocene, Zimov et al., 2009) over the last millennia (Schirrmeister et al., 2011; Zubrzycki et al., 2013). For example, during the Holocene there was an estimated accumulation of 15–30 gC m^{-2} yr^{-1}, which resulted in a 200–450 Pg carbon pool (Gorham, 1991; Tolonen and Turunen, 1996; Turunen et al., 2002).

The return of carbon from the terrestrial storage to the atmosphere is mostly driven by microbial decomposition (oxidation of organic carbon to inorganic form primarily to extend energy for growth) of the organic matter. The rates of decomposition depend on environmental conditions like temperature, nutrient and electron acceptor availability, and soil moisture (Schuur et al., 2008). Hydrologic conditions are a major controlling factor for carbon exchange processes in high-latitude ecosystems and the presence or absence of water-logged conditions can lead to significant shifts in the dominance of the produced carbon species.

Carbon dioxide (CO_2) is the carbon species dominantly produced under aerobic conditions. The net CO_2 flux (net ecosystem exchange, NEE) is the sum of two major flux components: i) CO_2 loss to the atmosphere through ecosystem respiration (Reco) and ii) CO_2 uptake by the ecosystem through gross primary production (GPP). The net CO_2 flux is the comparatively small budget of these two component fluxes of opposite signs, and is, like the Reco and GPP fluxes themselves, smaller in the high latitudes compared to other ecosystems due to cold temperatures, short growing season[1] lengths and the presence of consistently frozen ground.

[1] In contrast to the summer season that was used as an overall term with meteorological or calendar based definition, the growing season refers to a period that permits photosynthetic activity based on environmental conditions. For more details on the definition and the deviation into sub-seasons see Sect. 2.9.

Methane (CH_4) is dominant under anoxic conditions. Methane emissions from tundra ecosystems play a special role in Arctic wetland ecosystems (McGuire et al., 2009). A major source of CH_4 is anoxic respiration by microbes known as methanogens in anaerobic ecosystems such as wetlands. These emissions are the largest sources of atmospheric CH_4 world-wide with estimates of 100–230 Tg CH_4 yr^{-1} (Denman and Brasseur, 2007), including a contribution of Arctic wetlands of 23 Tg CH_4 yr^{-1} (Zhuang et al., 2004). In contrast to CO_2, CH_4 produced in the anaerobic soil layers has the potential to be oxidized while moving upwards to the atmosphere, thus transport pathways are important. Major pathways for CH_4 emissions are via i) diffusion through the soil, ii) ebullition (as release of bubbles), and iii) plant mediated transport by aerenchymatous vascular plants.

Besides CO_2 and CH_4 exchange, there are other components that contribute to the annual net C balance of an ecosystem, such as e.g. the lateral export of dissolved or particular organic and inorganic C by water.

1.1.3 Climate change

Over the last few decades observations in the Arctic have shown that, as a result of global warming, temperatures have risen faster than those observed over the Northern Hemisphere as a whole (ACIA, 2004; SWIPA, 2011) with double the warming than in lower latitudes (Overland et al., 2014). This tendency, primarily driven by ice-albedo effects (Curry et al., 1995), is expected to continue, and climate models project a strong future high-latitude warming (IPCC, 2013).

Carbon dioxide and CH_4 are both important greenhouse gases (GHG) with significant contributions to climate change processes. In general, the annual net C budget is more influenced by CO_2 than CH_4, but CH_4 has a significantly higher global warming potential in comparison to CO_2 (IPCC, 2013) and is therefore of global importance for the permafrost carbon feedback (Nzotungicimpaye and Zickfeld, 2017). Emission rates of these GHGs from permafrost environments are determined by the availability of organic carbon, and depend strongly on the ecosystem type and the time frame under consideration. In permafrost ecosystems, higher temperatures will lead to increased active layer thickness, and thus favor

substrate availability for microbial decomposition and enhanced release GHGs to the atmosphere (Schuur et al., 2008; Schuur et al., 2015). At the same time, warmer conditions may lead to prolonged vegetation periods with increased photosynthetic uptake, while higher soil temperatures may stimulate CO_2 production through enhanced soil respiration (Flanagan and Syed, 2011).

Under scenarios of modest climate warming potentially up to 30 % of Arctic lowlands (Jorgenson et al., 2006) could be affected by ice wedge degradation (Liljedahl et al., 2016), a processes that is expected to alter geomorphology and hydrology of permafrost landscapes. Through this process, a relatively homogeneous area could be transformed into a network of small water channels that drain water away from the remaining patches of soil surface. The resulting changes in the spatiotemporal patterns of soil water availability could potentially trigger significant shifts in ecosystem characteristics, such as soil thermal regime or vegetation and microbial community composition. These changes, in turn, would alter carbon cycle processes; for example, changing aerobic conditions in the top soil layers have the potential to change preferred pathways for microbial decomposition of CH_4 (Merbold et al., 2009; Zona et al., 2009; 2010). Such changes would promote CO_2 efflux due to higher soil respiration rates (Flanagan and Syed, 2011; Olivas et al., 2010).

1.2 MEASUREMENT METHOD

The eddy-covariance (EC) technique is a well-established method for the direct quantification of turbulent surface–atmosphere exchange processes (Aubinet et al., 2012). With the option to record continuous flux time series that are representative at ecosystem scale, the network of EC sites has grown considerably over the past decades, including coverage of complex terrain that is difficult to access with other monitoring techniques (Eugster and Merbold, 2015; Foken, 2017; Monson and Baldocchi, 2014; Wyngaard, 2010). With now more than 800 sites registered within the FLUXNET network, EC flux datasets cover a large fraction of ecosystem types globally (Baldocchi, 2014).

The application of EC instruments is in theory limited to stationary flow conditions and no net advection. For the application, the instrumentation must be capable of capturing fluctuations of wind and atmospheric constituents contributing to the flux, whereby a temporal resolution up to 10–20 Hertz is considered ideal. The vertical exchange flux is determined as the covariance of the fluctuations of the vertical wind component and a second scalar, typically computed over integration times of half an hour. The sign convention from the atmospheric point of view is to assign negative values for fluxes directed to the surface. The quality of the resulting flux is mainly dependent on the adherence to theoretical requirements (e.g. steady-state conditions and horizontal homogeneity), and the successful application of necessary correction procedures. The spatial representativeness of the flux data is dependent on the measurement height, terrain roughness and stability of the atmospheric stratification in the surface layer, all of which determine the 'field of view' of the sensors, the so-called footprint area that spans usually between several 100s of meters to a few kilometers, and thus has the potential to provide representative values of the effective exchange processes over a certain ecosystem.

To quantify the gas exchange flux, the gas content in the air can be measured with a fast-response gas analyzer. Depending on the site characteristics and research purpose, an open-path (OP) or closed-path (CP) setup can be used, with both having different advantages and disadvantages in their application (Munger et al., 2012). Open-path gas analyzer configurations provide *in-situ* measurements, having a comparably low power and maintenance demand. With the open optical measurement path in direct contact with ambient air, measurements are influenced by climatic conditions resulting in disturbed data collection (e.g., during precipitation events) and large correction terms with density fluctuations depending on pressure, humidity and temperature conditions. In contrast, closed-path gas analyzing systems need inlet tubes and, depending on the length of the tubing, an additional powerful pump, resulting in a delayed signal, frequency losses within the tubing, and a high power demand. Since temperature and pressure fluctuations are damped with tubing and for most systems the measurement cell can be climate-controlled, these systems are not

subject to changing ambient conditions and can perform well covering a wider range of climatic conditions.

1.3 IMPORTANT RESEARCH FIELDS

1.3.1 Carbon pool sustainability under future climate conditions

With the sustainability of the huge carbon pools of permafrost ecosystems being dependent on future climate conditions (Kaufman et al., 2009; Kirschbaum, 1995; Serreze et al., 2000), there is a high potential for global feedback if the permafrost carbon reservoir is destabilized under future climate conditions (Beer, 2008). One potential outcome could be that the soil carbon previously locked away in permafrost deposits could be released into the atmosphere as CO_2 or CH_4 as a consequence of changes in soil temperature and moisture conditions (Schuur et al., 2008). However, model simulations show a wide range of permafrost responses to climate change (Koven et al., 2011; Schaefer et al., 2011). Empirical studies on the sensitivity of permafrost to environmental drivers are urgently needed to corroborate comprehensive Earth system models.

The complexity of potential positive and negative feedback loops between climate change and carbon cycling leads to considerable uncertainties concerning the effects of long-term shifts in the carbon budget of an Arctic permafrost ecosystem. Most studies to date on the net effect of such a disturbance on biogeochemical processes in the Arctic have focused on short-term perturbations (Bret-Harte et al., 2013; Merbold et al., 2009); however, it is likely that the long-term effects of this disturbance may differ greatly from the short-term effects that immediately follow the disturbance event (Shaver et al., 1992). Studies addressing long-term (>10 years) manipulation effects for the high latitudes are rare. In one such study, Lamb et al. (2011) found that 16 years of a combined fertilization and warming experiment in Canada's high Arctic tundra showed limited effects on GHG fluxes and soil chemistry or biochemistry but strong increases in plant cover and height. A 2-decade warming experiment in Alaskan tundra revealed increased plant biomass and woody dominance, indirectly increased winter soil temperature, and increased net ecosystem carbon storage (Sistla et al., 2013). In wetting and

fertilizing experiments in the open heath of Zackenberg, an area in northeastern Greenland, the soil water supply was increased for 14 years, and occasional fertilizer pulses were added, resulting in increased soil respiration rates during summer and decreased CO_2 efflux in fall (Christiansen et al., 2012b). Results from a summer warming and wetting treatment in northeastern Greenland over 10 years indicated increased CO_2 uptake in response to altered environmental conditions; this increase was mostly caused by photosynthetic uptake of carbon (Lupascu et al., 2014). In a long-term (20 years) fertilization experiment in Alaskan tundra, Mack et al. (2004) increased nutrient availability, which led to a net ecosystem loss of carbon, with increased aboveground plant production outweighed by carbon and nitrogen losses from deep soil layers. Due to the multiple and unclear results of available environmental manipulations, additional and particularly long-term experiments are crucially needed.

1.3.2 Limitations of the measurement technique

The eddy-covariance technique has provided valuable insights into carbon exchange processes. For Arctic environments, however, data coverage is still comparatively sparse (Oechel et al., 2014). With extreme climatic conditions and limited access to infrastructure, additional challenges have to be met with respect to installation and selection of suitable instrumentation that does not overload available power supply, maintenance capacity and have a sensor heating option (Goodrich et al., 2016). In addition, such measurements may be affected by heating effects of the instrumentation, particularly during Arctic winter conditions (Goodrich et al., 2016). Such heating effects may introduce systematic biases to observed annual budgets.

The limitations of Arctic EC data coverage become particularly aggravated when it comes to flux observations beyond the growing season, since observations over the long winter season are still extremely rare. Consequently, in the past annual balances of Arctic EC fluxes were often estimated with crude approximations regarding wintertime fluxes, i.e. zero exchange from frozen soils was assumed. This approach has been shown to lead to systematic biases of the annual net CO_2 budgets in Arctic regions (Euskirchen et al., 2012; Lüers et al.,

2014; Marushchak et al., 2013; Oechel et al., 2014; Zimov et al., 1996). Non-zero wintertime CO_2 fluxes can e.g. be linked to plant and microbial respiration of cold-tolerant species (Bate and Smith, 1983; Coyne and Kelley, 1974; Kappen, 1993; Kelley et al., 1968; Panikov et al., 2006), CO_2 loss during freeze-thaw dynamics (Grogan et al., 2004; Pries et al., 2013), free soil water creating warm microenvironments in frozen soils (Zimov et al., 1993) and unfrozen patches during the re-freezing in the fall (Mastepanov et al., 2008; Zona et al., 2016). Consequently, the continuous coverage of cold season CO_2 fluxes is critically important to assess the role of Arctic ecosystems within the context of global climate change.

Open-path configurations are widely used to determine CO_2 fluxes between the surface and the atmosphere (Haslwanter et al., 2009), especially in the Arctic, because of the comparably low power and maintenance demand. However, the operation of an open-path gas analyzer (LI-7500) may lead to systematic biases of CO_2 fluxes towards implausible uptake (Amiro, 2010; Clement et al., 2009; Helbig et al., 2016; Oechel et al., 2014; Ono et al., 2007) that can be linked to instrument heating. Heat is artificially generated by the instrument electronics housed below the optical path and results in higher temperatures within the optical path, generating an additional sensible heat flux inside the open optical measurement path. This effect has implications on the determined covariance, since this process is not accounted for by the traditional Webb-Pearman-Leuning (WPL) density-flux correction (Webb et al., 1980). In an attempt to develop a direct instrumental solution for this problem, Grelle and Burba (2007) and Massman and Frank (2009) added fine-wire thermometers within the optical path of the LI-7500 to account for the influence of high frequency temperature fluctuations. As a simplified alternative, a correction procedure to amend the performance of the instrument without the need for additional sensor installations was developed (Burba et al., 2006a; Burba et al.; 2008). However, while the use of the self-heating correction has increased (Reverter et al., 2011), the application can vary depending on the instrumental setup (Burba and Anderson, 2010b). The self-heating correction allows offsetting the flux biases induced by instrument self-heating (Burba et al., 2008; Reverter et al., 2011). Alternatively, site-specific

corrections can be determined using parallel CP measurements as a reference (Järvi et al., 2009). If no parallel measurements are available, a generic scaling factor can be used (Rogiers et al., 2008). Still, the self-heating correction for OP sensors is subject to large uncertainties, and it has been shown that its correct application needs to be customized for individual cases (Bowling et al., 2010; Haslwanter et al., 2009; Wohlfahrt et al., 2008). Consequently, there is no general consensus on the application of the self-heating correction. Since the concept behind the correction assumes strongest heating effects under cold ambient air conditions (Burba et al., 2006b; 2008), the correction is usually applied only for cold ecosystems.

Another important technical aspect for the operation of EC systems under cold Arctic conditions is the application of a heating device to avoid riming and/or icing at the transducers of the sonic anemometer. During periods with high air humidity in combination with temperatures close to freezing, ice crystals can build up around the transducers of the sonic anemometer and disturb measurements (Makkonen and Laakso, 2005). Heating systems to avoid ice buildup can be implemented as built-in versions by the manufacturer. Alternatively, customized versions can be installed using, e.g., heating tape or resistive heating wires wrapped around transducers (Goodrich et al., 2016; Skelly et al., 2002). A suitable scheme to activate the heating device should be applied to ensure good instrument conditions and counteract icing events, but at the same time to minimize heating periods to avoid biasing the measurements. Increased sensible heat fluxes (Skelly et al., 2002) and resulting overestimations in CO_2 and latent heat fluxes (Goodrich et al., 2016) have been linked to active instrument heating. This calls for heating schemes that are based on meteorological conditions, triggering an activation, e.g., at high humidity and temperatures around freezing, instead of a continuous heating regardless of prevailing environmental conditions.

1.3.3 Year round observations of carbon exchange fluxes

As outlined in Sect. 1.3.2, extreme climate conditions pose special demands on both instrumentation and power sources (Goodrich et al., 2016). Moreover due

to the remoteness of the largest parts of the northern regions, these ecosystems are difficult to access, and continuous monitoring programs are impeded by logistical challenges, resulting in comparatively very sparse data coverage of carbon flux measurements for the Arctic (Oechel et al., 2014; Zona et al., 2016). Focusing on CO_2 fluxes in Arctic regions with underlying permafrost, summarizing the available studies yields a pronounced variability regarding the direction and magnitude of annual flux budgets, with results ranging from net sources (Euskirchen et al., 2012; Euskirchen et al., 2016; Oechel et al., 2014; Zimov et al., 1996) over CO_2-neutral (Lüers et al., 2014) to net sinks (Aurela et al., 2004; Aurela et al., 2007; Kutzbach et al., 2007). Also modelling results spread over a wide range (Belshe et al., 2013; McGuire et al., 2012). First year-round eddy-covariance measurements of CO_2 fluxes from continuous permafrost by Oechel et al. (2014) demonstrated that the non-growing season contributes significantly to the annual budget. Studies focusing on multi-year observations identified climatic conditions (Arneth et al., 2002; Merbold et al., 2009) with a specific focus on temperature and temperature-related variables such as snow-melt timing (Aurela et al., 2004; Philipp et al., 2016), growing degree days (Euskirchen et al., 2012) and maximum thaw depth (Lund et al., 2012) as most important controlling factors for interannual variability of CO_2 fluxes.

While Arctic ecosystems usually act as sustained sources of CH_4, flux magnitudes are associated with large uncertainties (Christensen, 2014) and are even more sparse than for CO_2. Published annual CH_4 emissions range between 7 gC m^{-2} (wet tundra ecosystem Zackenberg, NE Greenland, covering the period before snowmelt until early winter, Tagesson et al., 2012) and 13 gC m^{-2} (continuous eddy-covariance measurements over a boreal fen, Rinne et al., 2007). Recent observations found that the cold season contributions are estimated to account up to half the annual CH_4 budget with largest emissions during the so-called zero-curtain period that represents the refreezing of the active layer (Zona et al., 2016). While some studies observed burst events of CH_4 fluxes during the re-freezing of the active layer (Mastepanov et al., 2008; Tagesson et al., 2012) others report continuous CH_4 efflux during the fall period (Sturtevant et al., 2012; Wille et al., 2008). Environmental drivers like soil temperature and near-surface

atmospheric turbulence (Wille et al., 2008), soil moisture (Sturtevant et al., 2012), and vegetation (Turetsky et al., 2014) can influence the interannual variability of CH_4 fluxes (Emmerton et al., 2014; Mastepanov et al., 2013; Moore et al., 2011).

1.3.4 Disturbance experiment

Because of the huge carbon storage (Hugelius et al., 2014) in permafrost areas and the expected large temperature sensitivity of this carbon pool (Kaufman et al., 2009; Kirschbaum, 1995; Serreze et al., 2000), there is a high potential for global feedbacks if the carbon reservoir is destabilized. A release of enormous amounts of carbon due to destabilization could have disastrous consequences for the global climate system (DeConto et al., 2012; Dutta et al., 2006; Khvorostyanov et al., 2008a; Khvorostyanov et al., 2008b; Zimov et al., 1996). But sensitivity analysis of permafrost to rising temperatures is complicated due to complex interactions between the atmosphere, hydrosphere, pedosphere and biosphere.

Manipulation experiments, focusing on changes in spatiotemporal patterns of soil water availability, can give invaluable insights into the complex potential shifts in ecosystem characteristics associated with persistently drier conditions. These include shifts in, and interactions between soil thermal regime, vegetation and microbial community composition, and snow cover regimes, all of which trigger systematic shifts in carbon cycle processes. Only very few of such field manipulations have been conducted so far, and those available were performed on a small spatial (Oechel et al., 1998; Strack et al., 2006) or temporal scale (Merbold et al., 2009). Others focused on a combined effect of temperature and moisture manipulation (Chivers et al., 2009; Huemmrich et al., 2010). A large scale water table manipulation experiment in Alaska found an increase in the CO_2 loss (Zona et al., 2012) and a decrease in CH_4 emissions (Sturtevant et al., 2012; Zona et al., 2009) under drained conditions.

A long-term drainage disturbance experiment was established in a tundra ecosystem within the floodplain of the Kolyma river near Chersky in NE Siberia. The concept of the disturbance was designed to modify the local water regime and soil moisture conditions in the surrounding area in a way that is expected for degrading ice-rich permafrost under a warming climate. The manipulation

consisted of a circular drainage ditch with a diameter of ~ 200 m connecting to the nearby river through a channel of ~ 300 m length (Merbold et al., 2009). This drainage system was installed in fall 2004 and is still in place today, artificially modifying the local water table depth and thus significantly modifying biogeochemical and biogeophysical site characteristics during the last decade. The disturbance experiment aims to evaluate the effect of a lowered water table on the carbon cycle budgets.

1.4 KEY OBJECTIVES AND RESEARCH QUESTIONS

The primary objective is to improve the understanding of the spatiotemporal variability of ecosystem–atmosphere carbon fluxes in Arctic permafrost ecosystems. A central aspect of this research will revolve around the comparisons of recent observations with historic data, the evaluation of long term changes within these high latitude ecosystems and a quantification of trends in their sink and source strengths for greenhouse gases. This includes the identification of environmental drivers and processes that dominate this flux variability on various temporal and spatial scales. Furthermore, an in depth uncertainty analysis associated with micrometeorological flux observations within this climate zone is performed. To address the objectives, specific research questions were developed:

1. *Is there a significant difference in flux signals between the drained and the control site?*

   This difference would reflect changes in biogeochemical and biogeophysical site characteristics due to the altered water table and therefore modified conditions for the carbon cycle.

2. *Is there a significant difference between the recent datasets of both areas compared to the historic datasets?*

   By comparing recent to historic flux data, it can be evaluated how the tundra ecosystem adapted to climate change over the past decade, depending on the disturbance regime.

3. *What is the contribution of the non-growing seasons to net carbon budget of permafrost ecosystems, and which processes influence the winter season fluxes?*

   In order to adopt the eddy-covariance techniques to observe winter season fluxes, the quality of the flux data is evaluated to determine high quality signals. With those high quality year-round measurements, seasonal contributions are evaluated and annual balance of the permafrost carbon cycle are estimated.

4. *How is intra- and interannual variability linked to the environmental drivers that dominate the turbulent carbon dioxide and methane fluxes? Have these drivers changed due to the disturbance regime?*

   Depending on the disturbance regime, causal relationship between various environmental parameters and the observed spatiotemporal flux variability of CO_2 and CH_4 is characterized.

To answer the above listed research questions the work has been divided into three main chapters:

Impacts of a decadal drainage disturbance on surface–atmosphere fluxes of carbon dioxide

To improve the current understanding of links between carbon fluxes and long-term hydrologic disturbance growing season CO_2 flux rates between historic (2002–2005) and recent (2013–2015) data are analyzed. This allows assessing the combined effect of this disturbance and a changing climate. In both cases, the focus is on the net CO_2 flux between ecosystem and atmosphere, as well as its major components fluxes, i.e., GPP and Reco. These results are presented in Chapter 3 and aim to answer the first and second research question.

High-quality eddy-covariance carbon dioxide budgets under cold climate conditions

To assess the quantitative effect of instrument heating for improved quality of flux data during the wintertime, three full winter seasons with parallel operation of heated and unheated sonic anemometers as well as parallel operation of open-

and closed-path gas analyzers, the latter serving as a reference, are used. Measured scalars from both instruments, the vertical wind component from the sonic anemometer and the CO_2-signal from the open-path system are essential to determine the turbulent CO_2-flux. Upon the heating effect is quantified, reliable CO_2 wintertime budgets are estimated. Thus, Chapter 4 is a technical preparation for the third and fourth research question.

Year-round eddy-covariance measurements combining carbon dioxide and methane fluxes from a permafrost ecosystem

Chapter 5 aims to further improve the understanding of Arctic carbon flux budgets, and therefore also the ability to predict the sustainability of Arctic carbon pools under future climate change, building on Chapter 3. To evaluate the long-term effect of a persistently lowered water table on the net vertical carbon exchange budgets and its dominating biogeochemical mechanisms, an eddy-covariance dataset covering more than 3 years of continuous CO_2 and CH_4 flux observations in combination with ancillary measurements over the drained and a control area, respectively, is used. The vertical carbon flux exchange patterns at both sites are compared and the interannual variability with the dominating environmental drivers is analyzed depending on the disturbance regime. Furthermore, with year-round measurements, seasonal and annual budgets are derived to analyze the seasonal contributions.

2 METHODS AND DATASETS

2.1 SITE DESCRIPTION

The research site, located in a floodplain of the Kolyma river near Chersky (68.75 °N, 161.33 °E), NE Russia, consists of a wet tussock tundra dominated by tussock-forming *Carex appendiculata* and *lugens*, and *Eriophorum angustifolium* (Kwon et al., 2016b). An organic peat layer (0.15–0.2 m) overlays alluvial mineral soils (silty clay) with some organic material also present in deeper layers following cryoturbation (Corradi et al., 2005; Kwon et al., 2016b; Merbold et al., 2009). For the years 2014–2016 mean annual air temperature was -10.2 °C (daily means ranging between -49.8 °C in January 2014 and 24.6 °C in July 2015), which is warmer then the long-term average of -11 °C (Goeckede et al., 2016). A total annual precipitation of 160 mm was observed during this period, which is about 20 % lower than the average of 197 mm observed during the period 1960–2009. However, based on the fact that the growing season fraction of the total annual precipitation increased to ~ 50 % during our observation period, it cannot be ruled out that the recent datasets are subject to a systematic low bias in wintertime precipitation due to insufficient heating of the sensor. During the transition period in late spring (May/June) site hydrology is strongly influenced by flooding as a result of snowmelt and rising water levels in the nearby river, leading to standing water on the site (up to 0.5 m above ground surface) in most years. Afterwards the water table decreases gradually within days to weeks depending on fine-scale microsite conditions. The disturbance experiment resulted in a locally reduced water table by up to 0.3 m in summer (Kwon et al., 2016b; Merbold et al., 2009). The seasonal development of the vegetation is usually delayed in wet compared to dry areas where snow melt is followed by rapid greening. Vegetation height reached ~ 0.7 m during peak growing season. Snow cover thickness was on average 0.8 m and peaked around April with maximum snow depth reaching over 1 m in 2015.

2.2 INSTRUMENTAL SETUP

For the observation program, two sites were chosen: one within the circular drainage ring (and thus covering the areas affected by lowered groundwater levels) and another serving as a control site (close by but far enough away to represent natural conditions unaffected by the disturbance). Since both sites had to be close enough to share a power supply, the two observation sites were ~ 600 m apart. Ecosystem scale fluxes were monitored with eddy-covariance systems at a site elevation of 6 m above sea level. One tower (hereafter referred to as Tower 1 or drained tower, 68.613 °N and 161.341 °E) was placed within the drainage area (Figure 1, blue shaded area), so that its footprint (Figure 1, yellow to red shaded area) primarily covered areas affected by reduced groundwater levels. The control tower (hereafter referred to as Tower 2 or control tower, 68.617 °N and 161.351 °E) represented natural conditions (Figure 1).

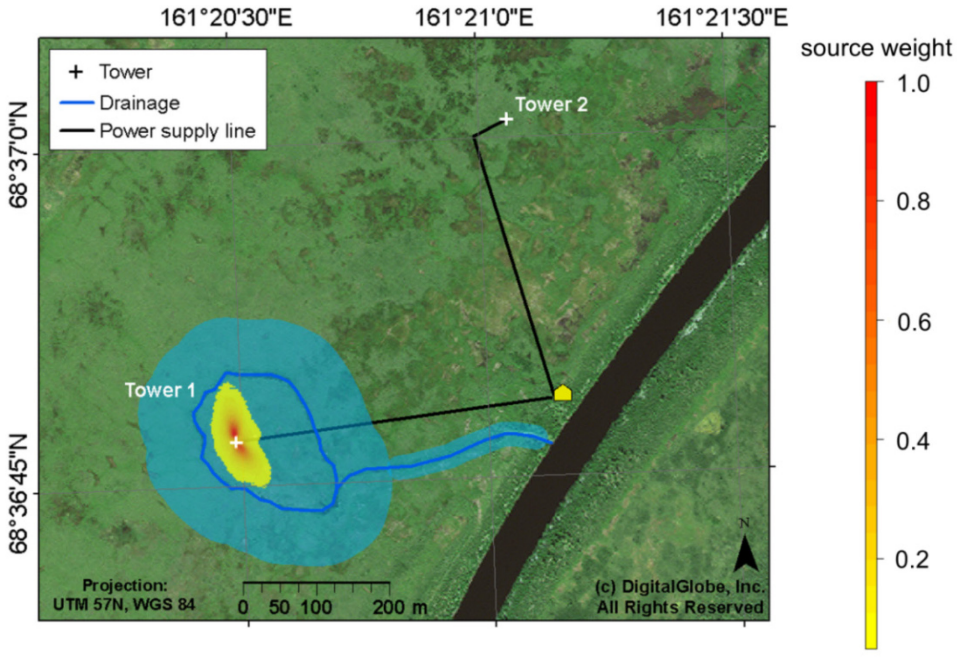

Figure 1: Overview of observational setup and site facilities on a wet tussock tundra near Chersky. The circular drainage ditch and drainage channel (blue lines) were installed in 2004 and are still in place today, altering the water table depth (blue shaded area outline the approximate area affected by the drainage). The image also depicts the towers (white crosses), power lines (black lines), and generator housing (yellow hut). The red-yellow colored area around Tower 1 indicates the weighted source function of footprints averaged over all stability classes from 15 May to 14 September 2014.

The EC instrumentation was mounted on top of each tower at a height of 4.9 m and 5.1 m for tower 1 and 2, respectively, including a heated sonic anemometer (uSonic-3 Scientific, former USA-1, METEK GmbH, Elmshorn, DE; with integrated 55 W heating) to monitor the three-dimensional wind field and the sonic temperature and two types of gas analyzers (GA). The open-path GAs (inclined by 15°, LI-7500, LI-COR Biosciences Inc., NE, USA) for CO_2 and H_2O flux densities were installed in mid-July 2013 next to the sonic anemometers, with a sensor separation of 0.38 m at both towers. In April 2014, the closed-path GAs (FGGA, Los Gatos Research Inc., CA, USA.) for monitoring CO_2, H_2O and CH_4 wet mole fractions were added to the setup. The CP systems consist of an inlet placed next to the sonic anemometer (vertical sensor separation: 0.30 m), a sampling line (heated and insulated Eaton Synflex® (former name decabon) with 6.2 mm inner diameter and a length of 16.0 m and 12.8 m for Tower 1 and 2, respectively), and an external vacuum pump (KNF N940 membrane pump, flow rate of 13 L min^{-1} at ambient pressure). Additional instrumentation to monitor environmental variables is listed in Table 1.

Table 1: Summary of the observed environmental variables available for both towers including instrumentation and measurement height. Tussock measurements describe the conditions in the middle of the tussock (0.2 m to the top of the tussock and 0.2 m to the soil surface). Heights above the soil surface are indicated as positive numbers, depths below the soil surface are given as negative numbers.

Environmental variable	Instrumentation	Measurement height [m]
Air temperature	KPK 1/6-ME-H38, Mela	2 and 5
Relative humidity	KPK 1/6-ME-H38, Mela	2 and 5
Barometric pressure	Pressure transmitter, 61302V, Young	5
Long/short up/downwelling radiation	CNR4, Kipp & Zonen	5
Up/downwelling photosynthetically active radiation	PQS1, Kipp & Zonen	5
Precipitation	Tipping bucket rain gauge, Thies	1
Soil moisture	ML-2x, DeltaT	-0.08, -0.16, and tussock
Soil temperature	Pt100, YUMO	-0.04, -0.08, -0.16, -0.32, -0.64, -1.28, and tussock

Data collection was running continuously at both towers since the installation mid-summer 2013. Both GAs were running in parallel on tower 1 since installation in spring 2014. On tower 2 the OP sensor was operational from July 2013 to July 2014, afterwards only the CP measurements were continued. For the final flux time series data from open-path (until April 2014) and closed-path (since April 2014) were merged.

2.3 METEOROLOGICAL DATA

The observed meteorological data (Table 1) were collected at 10 second intervals and stored on a data logger (CR3000, Campbell Scientific, UT, USA) as averages over 10 minute periods. The post-processing quality control scheme of the meteorological data included a test for failure of the power supply, a test that checks the range of parameters within a certain time window, a flat lining test, a spike test, and a test for identifying malfunctioning sensors and consistency limits. Remaining high quality data were subsequently averaged to 30-minute intervals.

2.4 EDDY-COVARIANCE DATA

2.4.1 Processing

For the EC towers, the data were collected at a rate of 20 Hz with analogue output for the GAs. All analog signals were first transmitted to the sonic anemometer, where they were digitized and sent to the site computer jointly with the wind signal. Data acquisition was handled through the software package EDDYMEAS (Kolle and Rebmann, 2007) on a local computer at the field site. The processing of the high-frequency EC data was based on the software tool TK3 (Mauder and Foken, 2015), which implemented all required processing steps and correction procedures. For both, OP and CP GAs, the 2D rotation of the wind field, the cross-wind correction (Liu et al., 2001), and a correction for losses in the high frequency range (Moore, 1986) was applied. For the CP GA the high frequency raw data (as wet mole fraction) were converted to dry mixing ratios before processing. Since losses in the high-frequency range occur when gases are transferred to the closed-path analyzers through inlet tubes, the flow rate of

13 L min^{-1} (ambient pressure) translated into a replacement of sample air in the measurement cell at a frequency of ~ 2–2.5 Hz for CO_2 and H_2O, respectively, which were used as cutoff frequencies for the spectral correction of the CP GA. The WPL density-flux correction (Webb et al., 1980) was applied for the OP data to account for density fluctuations within the open optical measurement path.

To calculate the global warming potential (GWP), CH_4 was weighted by a factor of 34, representing a 100-year time horizon with inclusion of climate-carbon feedbacks (IPCC, 2013).

2.4.2 Quality control

To ensure high data quality, the standard post-processing quality control scheme based on tests for stationarity and well-developed turbulence (Foken and Wichura, 1996) was extended by additional tests to detect implausible data points in the resulting flux time series. These tests covered a check for absolute limits for CO_2 flux data (-15 µmol m^{-2} s^{-1} < CO_2 flux < 5 µmol m^{-2} s^{-1}), the OP GA status information (gain control maximum < 75), errors messages in the log file reported by the sonic anemometer, a comparison of the absolute concentrations of CO_2 for the two towers for specific wind directions to detect potential contamination by the exhaust plume of the generator (based on a more than 5 % difference criterion), a test for T_a (< -40 °C, which is the lowest possible operating T_a for the sonic anemometer) and a flag for active sonic anemometer heating. Quality flags (QF) were combined and data covering QF 1–6 (Foken et al., 2004; 2012) were used to increase data coverage for reliable and robust gap filling procedure.

Data coverage of CO_2 fluxes for the closed-path system ranged around 80 % during the growing season and ~ 60 % during winter season. For the open-path systems data coverage was lower due to additional gaps caused by unfavorable weather conditions affecting measurements e.g., rain and condensation (see Table 3). Data coverage of CH_4-fluxes is reported in Table 2.

Gaps were commonly shorter than a day and distributed equally over all seasons. Longer gaps were caused by flooding events, when the entire system needed to be shut down to avoid damage, or resulted from a laser offset in the closed-path gas analyzer at Tower 1 in 2015. No data were available at the control

site from mid-November and mid-December 2015, for CH_4 and CO_2, respectively, until mid-July 2016. An overview of the active times for the different gas analyzing systems is given in Figure 2.

Table 2: Mean data coverage in percentage of CH_4 flux measurements per season and site, excluding data from mid-November 2015 to mid-July 2016 for both towers when the closed-path analyzer at the control site was not active.

Season	Drained [%]	Control [%]
Spring	74	77
Growing	83	86
Fall	73	71
Winter	69	63

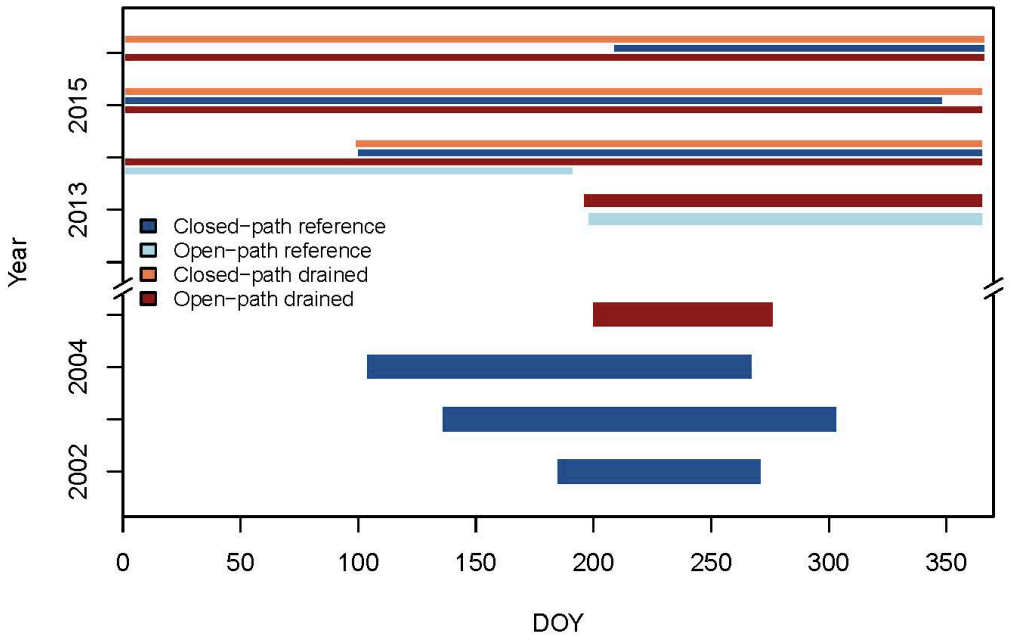

Figure 2: Measurement time frame for the eddy-covariance systems (open-path: LI7500, closed-path: LI6262 and FGGA) of both towers, for both the recent (2013–2016) and historic (2002–2005) observation periods.

2.4.3 Gap filling and flux partitioning

Gap filling and flux partitioning were both based on the so-called marginal distribution sampling method (Reichstein et al., 2005), implemented through the R-package "REddyProc" (https://r-forge.r-project.org/projects/reddyproc/). As there was a pronounced variability of environmental conditions the dataset was split into different seasons and sub-seasons during the growing season (for details

see Sect. 2.9), with individual gap filling and flux partitioning data pools for each sub-season.

The flux-partitioning algorithm that splits NEE into GPP and Reco signals is based on the estimation of the night-time respiration as a function of temperature and the extrapolation of this relationship for the daytime (Reichstein et al., 2005). In a subsequent processing step, GPP is derived from the difference between NEE and Reco (Reichstein et al., 2005). The results for the component fluxes GPP and Reco presented here are therefore not based on direct measurements, but rather represent a model-data hybrid product. The performance of this procedure is dependent on a number of user-defined settings, such as the definition of night-time conditions by setting a radiation threshold (present study: 20 W m^{-2}, e.g., Parmentier et al., 2011; Runkle et al., 2013). To address the temperature dependence of Reco, we used air temperature instead of soil temperature. This decision was based on our observance of implausible patterns in near-surface temperature measurements at our site, and, because of a damped diurnal cycle, higher-quality soil temperatures at 0.08 m below the surface cannot be correlated to short-term changes in respiration patterns. During the growing season, air and near-surface soil temperatures are closely linked, and both represent the temperature regime within the soil, driving respiration processes (Lloyd and Taylor, 1994). However, this flux-partitioning approach might be limited during the thawing and refreezing periods when energy is not used for heating, but instead for the phase change of ice water, and when soil temperatures do not change relative to air temperatures.

The gap filling procedure for CH_4-fluxes is based on weekly means with a moving window of daily shift. For annual budgets, mean annual cycles for each tower and gas species were used to fill long gaps.

2.5 ADDITIONAL FLUX-CORRECTION FOR SELF-HEATING OF THE OPEN-PATH SENSOR

Sensor geometry might be a crucial component if the OP sensor is mounted in an inclined position (Figure 3 a), while it should be independent for vertically

oriented instruments (Burba et al., 2008). For different directions of the horizontal wind, heated air might be blown further into (Figure 3 b) or out of (Figure 3 c) the optical path, with potential consequences for the impact of the self-heating effect, and therefore also on the necessary correction.

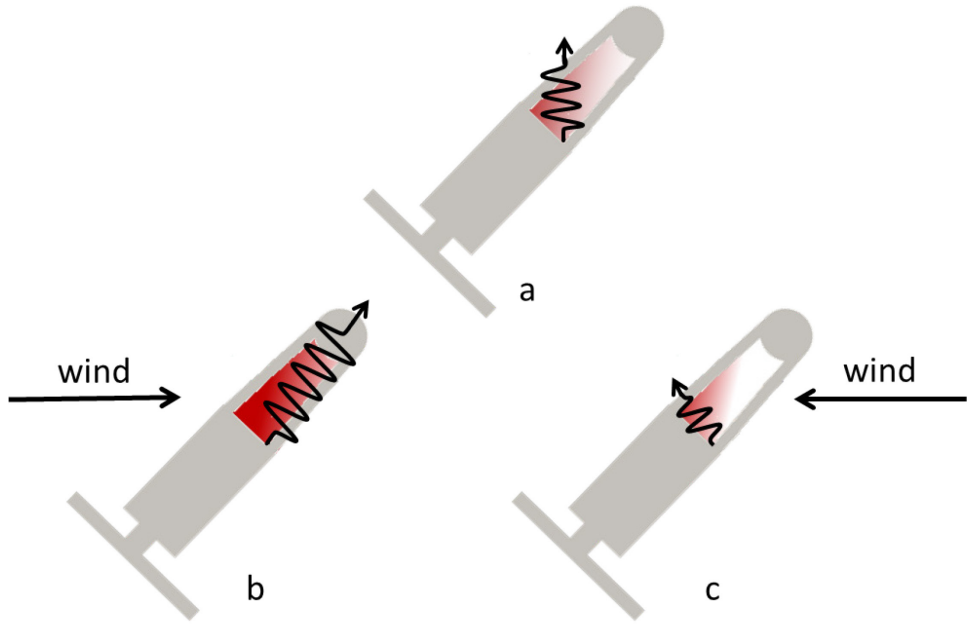

Figure 3: Conceptual overview of a potential wind direction impact on the self-heating effect for inclined OP sensors. We separate neutral conditions (a) from conditions when the heated air is blown into (b) or away from (c) the measurement path. Red shaded area mark the volume within the measurement cell that is influenced by the heating and the black curved arrow the heat flux direction.

An additional correction applied to the final fluxes was used to account for the self-heating of the OP analyzer, following Burba et al.'s (2006b) approach with an extension for inclined positions with available parallel CP measurements that can serve as a reference. The OP flux data (F_{op}) can be corrected as:

$$F_{corr} = F_{op} + \xi \frac{(T_s - T_a)q_c}{r_a(T_a + 273.15)}\left(1 + 1.6077\frac{\rho_v}{\rho_d}\right), \quad (1)$$

with scaling factor ξ as the fraction of the self-induced heat flux relevant for the correction of an inclined LI-7500 sensor. As pointed out by Rogiers et al. (2008) and further tested by Järvi et al. (2009) for inclined open-path analyzers only a small fraction of this additional heat flux actually influences the measurement path. Accordingly, ξ can theoretically vary between 0 (no self-

heating effect) and 1 (full self-heating effect needs to be applied, e.g. for a vertical sensor orientation). It was demonstrated by Järvi et al. (2009) that only a very small fraction of the full heat flux typically affects measurements that were taken with the recommended sensor inclination angle of 15°.

T_s is instrument surface temperature, T_a is air temperature, r_a represents aerodynamic resistance and q_c, ρ_v and ρ_d are partial densities of CO_2, H_2O and dry air, respectively. The instrument surface temperature is a crucial component of the self-heating correction that can be determined directly with additional measurements or can be estimated from T_a based on various empirical parameterizations. Since direct measurements of T_s are not available in most applications, the choice of a reliable parameterization scheme for T_s is an essential step for achieving good performance of the self-heating correction. Several approaches have been developed for this purpose, which vary in their test environment/conditions and therefore also differ in their specified area of applicability. Due to radiative heating over the day and radiative cooling during the night affecting measurements differently with increased effects under non-vertical OP sensor configurations (Burba et al., 2008) some T_s parameterizations differ between day- and night-time. Night-time conditions were defined by incoming shortwave radiation < 20 W m^{-2}. Consequently, Arctic winter with nearly no solar radiation is mostly represented by night-time conditions, while during summer (June/July) ca. 70 % of each day is characterized as day-time.

As the simplest solution,

$$T_s = 0.92T_a + 4.83, \quad (2)$$

was determined with climate chamber measurements ranging from -25 °C to 50 °C with a vertical sensor orientation (Burba et al., 2006b). During field experiments, a polynomial fit

$$T_s = 0.0025T_a^2 + 0.9T_a + 2.07, \quad (3)$$

was found to best reproduce the observed heating effects and increased thermal exchange. This equation is specified for a temperature range from -25 °C

to 20 °C (Burba et al., 2006b). For a forest site, Järvi et al. (2009) developed separate fits for day- and night-time conditions

$$T_{s\_day} = 0.93T_a + 3.17 \text{ and } T_{s\_night} = 1.05T_a + 1.52. \quad (4)$$

Individual fits for the top, spar and bottom part of the instrument can be used that further distinguish between day- and night-time conditions as described in Burba et al. (2008):

$$T_s = \frac{1}{3}T_s^{bot} + \frac{1}{3}T_s^{spar} + \frac{1}{3}T_s^{top}, \quad (5)$$

$$T_{s\_day}^{bot} = 0.944T_a + 2.57 \text{ and } T_{s\_night}^{bot} = 0.883T_a + 2.17, \quad (5.1)$$

$$T_{s\_day}^{spar} = 1.01T_a + 0.36 \text{ and } T_{s\_night}^{spar} = 1.001T_a - 0.17, \quad (5.2)$$

$$T_{s\_day}^{top} = 1.005T_a + 0.24 \text{ and } T_{s\_night}^{top} = 1.008T_a - 0.41. \quad (5.3)$$

The overall T_s was then calculated as the unweighted average of the three individual fits (Eq. 5).

The aerodynamic resistance is determined directly from the friction velocity u_* and the horizontal wind speed. The simplified approach described in Stull (1988) as

$$r_a = \frac{u}{u_*^2}, \quad (6)$$

includes the roughness of the surface via u_*.

Under the assumption that the true flux was represented by the CP data, ξ in Eq. (1) was optimized using a nonlinear least-squares method to achieve optimum agreement between corrected OP and reference CP fluxes. For this optimization, the starting value for ξ was set to 0.05, as suggested by other studies (Järvi et al., 2009; Rogiers et al., 2008). The ξ fraction was optimized separately for each of the T_s parameterization approaches, and also separately for day- and night-time conditions, without modifying any parameters of the T_s parameterization itself in the process. Through this optimization approach the OP CO_2 fluxes are corrected and, in comparison to the CP CO_2 fluxes, both the best equation for T_s estimation (from Eqs. 2–5) and the best fit of ξ for this equation can be determined for the given site-specific conditions.

To investigate the dependence of ξ on the wind field properties Eq. (1) was reorganized to determine ξ directly for each half-hour interval, and subsequently deriving statistics on the dependence of the ξ fraction for certain wind direction and wind speed classes. Since this approach does not account for nonlinear dependencies by minimizing the sum of squared residuals, values can vary systematically in comparison to the optimization approach. Accordingly, this analysis will only be used to identify how the sensor geometry and the angle of attack can influence the self-heating correction.

Since CP data serve as true reference for the optimization with Eq. (1), fully corrected CP fluxes are crucial for the application of the correction (e.g., data processing or software). Different factors such as type of instruments, length of inlet tubing, tube diameter and flow rate (see Section 2.4.1) will systematically affect corrections of CP fluxes (Aubinet et al., 2016; Aubinet et al., 2012; Burba and Anderson, 2010a; Metzger et al., 2016). For the CP system all applied corrections are seasonally independent and the CP system is used as a reference throughout the year. Furthermore, a correct application of the WPL density-flux correction (Webb et al., 1980) for the OP data is crucial, since otherwise a remaining bias would be projected on the self-heating correction. Here, we applied all recommended correction and used standardized methods for the data processing (Fratini and Mauder, 2014) to ensure highest data quality.

2.6 HISTORIC DATASET

Eddy-covariance measurements were conducted during the 2002–2005 growing seasons in the context of the TCOS Siberia project (Corradi et al., 2005; Merbold et al., 2009, Figure 2), at the same location that was used for the drainage tower in the new experiment starting 2013. Flux measurements until the end of October 2004 represented an undisturbed tussock tundra (Merbold et al., 2009). After the installation of the drainage channel in fall 2004, flux measurements at the same location in the subsequent year indicated that this modification in the local water regime resulted in no significant change to the seasonal budgets of net CO_2 fluxes (Merbold et al., 2009). However, these trends were based on a single

year of observations only, and thus did not reflect the long-term effects of such a disturbance.

To facilitate a direct comparison between recent (2013–2015) and historic (2002–2005) observations, the raw datasets from the period of 2002–2005 were re-processed using the same data processing and quality assessment procedure outlined in Sect. 2.4.1 to 2.4.3. This re-processing caused minor changes in the flux rates compared to the values reported in Corradi et al. (2005) and Merbold et al. (2009), because of changed assumptions and inputs when using a different flux processing software. However, general patterns in interannual variability of fluxes were not affected. For the data collected in 2004, a parallel run of open- and closed-path gas analyzers resulted in systematic differences in the seasonal dynamics and final budgets (see also Merbold et al., 2009) for CO_2 and H_2O fluxes. These differences remained ($R^2 = 0.75$) even after re-processing and applying additional corrections that have since become available (Burba et al., 2006b), as well as analyzer-specific corrections. Since the seasonal patterns in the open-path data displayed implausible patterns (e.g., near-zero fluxes at the beginning of the growing season, when dominating positive fluxes are expected) we decided to use only the closed-path data for 2004 in this study. More frequent gaps in the historic dataset compared to the recent dataset were caused by failures in the power supply system, as there was no continuous or stable power supply during this time (Merbold et al., 2009).

Methane flux measurements based on static chamber systems resulted in extrapolated budgets (mid-July to end of October) of 20 ± 15, 20 ± 11, 24 ± 19 and 0.6 ± 1.2 gC m^{-2} for the data years 2002–2005, respectively. Even if budgets are subject to a high level of uncertainty, the modification of the local water regime resulted in a significant decrease in CH_4 emissions.

2.7 Analysis of CO_2 flux rates during growing season

For the statistical analysis of the growing season during the data years 2002–2004 and 2013–2015, a linear regression with a moving window of 14 days was

used to analyze the peak uptake. An hourly shift was chosen to account for short-term variability. Maximum negative slopes were identified as maximum uptake rates while the center of the window represents the day of year (DOY) with the maximum uptake. To determine statistical differences between drained and control site a one-way analysis of variance (ANOVA) was performed to compare the means of the time series. Measurements and thus errors are independent, the data are normally distributed and the variances are equal in most cases. All statistical designs and analysis were performed with the software R (R Core Team, 2014).

2.8 ANALYSIS OF HEATING EFFECTS

Data with highest quality (QF 1–3, Foken et al., 2004; 2012) were used for the detailed analysis of the self-heating of the OP instrument and the sonic anemometer heating effect (Table 3). Figure 4 lists the timeframes used for all analysis.

Table 3: Quality flag (QF) of EC CO_2 fluxes as percentage of winter season (November–April) measurements from both sites.

Site	Winter season	QF 1–3 [%]	QF 1–6 [%]
Tower 1	2013/14	23.2	47.2
	2014/15	21.8	60.9
	2015/16	19.2	55.1
Tower 2	2013/14	18.5	44.2
	2014/15	21.9	55.6
	2015/16	-	-

2.8.1 Self-heating of open-path sensor

All statistical analyses were performed with the R software (R Core Team, 2014). The examination of the wind speed and direction with resulting figures were created with the R-package “openair” (Carslaw, 2015). Because both of the measurement signals have approximately the same error (Dunn, 2004), i.e., no one device is free of errors, the orthogonal regression was applied with the R-package “lmodel2” (Legendre, 2014). Orthogonal regression analysis was used to assess the agreement between OP and CP flux measurements, and Pearson’s correlation

coefficients (r) are given. Orthogonal regression is used in place of linear regression because it takes experimental uncertainties in both OP and CP measurements into account, and does not require the definition of an independent and a dependent variable.

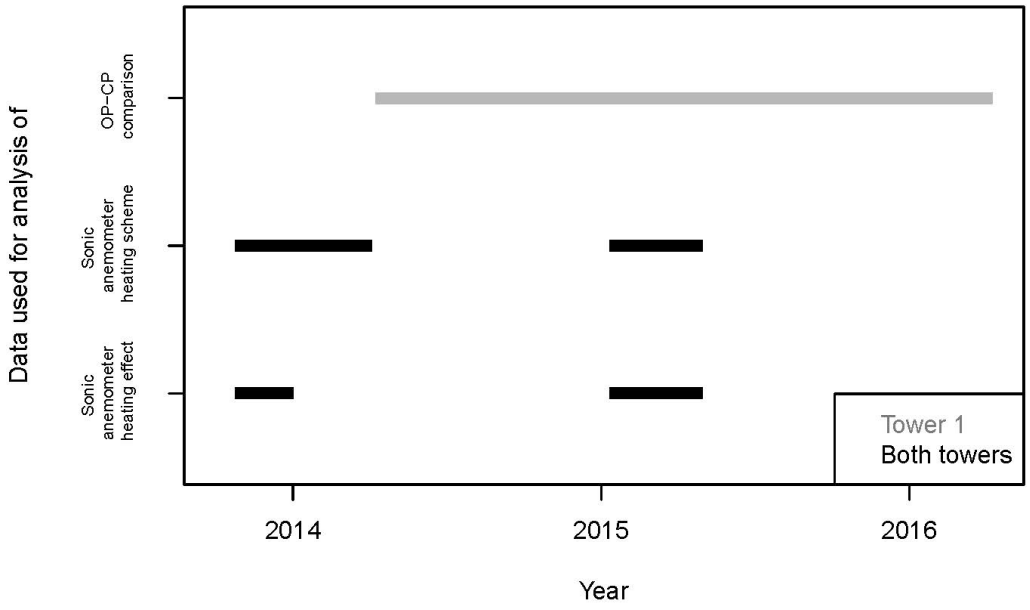

Figure 4: Time frames and used data for different analyses. Data coverage with QF 1–3.

2.8.2 Sonic anemometer heating and icing events

Using information from ancillary meteorological instrumentation the sonic anemometer heating was controlled by the data logger and was activated based on combined rH (> 85 %) and T_a (< 1 °C) conditions. Since the same heating schemes were applied at both towers, and both towers experienced almost identical meteorological conditions, sonic anemometer heating should be active synchronously at both towers. Due to a reset of sonic anemometer setup parameters, sonic heating was de-activated on tower 2 in the period from mid-October 2013 to beginning of April 2014, and on tower 1 in the period from mid-January to beginning of May 2015. For reasons of data quality assessment, the data analysis for the first period was restricted until the end of 2013. Heated and unheated conditions are compared during both winter seasons by combining data from both observation systems (e.g. heated conditions represent data from tower 1 during the first winter season and data from tower 2 during the second winter

season). It is assumed that during the polar winter with a closed snow cover, variability in microsite conditions between the towers can be neglected. In total 26 weeks are available for an in-depth analysis of the sonic anemometer heating effect.

For the identification of potential icing events, error messages given by the sonic anemometer were analyzed. Error messages were recorded with a frequency of 20 Hz and stored additionally to the high frequency EC data in an extra file and were counted per half-hour interval for the same temporal resolution as for EC data without distinguishing between individual error messages. These additional data logs indicate potential disturbance or blockings of the sonic anemometer signal. Icing events were identified as periods with the maximum number of error messages per half hour (36000), indicating a "permanent" disturbance of measurements that is unlikely to be caused by short-term meteorological conditions. Since EC data during icing events are inaccurate ancillary measurements are used to characterize meteorological conditions.

2.9 REMOTE SENSING AND ADDITIONAL DATA SOURCES

We used MODIS NDVI (MOD09GQ, MOD13Q1) with both daily and 16-day temporal resolution to analyze the interannual variability in phenology at the observation site. Raw data for the 250 m daily NDVI products were filtered for outliers based on the 16-day composite NDVI time series, and smoothed using a moving average approach (window size of 10 days).

For the seasonal classification the start of the spring season was defined by a net radiation threshold (> 0 W m^{-2} for 4 consecutive days) according to Oechel et al. (2014). The growing season was defined by daily mean air temperature (> 4 °C for 4 consecutive days as starting point) and fractional snow cover (> 50 % as ending point). The growing season was further divided into sub-seasons. Based on the "GreenBrown" R-package (Forkel et al., 2013) phenological key dates were derived from trends and patterns in the seasonal course of NDVI: start of season (SOS), peak of season (POS), and end of season (EOS), for each year

individually. From the temporal trends in MODIS time series of NDVI, the POS is determined by maximum value. For SOS and EOS a threshold of 46 % and 59 % of the corresponding POS was taken, respectively. These key dates allowed the growing season to be separated into four distinct sub-seasons: (1) pre-season (until SOS), (2) early-season (SOS to POS), (3) late-season (POS to EOS) and (4) post-season (after EOS). Mean values for SOS, POS, and EOS, as well as year-to-year variability of these key dates within the period 2000–2015, are provided in Figure 5. The end of fall was defined as the end of the so-called zero curtain period (Zona et al., 2016) by using 0.32 m soil temperature data at the drained site. The interannual variability of the starting dates for the seasonal deviations is shown in Table 4.

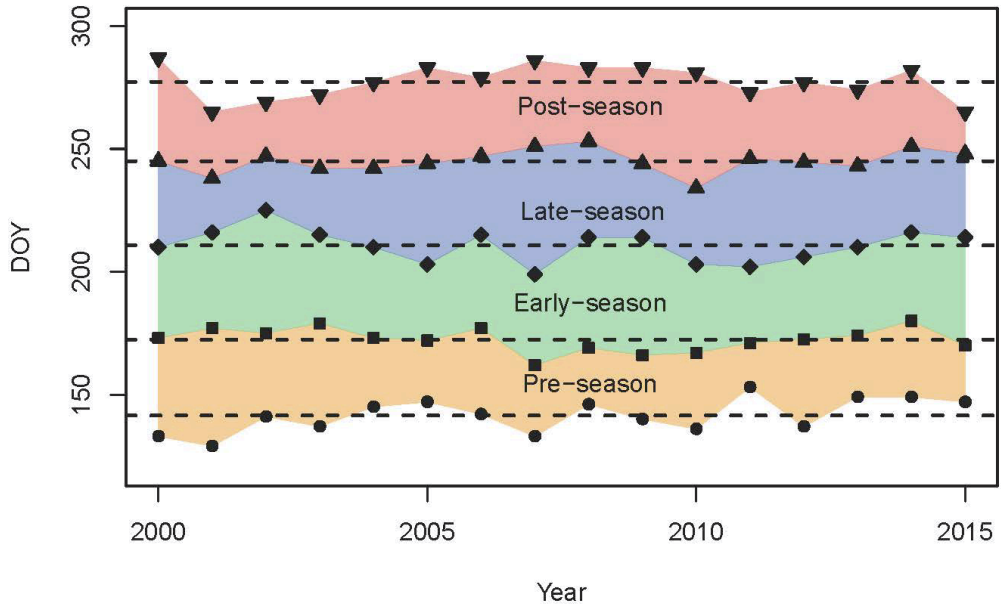

Figure 5: Interannual variability of all key dates with symbols marking the exact date, lines indicating the overall mean and colored areas representing the resulting sub-season during the growing season. Key dates from bottom to top: start of pre-season (circle), SOS (rectangle), POS (diamond), EOS (standard triangle) and end of the post-season (upside-down triangle). Due to cloud coverage, in 2012 the MODIS data coverage was not high enough to determine the key dates (SOS–POS); these dates are therefore linearly interpolated.

Table 4: Interannual variability of all dates as day of year (DOY) to determine the start of the season.

Start of season	2013	2014	2015	2016
Spring	-	116	105	99
Growing	149	150	148	135
Fall	273	281	264	269
Winter	338	340	336	360

A webcam (CC5MPXWD, Campbell Scientific) provided an additional data source for vegetation characterization. Pictures were taken daily at noon over the course of the growing season. Figure 6 provides an overview of the vegetation dynamics from pre-season (Figure 6 a) towards post-season (Figure 6 d).

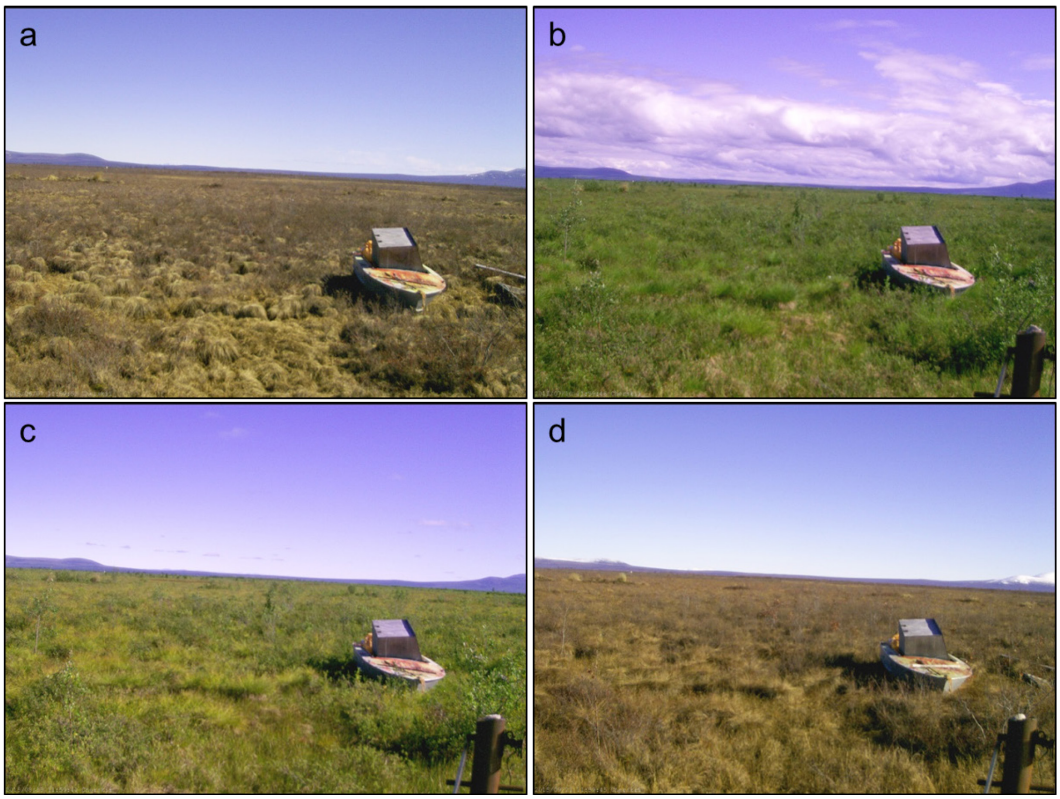

Figure 6: Webcam pictures representing the course of the 2015 growing season. All pictures were taken at noon in the middle of each sub-season: (a): mid-pre-season (6 June), (b): mid-early-season (10 July), (c): mid-late-season (9 August), and (d): mid-post-season (21 September).

3 IMPACTS OF A DECADAL DRAINAGE DISTURBANCE ON SURFACE–ATMOSPHERE FLUXES ON CARBON DIOXIDE IN A PERMAFROST ECOSYSTEM

3.1 INTRODUCTION

To improve the current understanding of links between carbon fluxes and long-term hydrologic disturbance in Arctic permafrost ecosystems (see Sect. 1.3.1) growing season CO_2 fluxes for two eddy-covariance towers running in parallel over a disturbed tundra ecosystem (i.e., one with a drainage ditch ring installed in 2004) and a control tundra ecosystem, respectively, are used. We directly compare CO_2 flux rates between both sites for three growing seasons (2013–2015) to evaluate the net effect of the long-term drainage on the carbon cycle. A comparison of disturbed and control flux rates between historic (2002–2005) and recent (2013–2015) datasets allows assessing the combined effect of this disturbance and a changing climate. In both cases, the focus is on the net CO_2 flux between ecosystem and atmosphere, as well as its major components fluxes, i.e., GPP and Reco. Furthermore, the seasonality of flux rates over the course of the growing season is analyzed.

3.2 RESULTS

3.2.1 Recent environmental conditions (2013–2015)

Large differences in all meteorological site conditions were found for all sub-seasons and over the entire year (Table 5). For example, in 2014 the mean annual temperature was -10 °C, with daily means ranging from -49 °C in January to

22 °C in July. Early- and late-season are the warmest periods of the year for both air and soil temperatures, with particularly high values observed during late-season 2014. Long-term air temperature averages (Rohde et al., 2013) for August 1982–2011 (data not shown here) indicate conditions above the monthly mean for 2014 and below the monthly mean for 2013 and 2015.

Table 5: Environmental conditions measured at Tower 1 (drained): air temperature (T_a) at a 2 m height, soil temperature (T_{soil}) at a 0.8 m depth and net radiation (Rn). Values are given as mean (± standard deviation), with the exception of precipitation (PPT, sum per season). Measurements from 2013 started mid-July (late-season); no data are therefore available before this time. The growing season is divided into sub-seasons; [length of season] is total number of days.

Year	Season	T_a [°C]	T_{soil} [°C]	Rn [W m^{-2}]	PPT [mm]
2013	Late-season [33]	8.7 ± 5.4	3.8 ± 1.1	80 ± 120	NA
	Post-season [31]	1.8 ± 4.8	0.9 ± 0.7	29 ± 82	NA
2014	Year	-10.1 ± 18.9	-2.8 ± 6.4	32 ± 103	173
	Growing season [129]	9.5 ± 7.4	3.8 ± 2.7	89 ± 137	153
	Pre-season [27]	8.6 ± 6.1	1.9 ± 1.7	143 ± 166	28
	Early-season [36]	14 ± 6.4	6.1 ± 1.5	121 ± 142	41
	Late-season [35]	12.1 ± 6.3	5.3 ± 1.8	80 ± 125	74
	Post-season [31]	2.2 ± 3.9	0.8 ± 0.9	19 ± 75	10
2015	Year	-11.3 ± 18.7	-2.4 ± 5.0	28 ± 96	118
	Growing season [114]	10.1 ± 6.8	3.3 ± 2.2	101 ± 141	99
	Pre-season [19]	8.1 ± 5.8	0.3 ± 0.9	148 ± 170	13
	Early-season [44]	14.9 ± 6.1	5.2 ± 1.5	126 ± 148	48
	Late-season [34]	7.7 ± 4.7	3.6 ± 1.1	72 ± 113	32
	Post-season [17]	4.9 ± 5.2	1.4 ± 0.7	39 ± 90	6

A pronounced seasonal cycle due to freezing-thawing dynamics is observed in the soil temperatures (Figure 7 c). For both sites, the active layer was completely frozen until early June, with thawing gradually beginning from the top down. During the growing season the active layer increases up to a depth of ~ 0.4–0.5 m (data not shown). Refreezing usually starts at end of September, and proceeds both from the surface downwards and permafrost upwards. For both the frozen and unfrozen conditions the drained site had higher soil temperatures (Figure 7 c). The largest differences during the growing season occurred during July and August with a ~ 2.5 °C higher soil temperature at the drained site.

While precipitation is variable throughout the year, over 80 % of the annual budget was collected during the growing season in our datasets for 2014 and 2015. Rain events are strongest during early- and late-season (Table 5 and Figure 7 b) with events ranging from 0.1 mm d^{-1} to 16 mm d^{-1}. These events have a direct influence on soil moisture (Figure 7). After flooding abates soil moisture drops rapidly, especially in the tussocks (data not shown). During rain events the soil moisture can increase to maximum values, depending on the intensity of the rain event. Soil moisture values are lower at the drained site than under natural conditions; this can be explained by the ~ 0.2 m difference in water table depth (over and under the soil surface for control and drained ecosystems, respectively) between treatments (Kwon et al., 2016b). While values for both 2013 and 2015 (Figure 7 b) indicated very dry conditions under disturbed conditions, saturation during late-season 2014 (data not shown) at both towers had the same value (soil water content at 0.08 m depth).

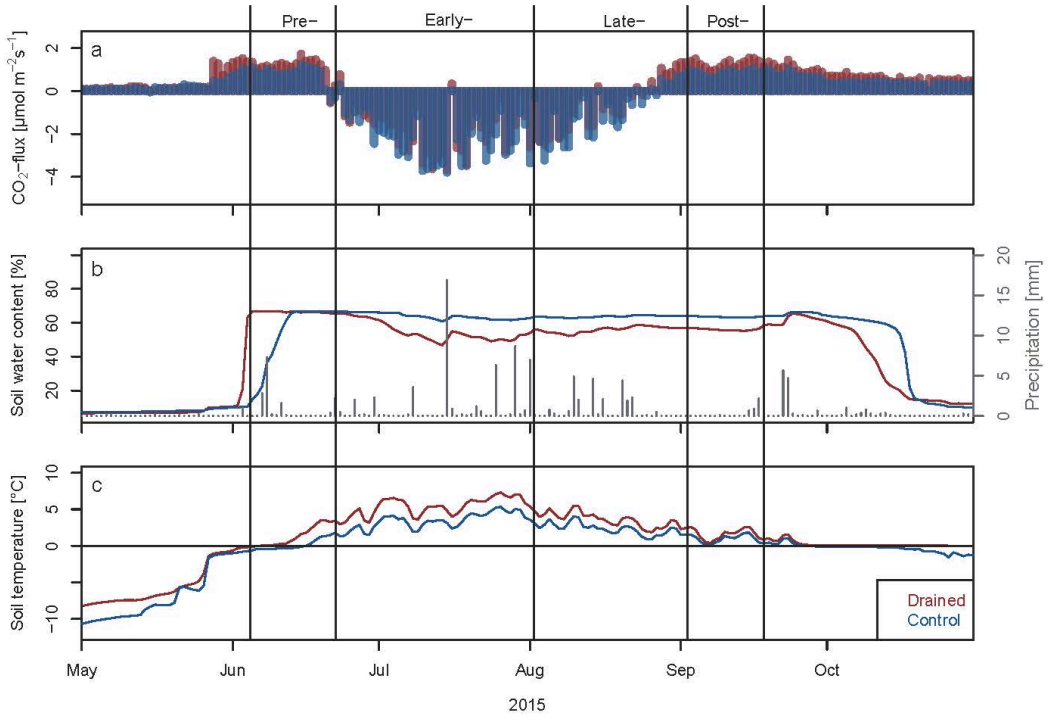

Figure 7: Daily mean (a) carbon fluxes, (b) soil water content at 0.08 m depth and (c) soil temperature at 0.08 m depth. Since precipitation patterns are very similar between sites, only data from the drained site are displayed. Vertical lines divide the 2015 growing season into sub-seasons.

3.2.2 Effects of drainage disturbance on recent carbon fluxes

Net ecosystem exchange and component fluxes varied considerably between 2013 and 2015 (Figure 8 and Figure 9). Splitting the time series into sub-seasons allows for an in-depth analysis of the changing impact of the drainage effects on the CO_2 flux over the course of the growing season:

1. Pre-season: The pre-season was characterized by a rapid increase in net radiation and rising air temperatures (see Table 5). In the weeks directly following snowmelt, cumulative NEE (Figure 8 a) shows a net loss of CO_2 from the system, while photosynthetic uptake is still weak. Both the drained and control study sites are continuous sources for CO_2, and only minor differences are observed between treatment sites and years. Averaged over all available time series, we found net releases of ~ 19 (± 4) gC m^{-2} over the course of 20–30 days.

2. Early-season: With the onset of strong photosynthetic uptake linked to rapidly greening plant biomass (Figure 6 b), both the timing and initial rates of net CO_2 uptake are very similar at the two sites (Figure 8 b). Still, over time, deviations in uptake rates become obvious. For instance, by the end of the 2015 sub-season the drained site showed a net uptake of ~ 20 gC m^{-2} less than the control site. The analysis of component fluxes (Figure 9 b) indicates that the difference in NEE can be attributed to the higher release of CO_2 via ecosystem respiration at the drained site, while photosynthetic uptake is close to uniform between sites for all years (Figure 9 b).

3. Late-season: Early-season differences in NEE between the drained and control sites continue during the late-season. With the onset of vegetation senescence both areas shift from a net sink to a net source of CO_2 (Figure 8 c), but for all data years the control site has a higher net cumulative uptake of CO_2 from the atmosphere. The timing of the peak cumulative budget (i.e., the date when the ecosystem shifts from a net sink to a net source of CO_2) differs by year and seems to be strongly influenced by air temperature conditions in August, with the latest peaks coinciding with the

warmest temperatures (data not shown). Differences in cumulative NEE between the two treatments amount to ~ 12 (± 4) gC m^{-2}; again, the effect was primarily driven by higher respiration rates in the drained area. The observed slight difference in GPP between the drained and control sites was non-uniform between years (Figure 9 c).

4. Post-season: Differences in the cumulative carbon budgets between both sites further increased, as evidenced by the consistently higher cumulative values presented at the drained site (Figure 8 d). Both sites are continuous sources for CO_2 during this sub-season, with decreased incoming radiation and air temperature conditions leading to the senescence of the last remaining active vegetation patches. This results in near-zero assimilation fluxes and thus no diurnal NEE cycle. Higher respiration rates in the drained area lead to higher net CO_2 emissions (Figure 9 d).

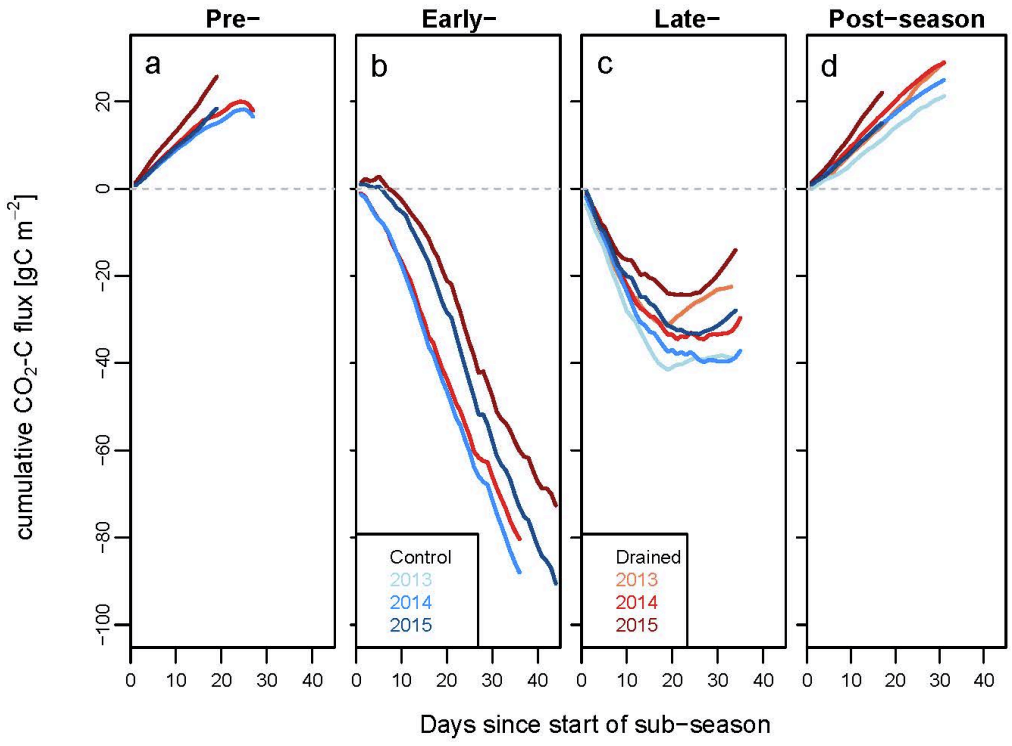

Figure 8: Cumulative CO_2 flux budgets for recent (2013–2015) eddy-covariance measurements for both sites (drained is in red, control is in blue). A grey line indicates the zero lines with a change from positive (i.e., release) and negative (i.e., uptake) fluxes. For these plots, timestamps have been normalized to account for interannual shifts in phenology. Time series were separated into the four different sub-seasons (see Sect. 2.9) using individual key dates for each year. Time series were then plotted in separate panels, resetting the budgets to zero at the beginning of each sub-

season. No measurements are available for the 2013 pre- and early-seasons, since measurements started mid-July 2013.

Across all of the sub-seasons, our results demonstrate that the control site was a stronger sink for CO_2 than the drained site. The majority of the observed CO_2 flux differences are caused by higher ecosystem respiration rates at the drained site, especially during the early- and late-seasons, while only negligible differences in GPP are observed. Over the entire growing season, the cumulative uptake at the control site is 20–40 gC m^{-2} higher than at the drained site, with significant differences (ANOVA, $p < 0.05$) between treatments in both 2013 and 2015 (in 2014 no significant difference in cumulative NEE between the sites was found). Daily mean flux rates over the course of the 2015 growing season are shown in Figure 7 a.

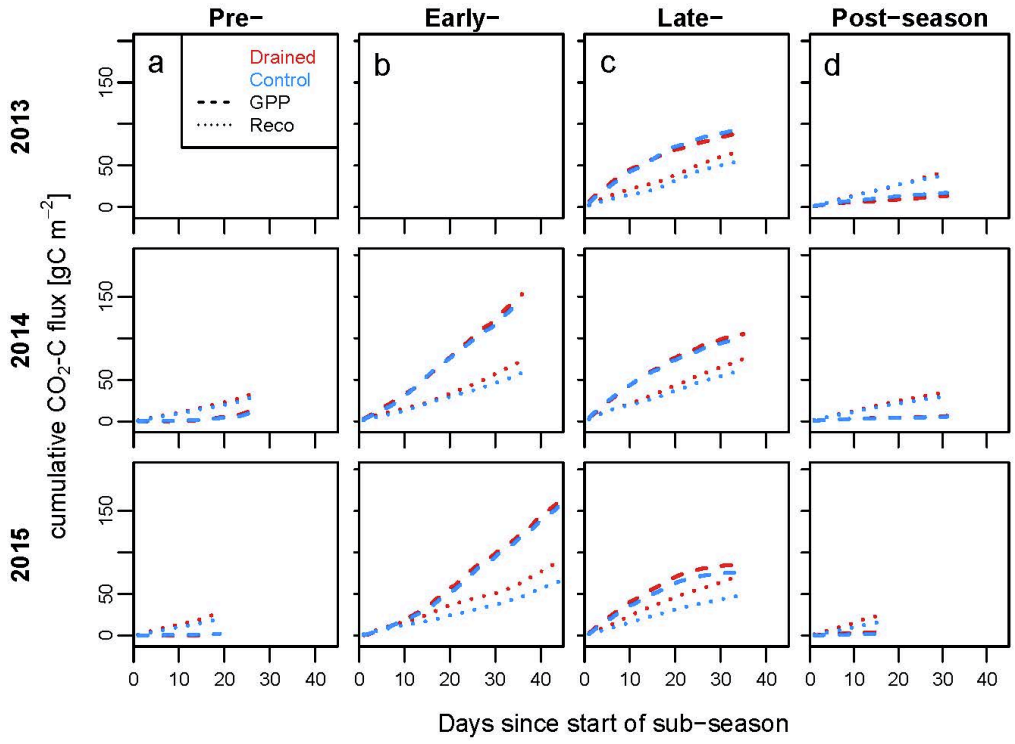

Figure 9: Cumulative ecosystem respiration (Reco, dotted line) and gross primary production (GPP, dashed line) from 2013 (upper panel) to 2015 (bottom panel) for both treatments (red and blue respectively as in Figure 8). Time axes within this plotting scheme are identical to those used in Figure 7.

3.2.3 Comparison of the recent (2013–2015) and historic (2002–2005) datasets

Data coverage between the historic and recent observation periods varied considerably, with measurement starting dates ranging from the beginning of May to mid-July and end dates differing by up to 2 months (Figure 2). To facilitate a direct comparison of the carbon budgets between all years, the starting dates for cumulative time series (Figure 10 and Figure 11) were set to 1 May. For time series that started later in the season, we used the available budget from the nearest year (either prior to or after the year of observation). Accordingly, not all displayed time series start with a value of zero, and final values therefore do not always represent the cumulative budget based on the available observations. This approach facilitates a qualitative comparison of seasonal trends in CO_2 exchange between different data years, while absolute numbers of the seasonal budgets are subject to significant uncertainty for years with data gaps.

The observed differences in cumulative uptake for the historic dataset reflect the interannual variability in CO_2 fluxes that can be expected in this type of ecosystem (Figure 10 a, 2002–2004). Such changes are primarily caused by varying climate conditions from year to year (Merbold et al., 2009). In contrast, 2005 – the year immediately following the installation of the drainage system – shows a systematic dampening in the seasonal course of net carbon exchange (Figure 10 b), even though the cumulative NEE budget at the end of the growing season is comparable to previous years' levels.

A direct comparison of the recent and historic carbon flux patterns in Figure 10 shows that the seasonal amplitude of the cumulative CO_2 budget has increased over the past decade. Maximum CO_2 uptake rates are higher at peak growing season in July, and initial carbon release immediately following snowmelt (~ May–June) seems to have increased as well. In contrast, net CO_2 emission rates in fall appear to be similar between recent and historic datasets. As a consequence, the average cumulative growing season uptake of CO_2 by the ecosystem has grown over the past ~ 10 years.

While the range of the cumulative CO_2 budget has partial overlap between the recent and historic data years for control conditions, the fluxes observed immediately after the disturbance (2005) and recent fluxes at the drained area display systematic differences, both in absolute values as well as in seasonal patterns. This finding suggests that the disturbed area may have rebounded from the immediate drainage effects and the resulting dampened seasonality that occurred shortly after the disturbance. Instead, recent CO_2 uptake rates at the drained section of the tundra partly exceed the rates observed for the control area before installation of the drainage (Figure 10, 2002–2004).

The seasonal CO_2 exchange for the overlapping data period (19 July to 23 September) for the years 2002–2004 summed up to -42, -21, and -16 gC m^{-2}, respectively, and -46, -63, and -41 gC m^{-2}, respectively, for the years 2013–2015 under control conditions. For the drained part of the tundra, we found -10 gC m^{-2} for 2005 and -20, -48, and -12 gC m^{-2} for 2013–2015, respectively. Negative budgets over most of the growing season in all observation years indicate that both the drained and control ecosystems act as net sinks for atmospheric CO_2 during this part of the year. However, the drained ecosystem displays slightly different exchange patterns for CO_2, with higher respiration rates throughout the growing season, making it a weaker CO_2 sink in comparison to the control site.

Separation of NEE into its individual component fluxes – GPP and Reco – demonstrates that the interannual variability in both cumulative time series (recent: 2013–2015; historic: 2002–2005) increased strongly after mid-July. Net flux variability is dominated by changes in photosynthetic uptake (Figure 11 b). Absolute cumulative flux rates of GPP and Reco tend to be higher at the drained site, indicating that the carbon turnover rates have increased as a consequence of drainage. The long-term tendencies toward higher net CO_2 uptake of the ecosystem during the growing season are mainly driven by increases in GPP since overall increases in photosynthetic uptake outweigh higher respiration losses.

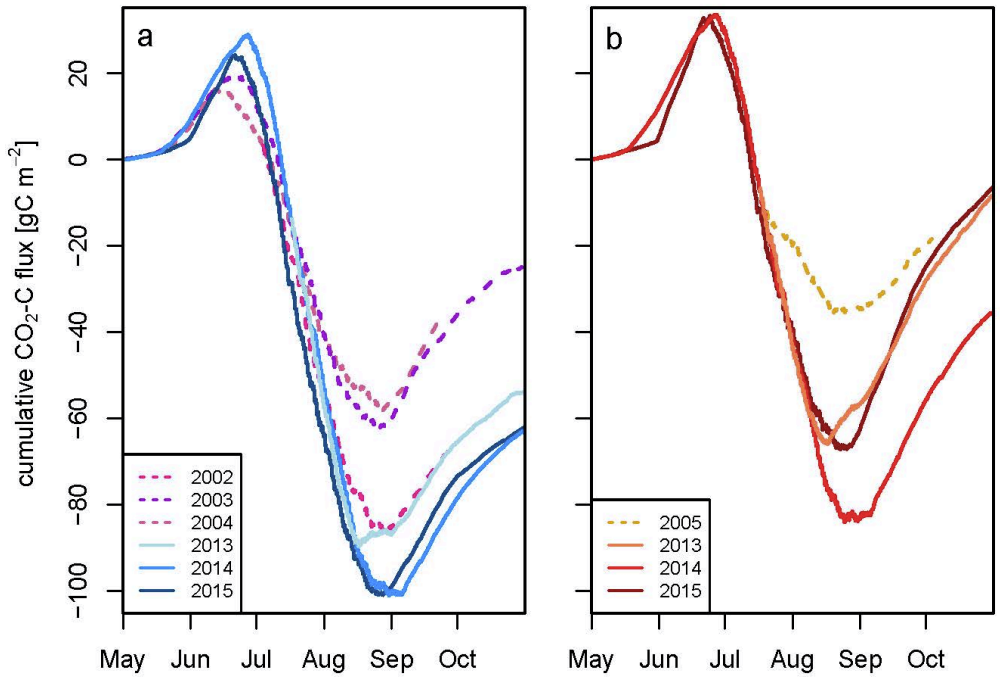

Figure 10: Recent (2013–2015) and historic (2002–2005) cumulative CO_2 budgets separated into disturbance regimes: (a): control area; (b): drained area.

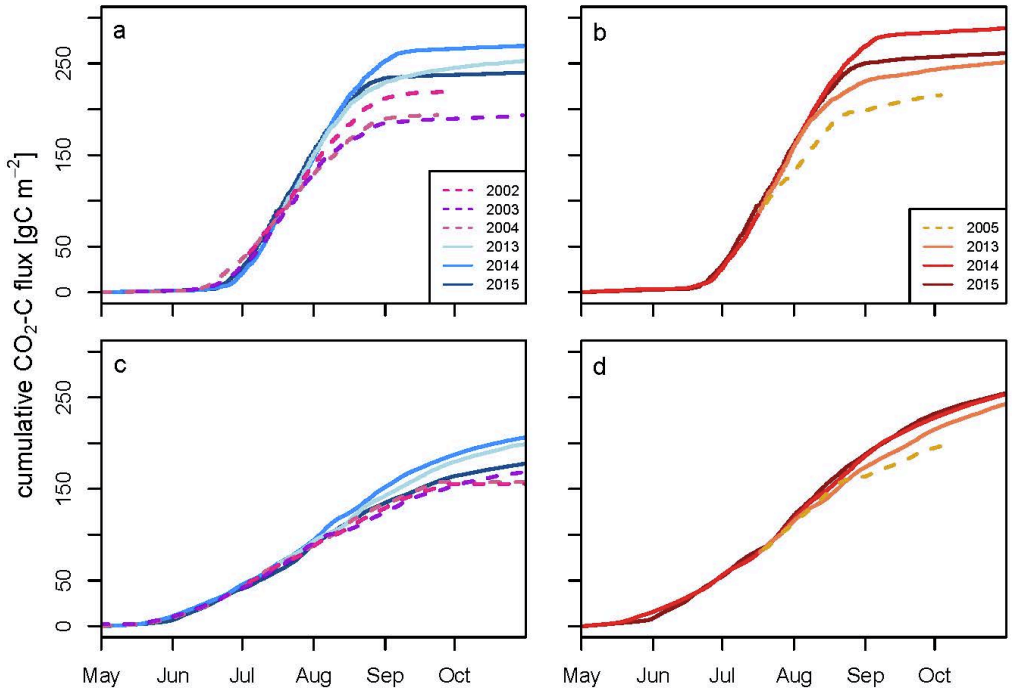

Figure 11: Cumulative signal of recent (2013–2015) and historic (2002–2005) gross primary production (GPP, top panel (a) and (b)) and ecosystem respiration (Reco, lower panel (c) and (d)),

separated into disturbance regimes: (a) and (c): control area; (b) and (d): drained area. Time axes within this plotting scheme are identical to those used in Figure 10.

3.2.4 Long-term environmental conditions

Variability in cumulative air temperature was observed, especially during pre- and post-season, while early- and late-season showed more uniform patterns (Figure 12). The most notable findings were the warm conditions during the 2004 pre-season, which, combined with a short sub-season, indicates a relatively early and intense start to the growing season (Figure 12 a). The same values at the end of the 2003 pre-season are attributed to a remarkably long sub-season. During the early- and late-season (Figure 12 b and c), air temperature developed very similarly in all observed years, with different data years marking the minimum and maximum thresholds. Extreme warm conditions are again observed in the 2002 and 2003 post-seasons, with values twice as high as for the remaining years in the dataset.

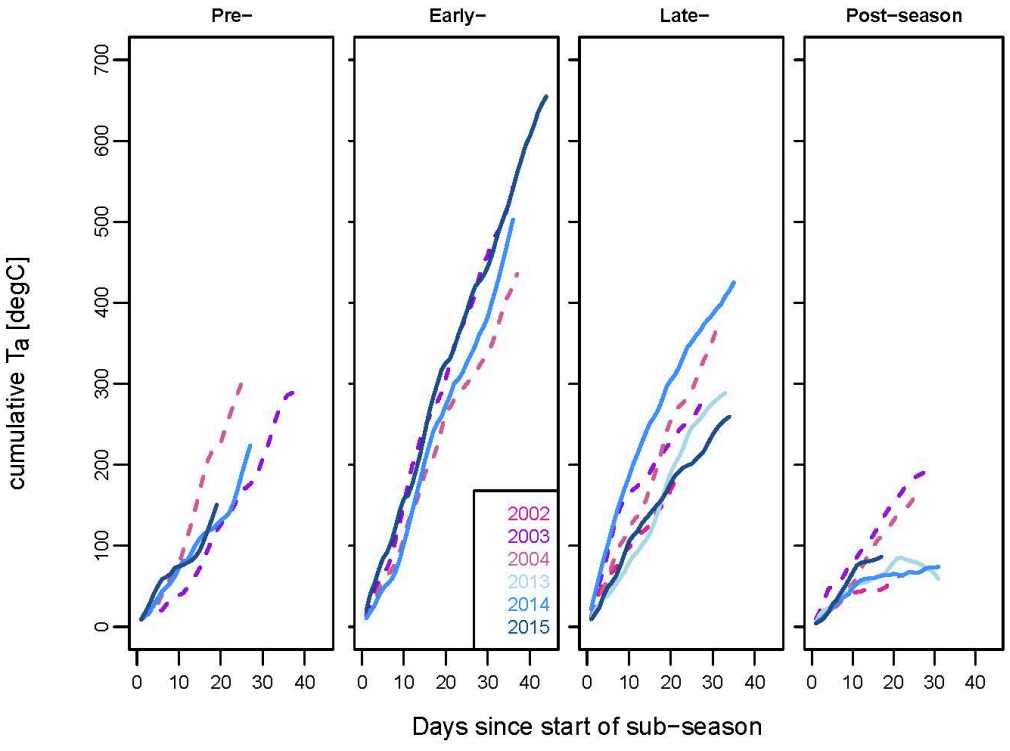

Figure 12: Sub-seasonal air temperature (at a 6 m height) budgets for the control area for the historic (2002–2004) and recent (2013–2015) datasets. Time axes within this plotting scheme are identical to those used in Figure 8.

A subtle trend was observed in cumulative NDVI values (Figure 13), with recent years at the upper range of the values observed for the historic period. At

the same time, all data years show very similar patterns within each sub-season, with differences in values mainly attributable to the individual length of specific sub-seasons.

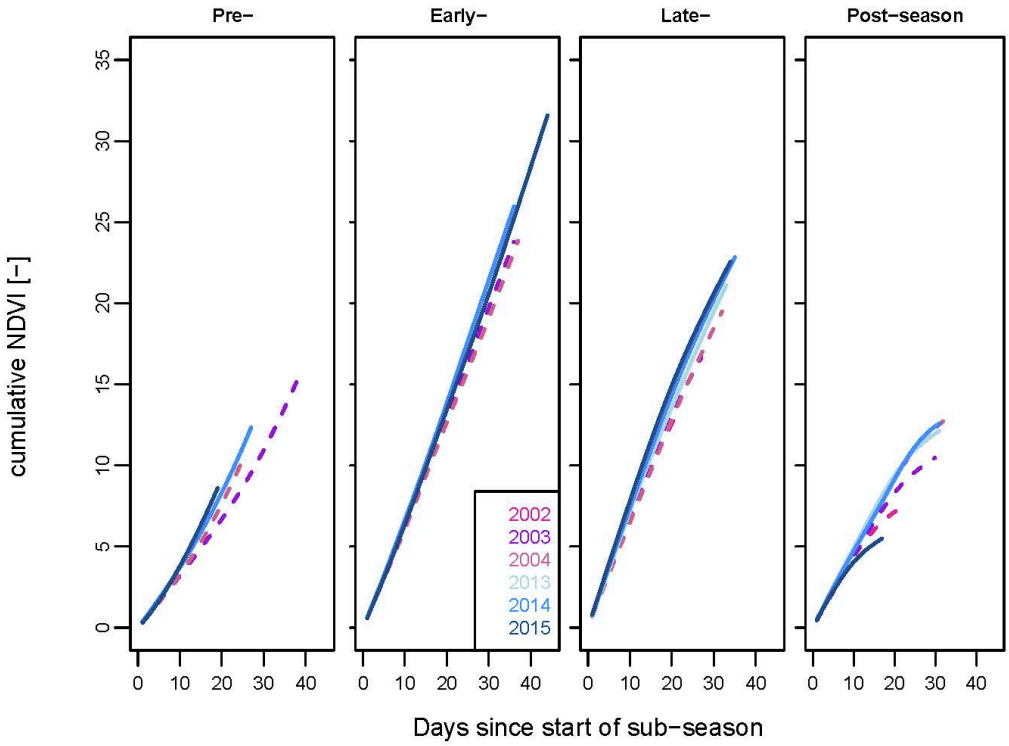

Figure 13: Sub-seasonal NDVI budgets for the control area for the historic (2002–2004) and recent (2013–2015) datasets. Time axes within this plotting scheme are identical to those used in Figure 8.

3.2.5 Linking interannual shifts in carbon fluxes to phenology

We found a strong interannual variability in timing for key phenological stages in the Chersky area (for the MODIS period, 2000 to present) with respect to the start (SOS), peak (POS), and end (EOS) of the season (Figure 5). Maximum year-to-year variability ranged between 18, 26 and 6 days for SOS, POS, and EOS, respectively.

Focusing exclusively on the observation periods 2002–2005 and 2013–2015, we found a maximum difference of 18 days between the shortest (118 days, in 2015) and longest (136 days, in 2005) growing season lengths. Neither the timing nor duration of seasons showed any long-term trends, resulting in no detected systematic differences in phenology between the historic and recent observation periods.

Our limited data availability precludes establishing significant links between phenology and NEE data. The analysis of the interannual variability of cumulative CO_2 flux budgets was executed only for the control site, limiting the data pool to just 6 years (2002–2004 and 2013–2015). Moreover, observations made during the historic period did not cover the entire growing season in some years, further reducing the database for the purpose of statistical analyses. It was therefore not possible to identify meaningful links between individual key dates and NEE patterns. Similarly, no direct correlation between growing season length and NEE budgets in either the recent or historic datasets was found.

Normalizing CO_2 time series to account for shifts in phenology (see Figure 5 and Sect. 2.9) removes interannual variability in cumulative flux budgets and separates the cumulative CO_2 budgets into two distinct groups, the recent (2013–2015) and the historic (2002–2004) datasets (Figure 14). Differences in CO_2 flux budgets become particularly obvious in the early- and late-seasons (Figure 14 b and c). A linear regression fit to identify the maximum gradient of the growing season CO_2 uptake (Table 6) confirms this separation, indicating a significant increase in this peak NEE uptake (ANOVA, $p < 0.05$) between historic and recent datasets. However, the timing of the maximum uptake (as DOY of maximum gradient, Table 6) seems not to be influenced, as dates vary from mid- to late July without any clear pattern. For this gradient analysis we tested different sizes of the moving window, and found no sensitivity of the obtained results towards this parameter. During both the pre- and post-season the net CO_2 release signal shows only minor differences between the recent and historic data (Figure 14 a and d).

Table 6: Results from the linear regression of cumulative CO_2 fluxes during the growing season with day of year (DOY) of maximum gradient and maximum gradient slope.

Year	DOY of maximum uptake	Maximum gradient
2002	204	-0.050
2003	195	-0.044
2004	203	-0.039
2013	210	-0.060
2014	195	-0.061
2015	191	-0.063

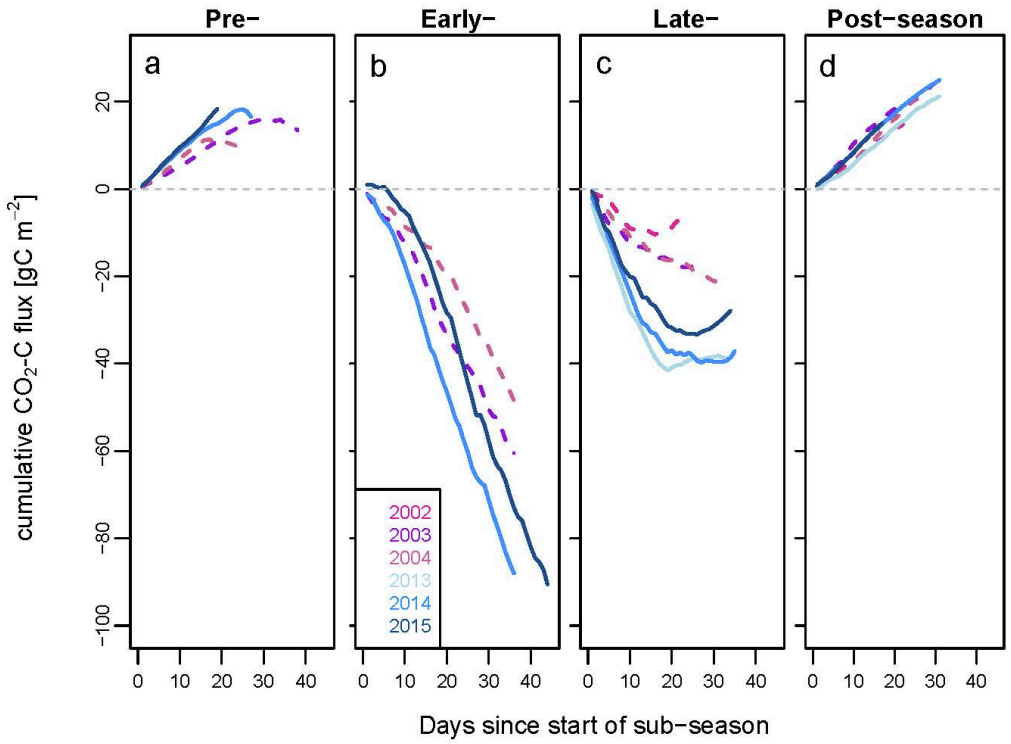

Figure 14: Sub-seasonal CO_2 flux budgets for the control area for the historic (2002–2004) and recent (2013–2015) datasets. Time axes within this plotting scheme are identical to those used in Figure 8.

Net radiation is dominated by strong changes in the albedo and pronounced differences in shortwave radiation. Shortwave radiation varies enormously, with 24h during polar summer, none during polar winter, and transition periods between. Levels of net radiation during the overlapping period of 2013–2015 (see Table 5) are comparable. Pre-season data indicate that the highest net radiation values trigger plant growth and that the rapidly decreasing radiation that occurs during late-season fuels an already early senescence of the vegetation.

3.3 Discussion

3.3.1 Impact of decadal drainage

In Arctic tundra ecosystems reduced soil moisture and the related decrease in water table depth increase the decomposition of soil carbon. This stems from the increased diffusion of oxygen into the soil (Billings et al., 1982; Oechel et al., 1998; Peterson et al., 1984), which induces higher CO_2 exchange fluxes to the atmosphere. In contrast, partitioning of the NEE signal indicates a minor increase

in GPP rates at the drained site, which can be attributed to a shift in the vegetation composition. Drainage has led to the establishment of more tussock-forming sedges (*Carex* species) and shrubs (*Betula exilis* and *Salix* species), while the undisturbed parts of this tundra ecosystem are instead dominated by cotton grasses (Eriophorum angustifolium, Kwon et al., 2016b). Such shifts in vegetation community structure have been associated with differing CO_2 uptake patterns (Christensen et al., 2000). Major differences – which were especially clear in the early- and late-season, when emissions at the drained site exceeded those found at the control site – are caused by higher respiration activity, triggered by higher soil temperatures (Kwon et al., 2016b; see also Figure 10 c and d) in the upper part of the active layer (Lloyd and Taylor, 1994).

In an earlier study, Merbold et al. (2009) could not show a significant change in the CO_2 exchange patterns immediately following this drainage disturbance. As this result can be attributed to the shorter observation period of only a single data year, neither long-term effects nor interannual variability could be taken into account. In contrast, in the present study we demonstrate that long-term (>10 years) drainage had a significant impact on the carbon cycle processes of this tundra ecosystem. Since recent CO_2 uptake rates at the drained site at times exceed the rates observed for the control area before installation of the drainage, we conclude that the drained section has largely adapted to the new conditions, with features such as vegetation and microbial community structures that can tolerate lower average water table depths and stronger fluctuations in water availability over the course of the growing season (Kwon et al., 2016b). Concerning interannual variability in the fluxes, ecosystem respiration seems to be relatively unaffected by annual shifts in either climate or water conditions, while assimilation can vary substantially from year to year. This variability in GPP is primarily due to changing temperatures and cloud cover, and is further amplified under the influence of fluctuating water regimes at the drained site. Finally, despite the fact that long-term changes in site conditions (e.g., water availability, plant communities) can lead to systematic shifts in both absolute fluxes and flux components, we found interannual variability to remain at approximately the same level between historic and recent data.

To our knowledge, our study represents the only long-term experiment focusing on the net impact of lowered water table depths on growing season CO_2 fluxes in Arctic tundra ecosystems. Existing water manipulation approaches have been conducted that can be used to evaluate our findings, despite the fact that differences between wet and dry sites , respectively, were obtained by wetting the natural tundra, instead of drying as in case of the presented study. For example, in one study, long-term water table depth increase triggered a stronger CO_2 sink during the growing season by promoting photosynthetic uptake during the summer (Lupascu et al., 2014). Other studies found lower CO_2 emissions during fall as a consequence of wetter conditions (Christiansen et al., 2012b). Similar conclusions were drawn in the present study, where wetter conditions under undisturbed conditions led to lower respiration rates and a higher CO_2 sink compared to the drained site. However, a direct comparison of our results with prior studies is compromised due to the different measurement techniques used, as well as the multi-factorial interaction of different treatments combined with the increased water table depth.

Similar findings to these long-term experiments have been described by studies that focus on short-term processes using an eddy-covariance method. Dry conditions are considered to be an important control factor for the terrestrial carbon cycle, and have been linked to increased respiration rates during the growing seasons (Aurela et al., 2007; Huemmrich et al., 2010; Lund et al., 2012; Zona et al., 2010). Such findings are in line with the results we obtained shortly after the setup of the drainage channel (2005). Although Zimov et al. (1996) observed the highest effluxes during the wettest year in an area close to our site, these results may have been influenced by small-scale heterogeneity and differences in measurement technique (i.e., chamber vs. eddy-covariance).

3.3.2 Seasonal development and interannual variability of CO_2 fluxes

The methods and limits used in determining the key dates for seasonality have a high degree of uncertainty. This uncertainty can influence the key dates derived to indicate SOS, POS, and EOS, which can in turn lead to uncertainty in the growing season and sub-seasonal NEE budgets. Variable spring flooding can also

affect the duration of the growing season through an indirect shift in key dates, and can reduce CO_2 uptake during the growing season (Zona et al., 2012). However, as we do not expect potential uncertainties in the key dates to cause systematic shifts in seasonal trends and budgets, the qualitative results presented in the present study should not be affected.

Here, we compare two observation periods, the historic (2002–2005) and the recent dataset (2013–2015), both covering 3 years of control measurements. These time frames might not be sufficient to fully represent conditions within each observation period, since surface–atmosphere exchange processes are often subject to pronounced interannual variability. Long-term continuous observations would allow a more in-depth statistical analysis. However, we observed characteristic patterns (e.g., the maximum CO_2 uptake rate during growing season) that clearly showed a distinctive trend between historic and recent periods. Thus, even from this limited database, we can see that the ecosystem has undergone a systematic shift over the past ~12 years.

Pronounced net CO_2 emissions to the atmosphere at the start of the growing season, as observed in this study during the pre-season, have previously been described by other studies for Arctic tundra sites (Corradi et al., 2005; Euskirchen et al., 2012; Grøndahl et al., 2007; Kutzbach et al., 2007; Nordstroem et al., 2001; Oechel et al., 2014; Oechel et al., 1997; Parmentier et al., 2011; van der Molen et al., 2007; Zimov et al., 1996). During the pre-season, respiration clearly dominates the CO_2 flux signal, while the onset of photosynthetic uptake is delayed even though environmental conditions are adequate (e.g., mean temperature = 8.1 °C, mean shortwave incoming radiation = 170 W m^{-2}). This observation, which differs markedly from the results of other studies focusing on Arctic tundra CO_2 flux exchange (Harazono et al., 2003; Kutzbach et al., 2007), might be associated with the very low abundance of mosses in this specific ecosystem (Kwon et al., 2016b).

The interannual variability of cumulative CO_2 fluxes is weak during the pre-season, even if environmental conditions (i.e., air and soil temperatures, soil moisture) are highly diverse both within and before the individual pre-seasons.

For example, 2004 showed exceptionally high air temperatures during this sub-season, while net CO_2 emissions remained at the same levels as had been observed for years with more regular temperature courses (Figure 13). In contrast, in 2015 release rates were higher than average during a relatively cold pre-season. We were unable to correlate the early start of the growing season and warm springtime conditions with increased uptake patterns during the growing season as described by other studies such as Aurela et al. (2004) and Euskirchen et al. (2012). These findings suggest that, for our study site near Chersky, early-season emissions may be affected by both conditions during winter (i.e., snow cover and depth, onset of snowmelt) and transition period (i.e., start and intensity of the flooding event). A detailed effect cannot be quantified here since all relevant snow regime dynamics happen before the start of the pre-season. Based on the available data, no direct correlation between the years with the lowest uptake over the growing season and the strongest flooding event were observed; an isolated effect of the flooding event therefore cannot explain the observed interannual variability.

Both peak uptake rates and the timing of these peaks at the end of the early-season (i.e., mid- to late July) agree with findings presented for tundra systems across the Arctic circle (Euskirchen et al., 2012; Grøndahl et al., 2007; Harazono et al., 2003; Kutzbach et al., 2007; Lafleur and Humphreys, 2007; Nordstroem et al., 2001; Oechel et al., 2014). During the late-season the shift of the balance between respiration and assimilation towards a net release of CO_2 is highly variable between years. Results from 2014 indicate that the length of the net uptake season is highly sensitive towards climate conditions in July to August. In 2014, warm temperatures (> 5 °C compared to the average monthly mean in August) led to an increased net CO_2 uptake from mid-July to the end of October by ~ 20 gC m^{-2}.

The year-to-year variability in NEE during the early- and late-seasons is dominated by variability in GPP (Euskirchen et al., 2012; van der Molen et al., 2007). In our study, we found GPP also to be the main driver of shifts in growing season CO_2 fluxes between the recent and historic datasets. The observed net increase in the CO_2 sink strength in recent years can be attributed to significant increases in CO_2 uptake rates around the peak of the growing season (Table 6).

This observed separation in the cumulative CO_2 patterns (Figure 14) between historic and recent periods cannot be attributed to systematic changes in climate: There are no systematic trends in air temperatures over the last decade in the Chersky region, and, particularly during the early- and late-season, average conditions were found to be very stable over the years (Figure 12). Small deviations in temperature during pre- and post-seasons are not correlated with the observed trends in CO_2 uptake. However, we observed a minor increase in cumulative NDVI values (Figure 13) in recent years (2013–2015), and these higher photosynthetic leaf areas might indicate an overall increase in light use efficiency within this ecosystem. Since the MODIS NDVI data result from a mixed product covering both the control and drained sites, values might have changed slightly due to changes in the vegetation composition at the drained site (Kwon et al., 2016b). However, considering these small differences without a trend between recent and historic years, this data product alone cannot provide a final answer regarding overall shifts in vegetation structure.

Another possible factor influencing the differences observed between recent and historic datasets is the location of the control site. Since the control site from the historic dataset was converted into a drained site in fall 2004 with the installation of the drainage ditch, a new control site had to be chosen for the recent measurements. Elevation measurements in 2014 indicated that parts of the drained site are slightly lower than the surrounding terrain (up to ~ 0.5 m). Within the floodplain environment, such minor topographic depressions preferentially collect melt and flood water; accordingly, control observations made during the historic period may have been subject to more pronounced flooding as compared to the recent control observations at the new tower position. More standing water surrounding the tower site could in turn cause differences in photosynthetic activity, respiration rates, and NDVI. Flooding dynamics can also influence carbon exchange fluxes and increase CO_2 losses (Zona et al., 2012). However, differences in elevation might have been less pronounced in the historic dataset, since subsidence may have been a secondary disturbance effect triggered by the lowered water table depth in this area.

Similar year-to-year patterns of pronounced CO_2 efflux rates can be observed in the post-season, where temperatures remain above freezing in most soil layers with favorable conditions for the microbial decomposition, triggering enhanced CO_2 emissions (Parmentier et al., 2011). However, unlike Oechel et al. (2014), respiration rates at our site are lower during post-season (~ 35 %) than during late-season. This is primarily due to biogeophysical differences in the site conditions in Chersky as compared to the Alaska North Slope sites near Barrow. While thawing of the active layer continues in fall near Atqasuk (Alaska, US), soil temperatures are already starting to decrease by August to September (see Figure 7 c and Table 5) in Chersky.

3.3.3 Data processing and uncertainties

The Burba correction was applied to adjust for the surface heating effects on the measurement performance of the open-path gas analyzer (LI-7500, LI-COR Biosciences); however, our approach is different from the original formulation of this procedure as detailed by Burba et al. (2008). Our approach was to customize the original equation for a non-vertical orientation of the instrument. Since our analyzer was mounted in an inclined position, the majority of the self-induced heating did not affect the measurement path; as a result, only a small fraction of the original Burba correction term needed to be applied (Järvi et al., 2009; Rogiers et al., 2008). We used a dataset of closed-path fluxes as a reference (data not shown), and found that 7 % of the original Burba correction optimized the agreement between open-path fluxes and the reference closed-path fluxes. As this value is dependent on changes in the reference closed-path dataset (e.g., data processing or software), the fraction of the applied correction might still be subject to change in future experiments. Still, with data processing based on standardized methods (Fratini and Mauder, 2014), the estimated fractionation factor is comparable to that presented by Järvi et al. (2009). A good correlation between open- and closed-path data after the correction (R^2 = 0.92; slope = 1.05 mmol m^{-2} s^{-1} and offset = -0.0001 mmol m^{-2} s^{-1}) was also obtained. We therefore assume that our correction is representative to remove systematic effects of sensor heating from the open-path flux data used in the present study.

Since the longest gaps have been present during pre-season - a critical transition period between winter and the growing season when environmental conditions change rapidly - even relatively short data gaps can have an impact on the final time series of CO_2 fluxes. For instance, as seen in the 2015 Tower 1 dataset, a poor performance of the gap-filling algorithm produced a sharp transition between winter (with near-zero fluxes) and the pre-season (with pronounced release, Figure 11 b). However, for long-term budgets, this short period with relatively low flux rates is not relevant, and during the remaining sub-season only short gaps occur, during which the algorithm performs well.

To account for the strong inter-seasonal variability, we computed flux-partitioning algorithms separately for each sub-season. With this approach we ensured that our method is based on adequate relationships between temperature and respiration rates at each point in the growing season. This seasonal separation also prevents potential overestimation of base respiration (Mahecha et al., 2010), which is related to growth in both microbial and plant biomass with increasing thaw depth and rising soil temperatures. Overall, the output of such a flux-partitioning algorithm is subject to increased uncertainties based on the chosen methodology and user-defined settings; the results on the component fluxes presented in the present study must be interpreted accordingly.

The comparability of the flux datasets between observation years has some technical limitations due to changes in instrumental setup (eddy-covariance equipment). For the historic dataset, both open-path (LI7500) and closed-path (LI6262) infrared gas analyzers (IRGAs) were used, while recent data are based on an open-path (LI7500) IRGA and a different type of closed-path analyzer (Los Gatos FGGA, off-axis integrated cavity output spectroscopy). Differences in the analyzer type also require different data post-processing and correction, and can result in deviations in the final flux rates even if the observed signals are similar. When integrating eddy-covariance fluxes over longer time periods (e.g., weeks, months, years), previous studies indicate that averaged cumulative NEE tends to be more positive when results are based on CO_2 signals from an open-path system (Bowling et al., 2010; Clement et al., 2009; Haslwanter et al., 2009). Even though most of these studies have been based on a newer version of the closed-path

instrument (LI7000), their results suggest that part of the differences found between the historic and recent datasets presented in the present study might be related to changes in the instrumental setup.

3.4 CONCLUSIONS

Our results demonstrate that a long-term drainage experiment (> 10 years) in a permafrost floodplain in northeastern Siberia has significant effects on growing season CO_2 exchange patterns in comparison to a control site reflecting undisturbed conditions.

1. Drainage effect on recent CO_2 fluxes: Our observations show that the net CO_2 sink strength of the drained ecosystem was reduced by 20–40 gC m^{-2} per year over the three observed growing seasons (2013–2015). Differences in NEE between the drained and control ecosystems are dominated by increased respiration rates at the drained site, primarily triggered by higher near-surface temperatures. In contrast, we found only minor effects on photosynthetic uptake, and the differences between the drained and control sites were less systematic across data years. Still, both ecosystems show negative flux budgets over the growing seasons, representing a net sink of CO_2 from the atmosphere.

2. Longer-term trends in CO_2 budgets: The comparison of recent flux data to historic conditions (2002–2005) indicates that this tundra ecosystem is now a stronger sink for CO_2 over the summer months than it was about 10 years ago. This finding can be linked to an increase in seasonality, with higher net emissions after the snowmelt, as well as to strongly intensified uptake rates at the peak of the growing season in July. The observed long-term shifts are dominated by higher photosynthetic uptake and a resulting stronger carbon sink capacity for CO_2 over the whole growing season, most likely linked to a trend towards higher plant biomass.

3. Ecosystem adaptation following disturbance: Our results demonstrate that the drained ecosystem did recover from the intermediate disturbance impact in 2005 (directly after the installation of the drainage), when net

carbon exchange rates showed a systematically damped seasonal course. CO_2 flux data from recent years indicate that the drained ecosystem has adapted to the disturbance, with changes in the biotic and abiotic conditions leading to a rebound to previous carbon flux levels.

4. Seasonality in summertime CO_2 exchange processes: Concerning recent effects of the drainage disturbance, 70 % of the observed differences in cumulative CO_2 budgets can be attributed to conditions in the high-summer period (July–August), when the effect of reduced water availability is most pronounced. Concerning long-term trends, the major part of the differences between historic and recent flux budgets was found in the early-season, when the long-term increasing trend in photosynthetic uptake has the strongest effect.

4 HIGH-QUALITY EDDY-COVARIANCE CARBON DIOXIDE BUDGETS UNDER COLD CLIMATE CONDITIONS

4.1 INTRODUCTION

There are several issues related to quantifying the turbulent CO_2 fluxes between the surface and the atmosphere and the estimation of reliable winter budgets in Arctic ecosystems (see Sect. 1.3.2). So far, no general recommendation to minimize associated data gaps, and particularly to avoid biases related to instrument heating, was developed. Here, the quantitative effect of different instrument heating options: 1) the self-heating of the OP gas analyzer and 2) the heating of the sonic anemometer that was activated based on meteorological conditions, is assessed. Measured scalars from both instruments, the vertical wind component from the sonic anemometer and the CO_2 concentration from the OP system are essential to determine the turbulent CO_2 flux. Findings build on continuous EC measurements from a field site near Chersky in northeastern Siberia covering three complete winter seasons. This dataset covers parallel operation of heated and unheated sonic anemometers as well as parallel operation of OP and CP gas analyzer systems. This setup allows for a comprehensive assessment of the effect of different instrument heating options on continuous eddy-covariance CO_2 flux measurements during Arctic winter and will be used to derive recommendations on how to minimize the bias in cases where only OP measurements are available. Therefore both heating effects are analyzed separately and the effect of each heating system on the determined CO_2 exchange fluxes is evaluated. Different formulations on the self-heating effect (1) were introduced in Sect. 2.5 and 2.8.1, corresponding results are presented in Sect. 4.2. The results are discussed in Sect. 4.4.1. For analysis of an active sonic

anemometer heating effect (2) the heating scheme was presented in Sect. 2.8.2 and results are described in Sect. 4.3 and discussed in Sect. 4.4.2.

4.2 RESULTS ON SELF-HEATING OF OPEN-PATH SENSOR

4.2.1 Differences between open-path gas analyzer and closed-path reference data

Wintertime CO_2 fluxes obtained from the OP and CP were correlated (r = 0.97, N > 5700) showing that both measurement systems generally capture the same signal. With an orthogonal regression analysis an intercept of -0.249 µmol m^{-2} s^{-1} and a slope of 0.876 were obtained. A positive intercept indicates that the OP has the tendency towards more negative CO_2 fluxes, i.e. more uptake by the ecosystem. Even under cold ambient conditions with completely frozen soils and monthly mean T_a below -30 °C (DJF) where active assimilation of CO_2 by the ecosystem is virtually impossible, average CO_2 fluxes ranged around or below zero with the operation of an OP (-0.18 ± 0.7 µmol m^{-2} s^{-1}, Figure 15 a), while the reference CP shows district positive mean CO_2 fluxes (0.19 ± 0.4 µmol m^{-2} s^{-1}, Figure 15 b).

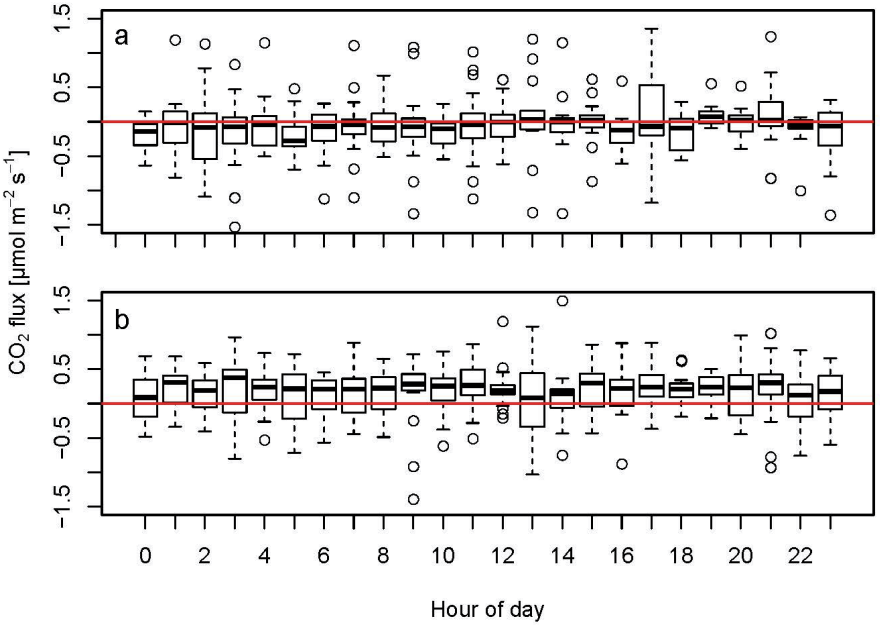

Figure 15: Boxplot for CO_2 fluxes in January by hour of the day from the OP (a, without self-heating correction) and the CP (b) systems. Red lines indicate the zero lines.

These observations suggest a systematic bias in OP measurements that can only be clearly demonstrated during wintertime, since no other influence factors (e.g. uptake by meteorological or biological forcing) besides instrument self-heating can cause negative flux rates. However, CO_2 flux offsets between OP and CP systems show similar tendencies over the full annual cycle (Figure 16 a and b), resulting in a cumulative offset of 92 gC m^{-2} for the data year 2015. Discrepancies in net flux rates between the OP and the CP were found to have different gradients for different seasons:

1. Winter: Strong offsets between OP and CP fluxes were observed in the period December through February. These differences already amount to 16 gC m^{-2} in the first months of the year (January–February, period 1 in Figure 16 b). In December, the CP shows higher positive fluxes adding another 11 gC m^{-2} to the observed differences (period 5 in Figure 16 b).

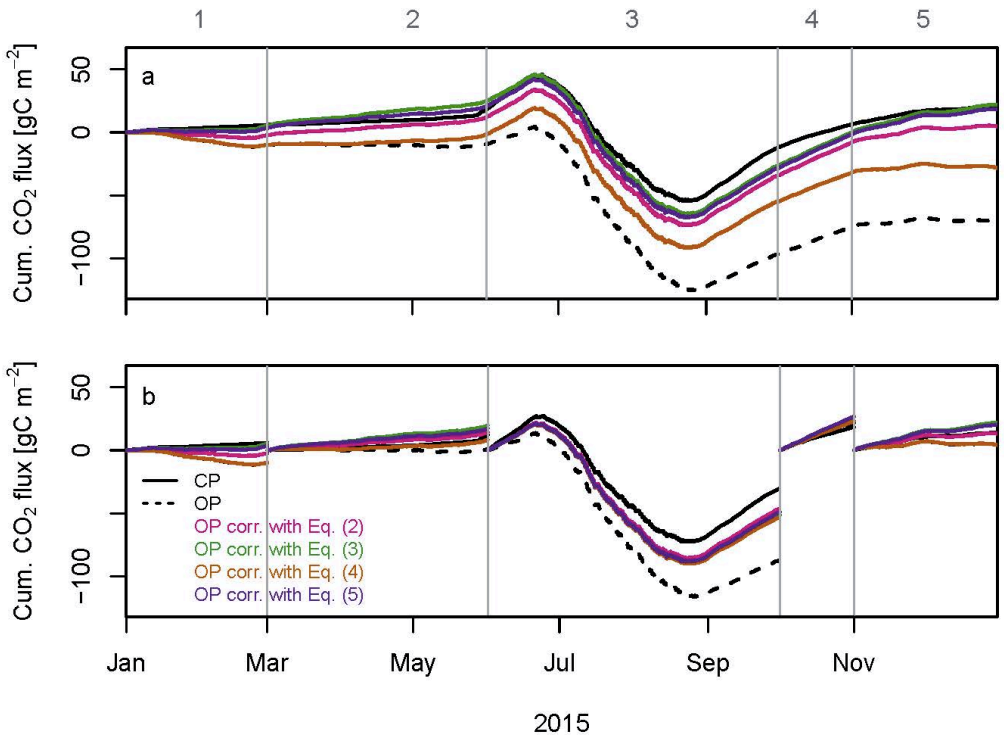

Figure 16**:** Comparison of cumulative CO_2 fluxes for the CP and OP (black lines) and four versions of the self-heating correction for the OP using different instrument surface temperature equations (colored lines) calculated for a full year (a) and per season (b).

2. Transition seasons: During the last months of winter towards spring (March through May, period 2 in Figure 16 b) and in fall (October, period 4 in in Figure 16 b) flux rates between OP and CP generally agree, thus no systematic differences are observed. Accordingly, in this period the offset between the two GAs remains nearly constant.
3. Summer: Large differences arise again during the season from June to September (period 3 in Figure 16 b) with the OP showing higher uptake rates. As a result, the gap in cumulative fluxes between OP and CP steadily increases, summing up to 57 gC m^{-2} for this season.

4.2.2 Application of the self-heating correction scheme

The apparent enhancement in net uptake of CO_2 as measured by the OP is likely to be caused by the self-heating of the instrument linked to the additional heat flux within parts of the optical path disturbing the measurements (Burba et al., 2006a; 2006b; 2008). For the application of the self-heating correction using Eq. (1) a combination of input parameters is required with different magnitudes and seasonal courses (Figure 17). Parameterized T_s is higher than T_a used as input, except for Eq. (4) during the winter period (Figure 17 a). Overall highest mean differences are observed for Eq. (2), while the annual amplitude is largest with Eq. (3). Air and instrument surface temperatures show a pronounced seasonality. For the densities of CO_2, H_2O and dry air, strong seasonal variations are observed with similar characteristic, showing lowest values in summertime for CO_2 and dry air, and opposite tendencies for H_2O density (Figure 17 b). Increased friction velocity values during the summer result in decreased aerodynamic resistance since horizontal wind speeds fluctuate between 2.3 and 3.9 m s^{-1} year-round (Figure 17 c).

The aim of the self-heating correction is to reduce the differences between both GAs. To analyze the performance of the correction, an orthogonal regression analysis is performed before and after the application of the correction with the intercept representing the offset (Table 7). Different linear relationships between CO_2 fluxes from OP and CP reference during day- and night-time (Table 7) are observed. Therefore ξ fractions were fitted separately for day- and night-time

conditions, and also separately for the four different T_s estimations tested (Table 7). Fitted ξ are tightly linked to T_s inputs and due to large differences in the estimations of T_s, ξ varies over a large range with maximum ξ of 0.13 during daytime (0.07 during night-time). Fitted ξ during daytime are by a factor of 2 to 8 larger than during the night. Intercepts after the self-heating correction stay above zero, indicating that there are remaining flux patterns that cannot be corrected for.

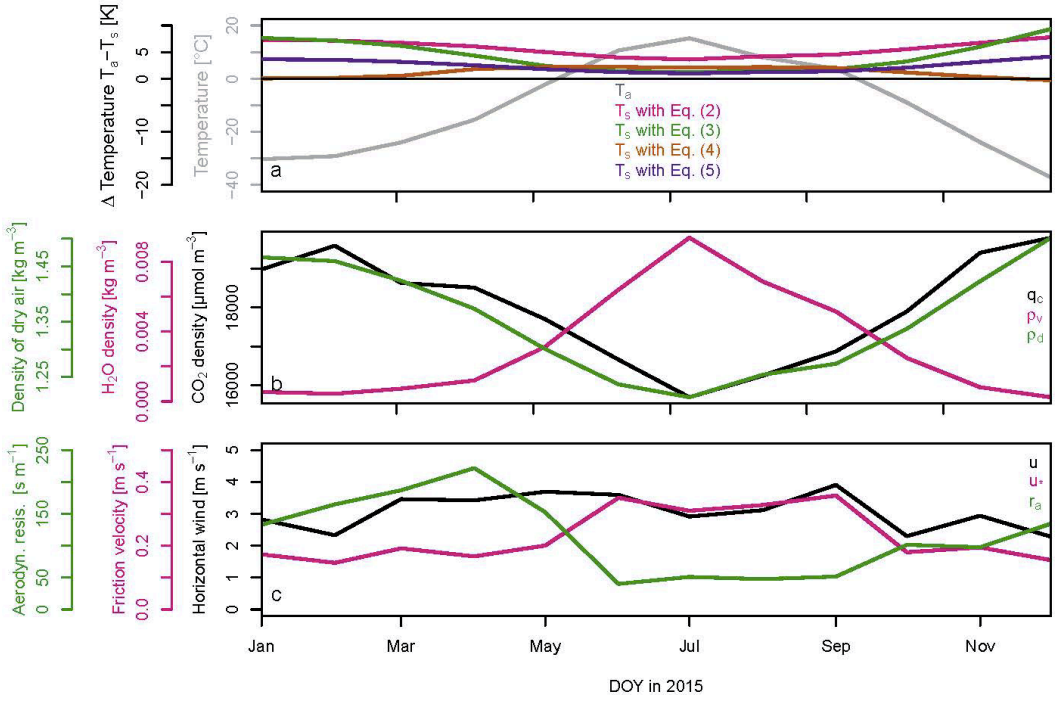

Figure 17: Input parameters for self-heating correction with temperatures (a), densities (b) and turbulent parameters (c) as monthly means. For (b) and (c) axes are color-coded according to lines. For (a) air temperature (grey) and difference to instrument surface temperature (colored line) are shown with the black line indicating the zero line.

To evaluate the seasonal performance of implemented T_s estimations for the self-heating correction, i.e. combinations of Eq. (1) with Eq. (2)–(5), corrected cumulative CO_2 budgets were compared to the CP reference (Figure 16). For all four versions tested, residual differences remained after correction, with gradients of cumulative deviations to the reference varying by season, indicating that the chosen self-heating correction cannot fully remove the offset found in the OP signal. This demonstrates that the self-heating correction is only accounting for an overall intercept, capable of removing a net bias while being unable to change the shorter-term flux patterns. Still, all variants, CO_2 flux differences to the CP can be

reduced and the cumulative annual difference to the CP reference is brought down to a range between -1 and 49 gC m^{-2} for 2015.

Table 7: Overview of results from non-linear fit with Eq. (1) as fraction ξ depending on the instrument surface temperature input. For the statistical analysis between CP and OP CO_2 flux data before (first line for day- and night-time conditions) and after the application of the self-heating correction an orthogonal regression (slope and intercept) is performed and Pearson's correlation coefficients (r) are given.

Time of day	T_s function	ξ	Slope	Intercept [µmol m^{-2} s^{-1}]	r
Day-time	-	-	0.900	0.385	0.96
	Eq. (2)	0.048 ± 0.001	0.888	0.047	0.97
	Eq. (3)	0.130 ± 0.004	0.900	0.054	0.97
	Eq. (4)	0.078 ± 0.003	0.892	0.059	0.97
	Eq. (5)	0.129 ± 0.004	0.900	0.051	0.97
Night-time	-	-	0.805	0.239	0.81
	Eq. (2)	0.019 ± 0.002	0.843	0.134	0.82
	Eq. (3)	0.042 ± 0.003	0.824	0.106	0.82
	Eq. (4)	0.011 ± 0.006	0.849	0.224	0.82
	Eq. (5)	0.068 ± 0.005	0.829	0.113	0.82

4.2.3 Performance of different parameterizations of the self-heating correction scheme

Regarding the performance of the T_s parameterizations, we found systematic differences during different parts of the year (Figure 16 a). In period 3, which represents the four month summer period with the largest differences between OP and CP (see Section 3.1.1), all self-heating corrections agree well with negligible differences of maximal 7 gC m^{-2}, and corrected OP CO_2 fluxes yield a good agreement with the reference measurements (cumulative differences about 20 gC m^{-2}). For periods 1 and 5 representing Arctic winter conditions, the self-heating corrections using Eq. (2) or (4) have nearly no impact on the fluxes and patterns remain close to the input signal. Under night-time conditions, temperature differences between ambient air temperature and estimated T_s are small with Eq. (4), resulting in a negligible ξ and therefore no substantial self-heating correction. Also with Eq. (2) a small ξ is fitted for night-time, leading to only a minor self-

heating correction. During the remaining parts of the year (transition periods in periods 2 and 4), Eq. (3) and (5) seem to slightly overcorrect CO_2 fluxes.

Overall, annual CO_2 differences between corrected OP and CP are 16, -1, 49 and 3 gC m^{-2} for eq. (2) to (5), respectively. Both Eqs. (3) and (5) demonstrate that, given a good parameterization for T_s has been chosen, the self-heating correction can yield OP flux results where annual budgets are comparable with those obtained by a reference CP. Still, even for those cases small seasonal fluctuations remain that lead to non-zero offsets, which may be linked to large seasonal differences between CP and the OP signal, and also differences between daytime and night-time conditions. Since the correction with Eq. (3) yield smallest differences in annual cumulative CO_2 budget in comparison to reference measurements and it represents a simple approach associated with low uncertainty, this combination appears to be suited best for the application of self-heating corrections at our site and will be used for further analysis.

The self-heating correction in total has a pronounced seasonality, with a bimodal course and maximum values during summer and winter (Figure 18 a). By separating into individual terms (Figure 18 b), it can be demonstrated that single terms can have diverse dynamics over the course of a year. The first term of the correction (light blue lines in Figure 18 b) is a combination of CO_2 density and the difference between T_a and T_s. The general shape of the term is determined by the CO_2 concentration with a mid-summer minimum. This term is the only one including the T_s parameterization scheme, thus differences can arise with other estimation approaches (data not shown). The second term of the self-heating correction (dark blue line in Figure 18 b) as reciprocal of aerodynamic resistance and ambient air temperature is characterized by a strong increase in May and decrease in September with quasi-flat stages in-between, strongly influenced by the aerodynamic resistance as a result of the friction velocity (see Supplement Figure S2c). While the first and second term of the self-heating correction have comparable magnitudes with opposing tendencies over the course of a year, the third term composed of the densities of water and dry air (dark green line in Figure 18 b) varies by just 1 % over the course of the year, thus has no systematic effect on the overall correction. A seasonality of ξ is caused by the separation into

day- and night-time conditions representing summer and winter, respectively. In summary, the first term of the correction dominates winter, even if the total correction is reduced by small ξ (e.g., night-time conditions). The summer maximum is caused by the second term due to increased aerodynamic resistance that gets amplified by high ξ (e.g., day-time conditions).

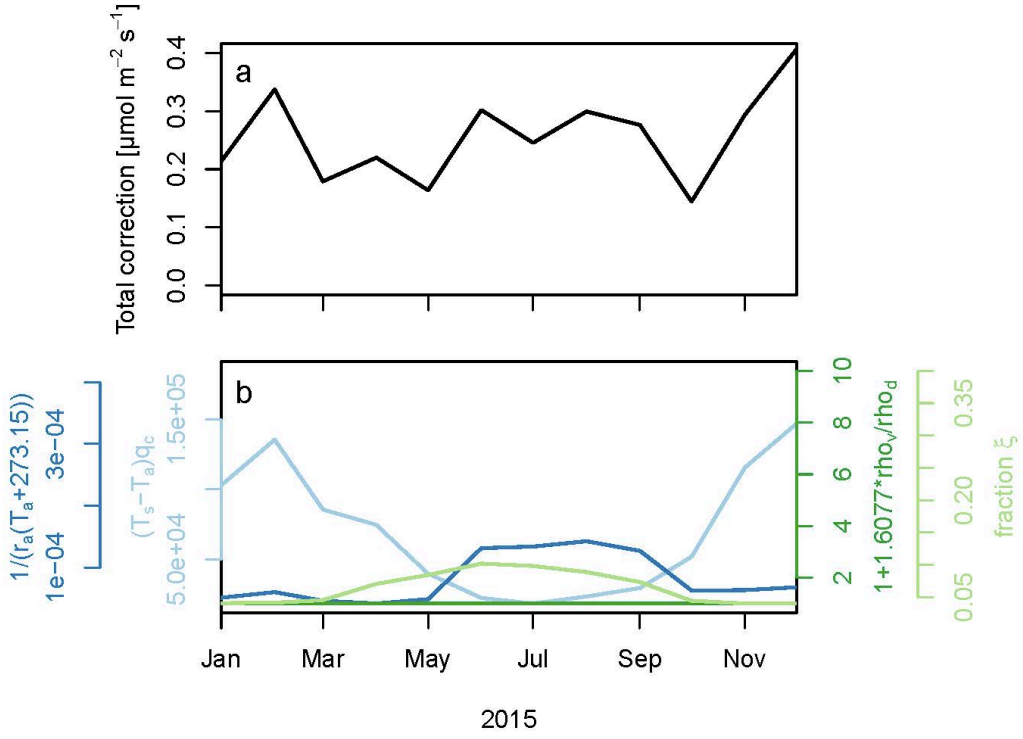

Figure 18: Monthly means for self-heating correction in total (a) and for individual terms (b) that are displayed in absolute numbers by spanning the same relative range. Eq. (3) is used for the surface temperature estimation. The seasonal variability of the fraction ξ is caused by the varying proportions of day- and night-time over the course of the year, since the values optimized for daytime conditions are significantly higher than those for night-time.

4.2.4 Influence of sensor geometry

The wind field dataset was split into seasons, since the properties at our site vary considerable between summer and winter (Figure 19). The prevailing wind directions differ between strongly dominant northern winds during summer, prevailing SE wind directions during winter, and varying directions during spring and fall. Summarized over the annual cycle 2015, the overall dominant wind direction is the SE sector (150°). Wind speed averages are lowest during winter and highest during summer, with an annual mean of 3.8 m s^{-1} for 2015. There is no direct connection between dominating wind direction and wind speed: e.g. in

winter highest wind speeds are commonly attributed to northern winds, a section that is not dominating the wind directions.

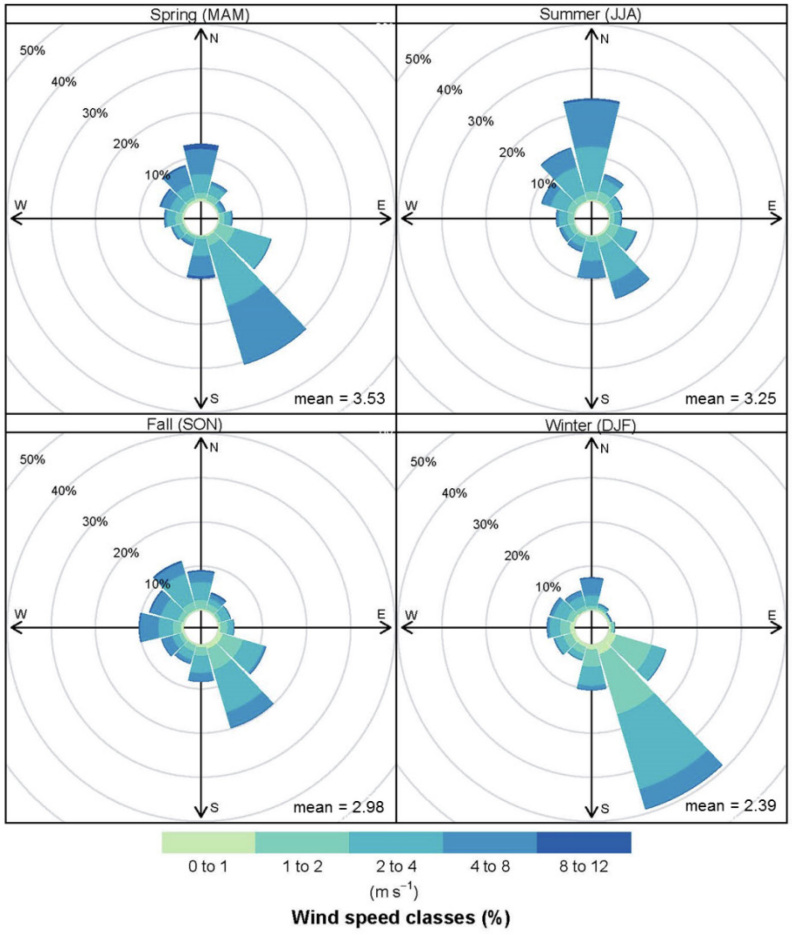

Figure 19: Frequency distribution of wind direction separated in wind directing sectors (30°) and classified into five wind speed classes. Dataset was divided into seasons spring (MAM, top left), summer (JJA, top right), fall (SON, lower left) and winter (DJF, lower right). Mean wind speed values (lower right of each panel) are aggregated per season.

To investigate the dependence of the sensor geometry and wind fields on the self-heating correction, ξ was computed individually for each 30-minute interval ($N > 5000$, mean = 0.15, standard deviation = 0.39). Analyzing the resulting set of ξ in dependence of the wind conditions reveals distinct structures (Figure 20) that hint at an influence of the flow pattern on the self-heating effect. The fraction ξ is generally smallest within the SE sector (0.12 ± 0.28) followed by NE (0.13 ± 0.45), SW (0.16 ± 0.38) and highest values are observed in NW (0.22 ± 0.47). Under low wind speed conditions (e.g., around 300° in Figure 20) ξ tends to be highest.

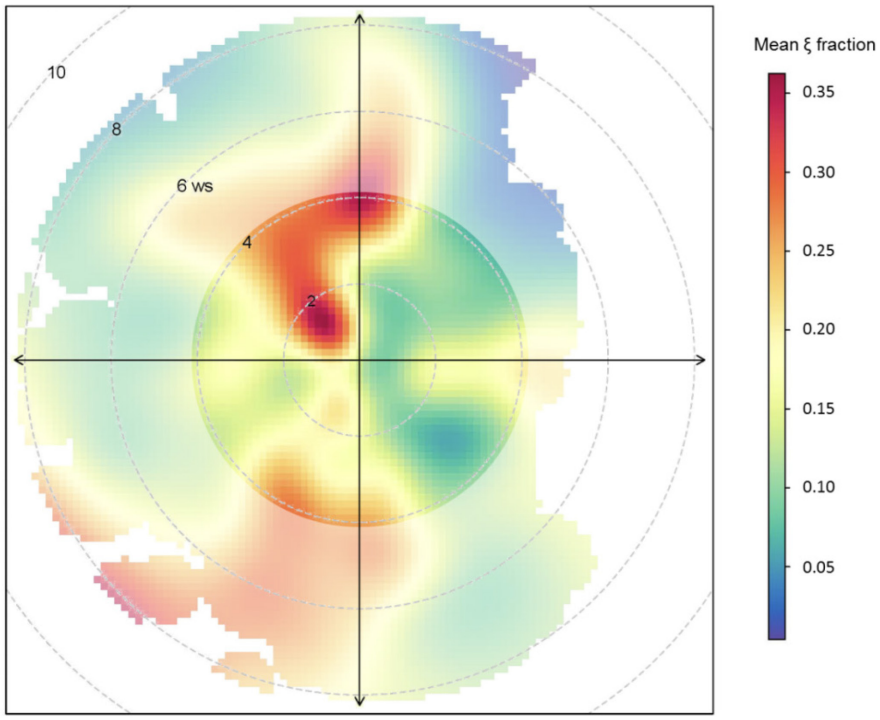

Figure 20: Averaged fraction ξ (color coded) binned by wind direction ([°], black compass rose) and wind speed ([m s^{-1}], grey dashed circles). For the instrument surface temperature estimation Eq. (3) was used. The focus is set to small wind speeds up to 4 m s^{-1} with semi-transparent colors for higher wind speeds.

The OP sensor was installed on a boom pointing towards 55° with an inclination position oriented almost perpendicular to that boom towards ESE (120°). Accordingly, with horizontal wind coming from the NW sector (240°–360°), air will be blown directly into the optical path, reinforcing the self-heating effect (Figure 1b). In contrast, the extra heat flux induced by the instrument self-heating will be transported out of the optical path with wind directions from the SE (60°–180°, Figure 3 c). Focusing on the lower wind speeds (< 4 m s^{-1}), exactly this pattern can be observed in Figure 20: comparatively small ξ are fitted for the E–SE sectors, indicating that the self-heating effect within these directions is smaller than average. In contrast, winds from the W–NW sectors can be associated with higher-than-average ξ, suggesting that heated air is directed into the optical path and leads to an amplified self-heating effect. For higher wind speeds (> 4 m s^{-1}), we assume that the associated increase in mechanical turbulence generates a better mixing of the air around the sensors, therefore reducing the relative impact of the self-heating effect, and accordingly also the

required ξ to correct the fluxes. This can be seen in Figure 20 for almost all directions, except for the SW sector (190°–230°): For these directions, flow distortion by the sonic anemometer (Göckede et al., 2008; Mauder et al., 2007) under high wind speeds appears to influence the performance of the OP sensor, leading to highly elevated ξ that are unlikely to be caused by the instrument self-heating alone.

4.2.5 Implications of the self-heating correction on CO_2 budgets

In the discussion to follow, we focus on the use of Eq. (3) in combination with Eq. (1) to apply the self-heating correction and offset the self-heating effect of the OP analyzer. With this self-heating correction for the OP, CO_2 fluxes are shifted towards smaller negative and higher positive fluxes. Formerly predominantly negative wintertime CO_2 fluxes now show a distinct positive mean value (Figure 21 a and b). In summer, the CO_2 loss is increased and therefore the net uptake is reduced. Results corrected for the self-heating are much closer to the reference CP fluxes (Figure 21 a and b) than results without the application of this additional correction.

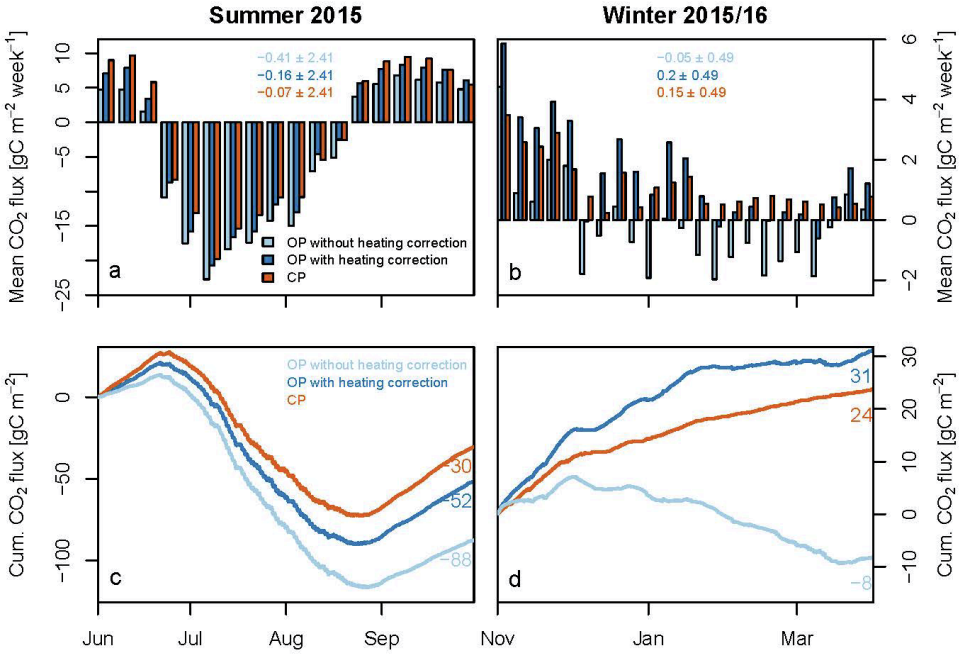

Figure 21: Weekly averaged fluxes (a and b) with mean flux rates (top center as mean ± standard deviation [µmol m^{-2} s^{-1}]) and cumulative budgets (c and d) with seasonal budgets (as [gC m^{-2}], with number representing seasonal budgets for both GA with corresponding color coding). Left panels give results for the summer season 2015 (June–October) and the right panels for the following winter 2015/16 (November–April). Note that axes for summer and winter are different due to systematically different flux rates for each season.

Still, systematic discrepancies remain within individual seasons, e.g. in winter some of the weekly mean flux rates remain close to zero or in the negative range, even though absolute values are small. Overall, the best fit of the self-heating correction overcorrects OP fluxes during winter, and undercorrects them in summer (see intercepts in Table 7 and cumulative CO_2 budgets in Figure 21 c and d). The residuals between corrected OP and CP reference (summer: -22 gC m^{-2}; winter: 7 gC m^{-2}) partly balance each other over the course of the year, resulting in annual CO_2 budgets in close agreement with the CP references (see Figure 16 a).

4.3 RESULTS ON THE HEATING OF SONIC ANEMOMETER

4.3.1 Heating scheme and icing events

The scheme based on meteorological conditions (rH and T_a) to control the activation of the sonic anemometer heating worked as planned for the tower with active heating and was always switched on when corresponding meteorological threshold conditions were reached. In total 1365 and 849 half-hour intervals with active heating for winter 2013/14 and winter 2015 as well as 6387 and 4449 half-hour intervals without heating for winter 2013/14 and winter 2015, respectively, are observed (Figure 22 a and b). Air temperature during both winter periods is almost always under 1 °C, therefore rH is the driving parameter for controlling the sensor heating. Monthly means for rH, averaged over both winter seasons, are highest during Oct, Nov and Dec (82 %). Accordingly, periods with active heating occur more often during winter 2013/14 covering October, November, December with most humid conditions and active heating for 26–33 % of the time. An exception is April 2015 with large fluctuations in rH, resulting in an overall low mean but activated heating around nearly one quarter of the time.

During the first winter period (2013/14), continuous error messages were observed at both towers more or less simultaneously in January 2014 (Figure 22 a). During this time, air temperatures dropped mostly below -40 °C, i.e. outside of the measuring range of the sonic anemometer, thus it cannot be determined if low

temperatures or icing of the sensor was triggering these error messages. Therefore the period of January 2014 was excluded and the focus was set to December 2013.

All documented icing events occur under inactive heating before, during or after the event. Following the icing event, ice was either removed manually by the site technician after the detection or may have disappeared due to sublimation. This can alter the residence time and might cause differences in the icing event length between towers, shorten icing events even if conditions would continue to promote icing or lead to icing at individual towers.

In mid-December 2013 (Figure 22 c), sustained high frequency (around 36000 error messages per half hour) of error messages were observed at the unheated tower, indicating icing of the sensor over duration of several hours. For the same period, at the heated tower error messages are scattered and small (<550 error messages per half hour). This demonstrates that icing has been prevented by the sonic anemometer heating while without this heating ice could build up and disturb instrument performance. We assume that the icing at the unheated tower was eventually removed manually by the site technician, since it appeared only for a very short time period, while meteorological conditions did not change substantially during this event.

In the second winter period (2015) both towers showed high error message counts independently from each other. The icing in both cases lasted for a more extensive period (2–3 days) for both the heated and unheated tower, respectively (Figure 22 d). The second ice buildup during the second winter period (2015) only occurred at the unheated tower in mid-February. The previous discontinuous heating at the heated tower switched off 3 hours before the ice buildup started at the unheated tower. We assume that the heating prevented the initial stages of ice buildup at the heated tower, so even though the heating was not running at the time the ice finally closed around the unheated sensor, it can be assumed that the active heating made the difference in this case.

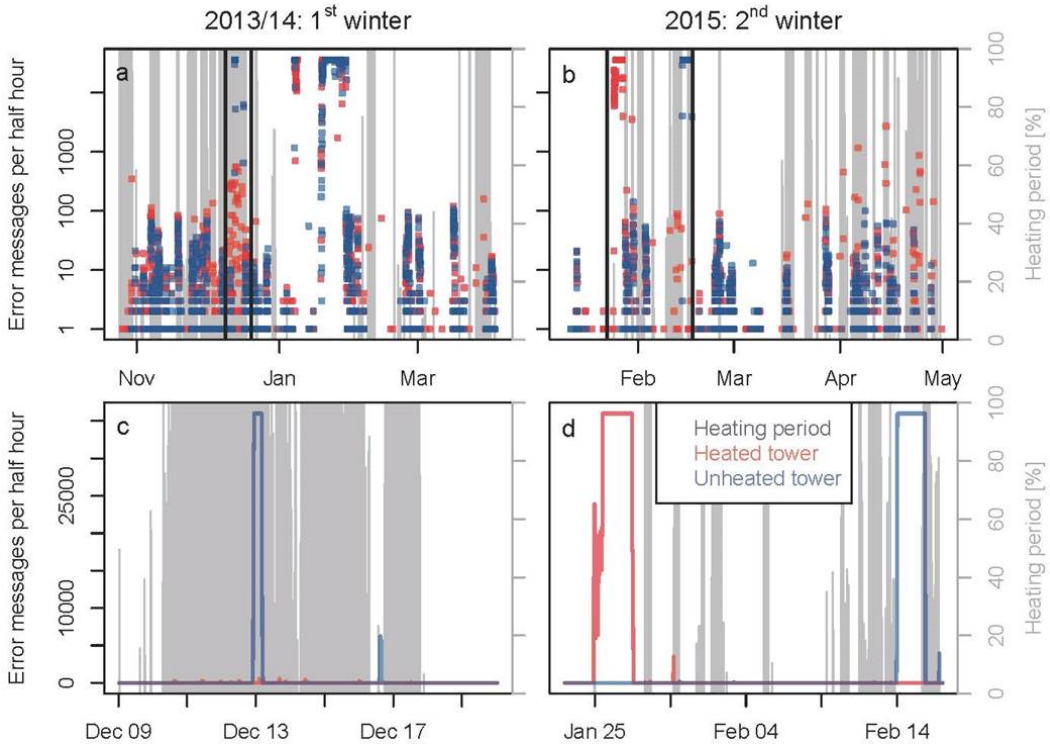

Figure 22: Active heating periods and recorded error messages from the sonic anemometer during both winter seasons. Lower panels (c and d) focus on a more detailed period that is marked with black bars in the top panel (note changes of the y-axis from logarithmic to linear scale from the top to the lower panel).

4.3.2 Heating effect on sensible heat and momentum fluxes

With sensor heating deactivated, T_a measured by the sonic anemometers and the ancillary instrumentation at the same tower agree well (Figure 23 c and d). Positive offsets between sonic anemometer and ancillary sensor in both observation periods indicate that T_a measured by the ancillary sensor gives slightly lower values, which is likely to be caused by instrument calibration effects. Differences in mean T_a averaged for both towers are close to zero with 0.2 °C and -0.3 °C for the first and second winter period, respectively (Figure 24 c and d).

With activated heating, there is a systematic shift in T_a measured by the heated sonic anemometer in comparison to the unheated sonic anemometer (Figure 24 a and b) as well as to the ancillary sensor (Figure 23 a and b). The T_a difference between heated and unheated sonic anemometer increased slightly over

time (first winter: -1.5 K; second winter: -1.9 K), resulting in a mean T_a reduction of approximately -1.75 K as a consequence of sensor heating.

Differences in the sensible heat flux between both EC systems during inactive heating periods are close to zero, with median values of -2.9 and 1.6 W m^{-2} (Figure 24 c and d), for the first and second winter period, respectively. With active heating, sensible heat fluxes tend to increase, with mean offsets of 5.8 and 4.5 W m^{-2}, for the first and second winter period, respectively. Overall, across towers and data years we found an increase in sensible heat fluxes of 6 W m^{-2} with active heating (Figure 24 a and b).

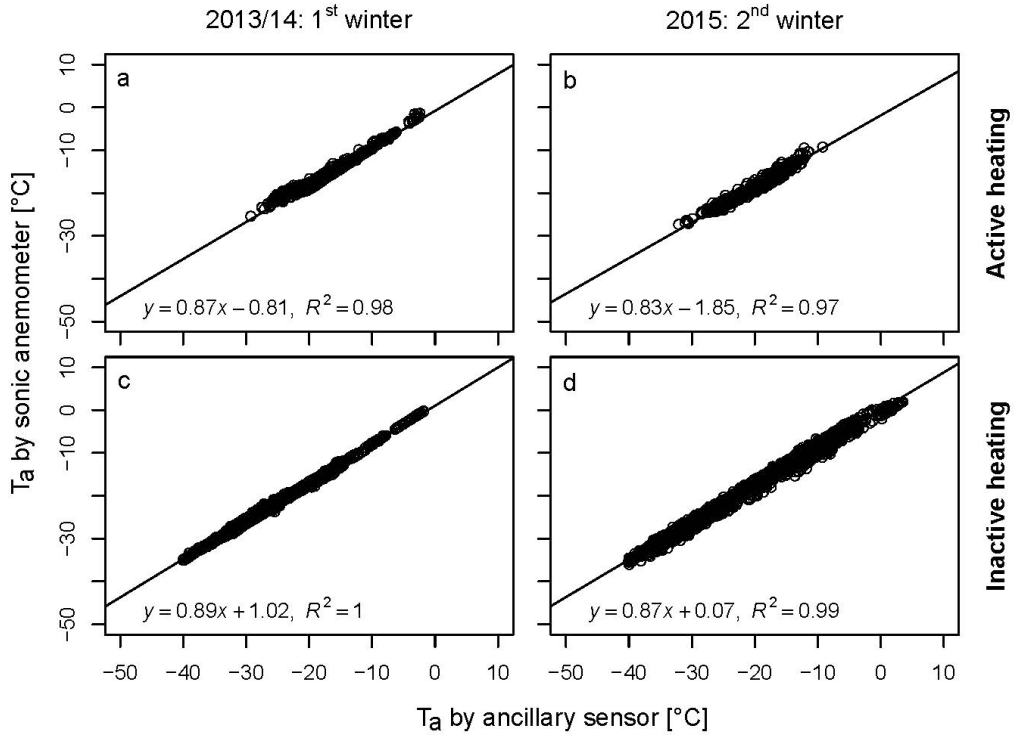

Figure 23: Comparison of air temperature retrieved from different sensors during both winter seasons with distinction between active and inactive heating periods. Statistical coefficients based on a standard least squares regression (black line) are given at the bottom of each panel.

Since double axis rotation is applied within the flux-processing sequence, implications of the sonic anemometer heating on the fluctuations of the vertical wind component can only be investigated by analyzing the variance of the w-signal ($\sigma^2(w)$). Negligible differences between both tower systems are observed in $\sigma^2(w)$ both with (0.002 and 0 m s^{-1}) and without (0.002 and -0.002 m s^{-1}) active heating at one of the towers (Figure 24). Consequently only minor

differences of sonic anemometer heating can be found also for the friction velocity with active heating (0.02 and -0.01 m s^{-1}) in comparison to unheated (0.01 and -0.02 m s^{-1}) conditions.

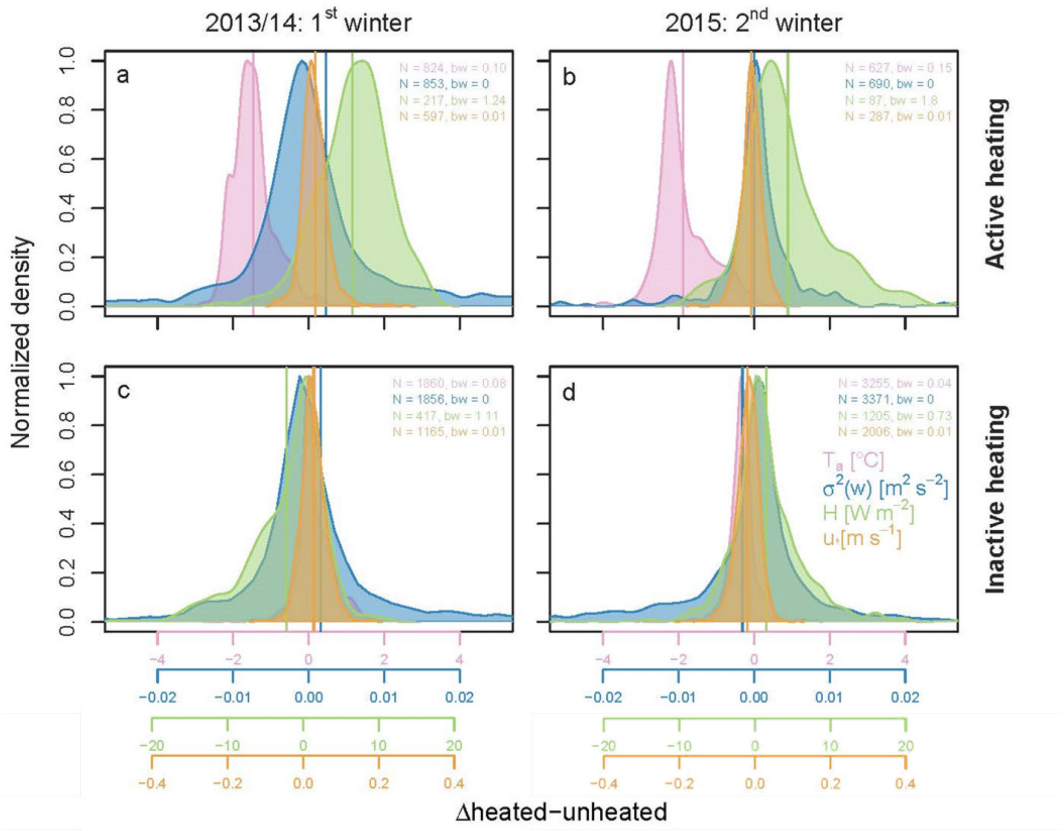

Figure 24: Comparison of differences of air temperature (T_a, purple), variance of the vertical wind speed ($\sigma^2(w)$, blue), sensible heat flux (H, green) and friction velocity (u_*, orange) retrieved from the sonic anemometer for both winter periods (a and c for the first winter season and b and d for the second winter season) between heated (a and b) and unheated (c and d) conditions. Total number of data (N) and bandwidth (bw) of the kernel density estimation for each variable and heating-case are given in corresponding colors in each sub-plot. Note that each variable has its own color-corresponding x-axis and that ranges between x-axes differ. Densities were normalized by their range. Vertical lines indicate means.

4.3.3 Heating effect on CO_2 fluxes

Carbon dioxide flux measurements based on the CP gas analyzing system are not affected by the sonic anemometer heating, i.e. mean CO_2 flux offsets between both towers with (-1.6x10^{-2} µmol m^{-2} s^{-1}) and without (-4.1x10^{-3} µmol m^{-2} s^{-1}) heating one of the instruments do not differ systematically (Figure 25). On the other hand, computing fluxes based on the OP gas analyzing system we observe a more pronounced sonic anemometer heating effect systematically shifting the offsets in mean CO_2 flux rates between both towers (active: 9.4x10^{-2} µmol m^{-2} s^{-1};

inactive: -0.14 µmol m^{-2} s^{-1}; Figure 25). Assuming continuous operation of the sonic anemometer heating, this mean increase in CO_2 fluxes of 0.23 µmol m^{-2} s^{-1} would sum up to an additional 36 gC m^{-2} in wintertime efflux over the entire winter season (November–March).

The fact that systematic shifts in fluxes were only observed when calculating fluxes based on OP data suggests an indirect heating effect that can be attributed to the WPL density-flux correction (Webb et al., 1980). This correction, which has to be applied for OP gas analyzers only, includes air temperature and sensible heat flux as input data. Accordingly, biases in those will indirectly influence density-corrected OP CO_2 fluxes via this correction. In a sensitivity study, we found that the net bias was almost exclusively caused by offsets in sensible heat fluxes, while systematic shifts in the air temperature caused negligible net effects in the CO_2 fluxes.

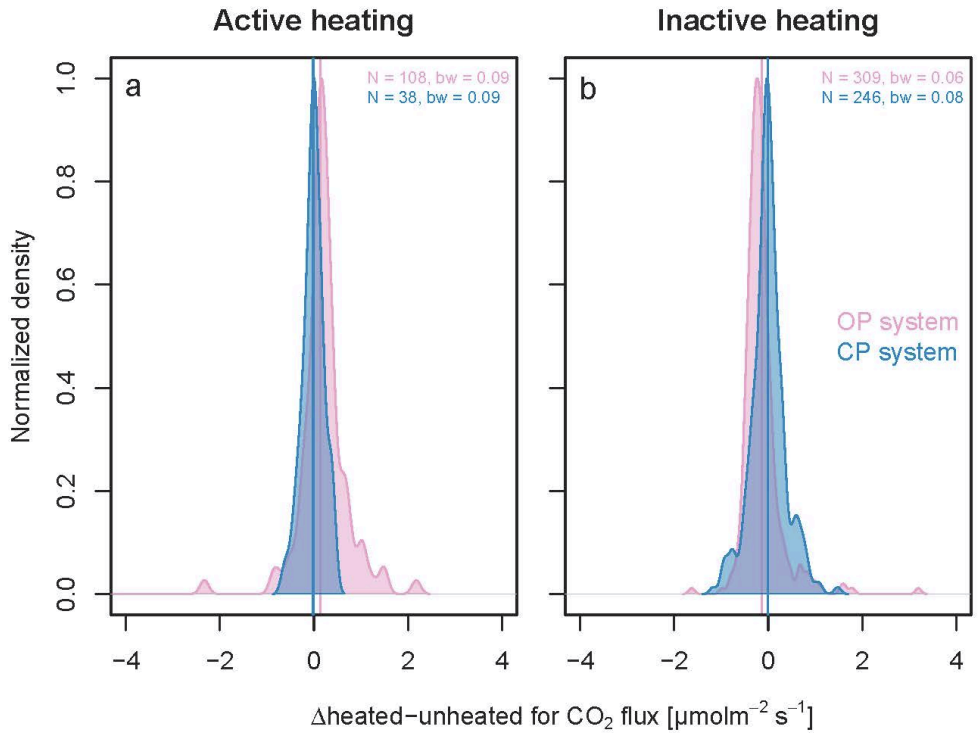

Figure 25: Comparison of NEE differences from the OP (purple, representing the first winter season 2013/14) and CP (blue, representing the second winter season 2015) between heated (a) and unheated (b) conditions. Total number of data (N) and bandwidth (bw) of the kernel density estimation for each variable are given in corresponding colors in each sub-plot.

4.4 DISCUSSION

4.4.1 Self-heating of the open-path LI7500 sensor

The apparent enhancement in net uptake of CO_2 with 92 gC m^{-2} as measured by the OP is likely to be caused by the self-heating of the instrument linked to the additional heat flux within parts of the optical path disturbing the measurements (2006a; Burba et al., 2006b; 2008). Järvi et al. (2009) determined a 140 gC m^{-2} difference between an OP and CP during roughly 2 months (Oct–Dec) for a beech forest site in Finland. However, their data were not gap filled, and the study time frame is very short in comparison to the data presented here. If no reference measurements are present, the potential uptake that may be caused by self-heating of the sensor can be estimated by comparing flux differences between the OP sensor with and without the self-heating correction. Based on this concept, existing studies found differences of 20 gC m^{-2} (Barrow, Ueyama et al., 2012) and 87 gC m^{-2} (Atqasuk, Oechel et al., 2014) per year at two Alaskan sites representing similar environmental conditions as our sites near Chersky. Reverter et al. (2011) identified a linear fit between mean annual temperatures and the net effect of the self-heating correction, where the correction effect was clearly elevated at sites situated in cold regions. Applying their suggested approach with a mean temperature of -11 °C found in Chersky (see Table 5) suggests a reduction of the CO_2 uptake of 240 gC m^{-2} through application of the self-heating correction. This apparent over-correction can be explained by the fact that environmental conditions in Chersky (e.g., annual mean temperature and ecosystem type) are far outside the range analyzed by Reverter et al. (2011). Accordingly, our findings indicate the linear fit between magnitude of the self-heating correction and prevalent temperature cannot be applied across a broad temperature range, and that instead non-linear elements need to be included when extending the approach by Reverter et al. (2011) to the Arctic domain.

The greatest impact of the self-heating is expected during winter with lowest air temperatures and hence relative highest contribution of the heating effect to the total sensible heat fluxes (Burba et al., 2008; Grelle and Burba, 2007). This theory is supported by some existing studies that achieved a good agreement between OP

and reference measurements during the growing season (Goodrich et al., 2016). However, other references demonstrate that the self-heating effect is not only affecting fluxes during the cold season, but corrections for sensor self-heating have to be applied to warm season measurements as well (Järvi et al., 2009; Ueyama et al., 2012), with different magnitudes in the heating effect (Reverter et al., 2011). Oechel et al. (2014) found similar seasonal patterns as observed in the presented study, i.e. with high impact of self-heating during both summer and winter seasons, while spring and fall provide just minor contributions to offsets in cumulative flux budgets.

Taking into account the differences in T_s parameterizations between day- and night-time (e.g., Eq. 3), we decided to separately fit the ξ fractions for day- and night-time conditions. With this separation, different linear relationships between CO_2 fluxes from the OP and the CP can be observed, with a closer agreement during night-time. This is also reflected by some instrument surface temperature estimations with systematically higher offsets during day-time, indicating a stronger heating effect. Radiative heating over the day and radiative cooling during the night can affect measurements and this effect might be increased under non-vertical OP sensor configurations (Burba et al., 2008) as it is used in this study. This has implication on the fitted ξ that are a magnitude smaller under night-time conditions, compared to the daytime fits. Since our study site is situated in the Arctic, this difference leads to a ξ fraction seasonality in the overall self-heating correction, because the fractions of day- and night-time vary strongly between summer and winter seasons, respectively.

For all self-heating correction approaches a strong dependency of ξ on the instrument surface temperature was demonstrated.

1. Equation (2) represents the simplest approach, i.e. without differentiation for day- and night-time conditions. Burba et al. (2006b) derived the equation from climate-chamber measurements that may not reflect natural conditions. Moreover, the sensor was installed in a fully vertical position, not accounting for inclination. Consequently, this simple method shows discrepancies, mostly during winter.

2. In case of Eq. (3), negligible differences in cumulative CO_2 fluxes in comparison to the CP are observed, even though the equation follows a similar structure than Eq. (2). The main difference is that Eq. (3) was tested under field conditions. For another study this method with an empirically determined ξ of 0.05 yielded reasonable results (Rogiers et al., 2008). During night-time, absolute values of ξ fits from the presented study agree with this finding, but under daytime conditions the value is 3-times higher. This difference may be explained by the overall colder temperatures in Chersky, which imply a higher contribution of the self-heating.
3. While the apparent uptake during the Arctic winter is not corrected properly by using Eq. (4), the fitted ξ for daytime is comparable to the one for the Finnish beech forest (Järvi et al., 2009), achieving a good agreement with the reference measurements during the non-winter season. Still, the overall fit of the annual correction is poor within the context of our study.
4. Results for the corrected OP fluxes are close to the CP reference when parameterizing T_s with Eq. (5). However, this approach is impaired by its complex structure, dividing the sensor into different sensor elements, and additionally separating day- and night-time conditions. Moreover, with a lacking definition how to combine these elements into a final parameterization scheme, the good agreement found in this study might be coincidental, and a general applicability might not be given.

In general, both, the instrument surface temperature estimation and the fitted ξ are closely linked, and it is important to use related values in the context of the self-heating correction to avoid additional uncertainties. Thus, further experiments with direct measurements of instrument surface temperature under natural conditions with different instrument configurations are necessary to improve the performance of estimates and reduce uncertainties. Furthermore, we found evidence that self-heating correction in general is influenced by flow patterns indicating that the method is subject to methodological uncertainties that need further investigations.

4.4.2 Heating of sonic anemometer

Our results demonstrate that the chosen heating scheme can prevent ordinary ice buildup under expected meteorological conditions, and in this way can reduce the power consumptions considerable below that of a continuous or intermittent heating strategy (Goodrich et al., 2016). Still, there are special meteorological conditions, not being captured with this regular heating scheme, that can cause ice buildup and disturb measurements. We hypothesize that the ice buildup event which occurred at the heated tower in late January 2015 might have been caused by icing fog introducing riming. Consequently, the riming should also appear at the unheated tower because of very similar meteorological conditions between towers but might have been removed manually before major buildup started. Under this special meteorological situation, ice buildup cannot be anticipated by an activation scheme based on ancillary meteorological conditions. Accordingly, any such scheme to prevent sensor icing must fail.

In both existing studies focusing on the effect of sonic anemometer heating, continuous heating was found to increase the apparent sensible heat flux (Goodrich et al., 2016; Skelly et al., 2002), but a uniform explanation for this effect was not provided. Findings from this study suggest that temperature measurements from the heated sonic anemometer are the driving element for the observed differences in sensible heat fluxes while the wind components only show a minor influence. The most likely explanation of the observed differences in T_a with activated heating is an instrumental issue related to biases in sonic pathway length, i.e. heating of arms and transducers influences signal runtimes between the transducers. With an observed reduction in T_a the path length is increased and that effect might be amplified under very cold environmental conditions.

Since no direct heating effect on the variability of the vertical wind speed and the resulting friction velocity was observed, it is also not expected to find a direct heating effect on the determined CO_2 mixing ratios and fluctuations. This assumption is confirmed by the finding that the activated heating does not lead to a shift in CO_2 fluxes based on the CP gas analyzing system. However, systematic

indirect effects can occur when observations from a heated sonic anemometer (sonic temperature, sensible heat flux) are used as input for the WPL density-flux correction of OP flux measurements. In this context, shifts in sensible heat fluxes were found to be the major driver for a biased WPL-correction when sonic anemometer heating is activated. The sonic anemometer heating holds the potential to significantly alter the seasonal CO_2 budget indirectly through biasing the WPL density-flux correction. The mean bias in CO_2 fluxes with active heating is a magnitude larger than the overestimation reported by Goodrich et al. (2016) with -0.03 μmol m^{-2} s^{-1}. The mean bias was found to be caused by a higher variance in the vertical wind component having a direct effect on the determined fluxes of CO_2 with a CP and the same type of sonic anemometer as used in this study (Goodrich et al., 2016).

4.4.3 Relevance of wintertime CO_2 budgets

Correcting the self-heating of the open-path LI7500 gas analyzer, and accounting for potential biases linked to the active heating of the sonic anemometer, both are essential elements in the eddy-covariance flux processing protocol to obtain high quality budgets of CO_2 fluxes during Arctic winter. At the site close to the city of Chersky that has been investigated in the context of this study, appropriately corrected wintertime emissions amount to about 25 gC m^{-2}. These net emissions are comparatively low compared to the substantial net releases of CO_2 during wintertime which have been reported across different Arctic permafrost ecosystems like wet sedge (115 gC m^{-2}), heath (99 gC m^{-2}, both Euskirchen et al., 2012) , or forest tundra (89 gC m^{-2}, Zimov et al., 1996), all representing 3 years of measurements covering a period from September–April/May. Assuming a temperature dependence of winter CO_2 flux as suggested by e.g. Zimov et al. (1996), shorter study time frames focusing on e.g. just the core winter period might lead to smaller winter effluxes. Such results were presented e.g. by Oechel et al. (2014) with 12 gC m^{-2} covering a period from October to April for a moist acidic tundra, or Lüers et al. (2014) with 6 gC m^{-2} during November to April for a semi-desert ecosystem. Given that the largest portion of wintertime CO_2 emissions observed at our site near Chersky can be attributed to the fall shoulder season and the transition into early winter, our

observations generally agree with these findings, but also indicate slightly higher efflux also at the peak of polar winter than found at both of the other sites with continuous permafrost (Lüers et al., 2014; Oechel et al., 1997)

4.5 CONCLUSIONS

In this study, we investigated the impact of different set-up options and instrument configurations on the data quality of wintertime EC CO_2 fluxes under cold conditions in the Arctic. The first part focused on the correction of the self-heating effect of the open-path gas analyzer, while the second part deals with the effect of the sonic anemometer heating on the determined scalars and fluxes. Based on three winter seasons of continuous eddy-covariance measurements from a site close to the city of Chersky, we developed the following measures to avoid biases of instrument LI-7500 self-heating and controlled sonic anemometer heating on flux data quality:

1. A self-heating correction for CO_2 flux time series based on the LI-7500 gas analyzer is essential to avoid systematic biases in long-term budgets. For an inclined sensor setup, only a small percentage of the correction proposed by Burba et al. (2006b) needs to be applied (for our setup ca. 7–13 %).
2. Strongest self-heating biases in LI-7500 flux data were found not only in winter but also during the summer, while shoulder seasons were largely unaffected. Accordingly, self-heating correction not only needs to be applied for cold-season observations, but is also essential for summertime flux time series. Therefore a year-round application of self-heating correction is necessary to avoid systematic bias on annual flux budgets.
3. Sonic anemometer heating affects measurements of sonic temperature and sensible heat fluxes, but no direct effect on the variability of the vertical wind speed and the resulting friction velocity was observed. Accordingly, scalar fluxes based on a CP gas analyzer are unaffected by sonic anemometer heating, and longer heating periods are likely to have a positive effect on the data quality of these fluxes. For OP sensors (see item

4.) below), a shorter but recurring application of heat pulses to avoid icing of the sensor may prove beneficial for eddy-covariance flux data quality in cold climates, particularly if icing fog events can occur.

4. A small but systematic indirect bias of sonic anemometer heating on CO_2 flux data occurs through the application of a density-flux correction (e.g. WPL correction) for open-path analyzers, since this correction scales with the sensible heat flux, which is biased when the heating is activated. No such effect could be observed for flux time series obtained from closed-path instruments.

Based on our analyses at the Chersky site, we recommend a heating scheme for Arctic conditions that is not controlled by meteorological conditions, but instead either is activated at regular intervals independent of prevailing weather conditions, or use extended heating periods up to permanent heating. For the first option possible solutions might be to activate the sonic anemometer heating for an hour per day in staggered cycles to avoid preferentially exclusion of a specific period while removing potential icing to guarantee high quality measurements. However, a strong disturbance of the observed turbulent fluxes takes place during activation/deactivation periods of the sonic anemometer heating, so these transition periods need to be flagged as lowest data quality, and discarded from further flux data analysis. For EC systems employing CP gas analyzers, our findings indicate that there is no negative effect of sonic anemometer heating on the CO_2 flux. If an OP system is used, CO_2 fluxes should be treated with caution due to the indirect heating effect of the sonic anemometer. Accordingly, to avoid systematic biases in the OP CO_2 budget, either an alternative data source for the sensible heat flux (e.g. ancillary instrumentation, or gap-filling) needs to be used as input for the WPL correction, or a suitable correction procedure to minimize the systematic offsets in sensible heat fluxes during sonic anemometer heating periods should be applied.

5 YEAR-ROUND EDDY-COVARIANCE MEASUREMENTS COMBINING CARBON DIOXIDE AND METHANE FLUXES FROM A PERMAFROST ECOSYSTEM

5.1 INTRODUCTION

As summarized in Sect. 1.3.3, the understanding of Arctic carbon flux budgets is significantly hampered by the limited database of year-round observations. Particularly for CH_4 fluxes, only very few continuous flux time series for the non-growing season have been published, and also for CO_2 year-round observations are compromised by very high percentages of data gaps during the harsh polar winter conditions. Therefore, a comprehensive assessment of sustained drainage on year-round Arctic carbon budgets is not available to date. To improve this situation, and advance the understanding of carbon exchange between surface and atmosphere in Arctic permafrost ecosystems, seasonal flux patterns and annual budgets of CO_2 and CH_4 of two eddy-covariance towers running in parallel over a disturbed tundra ecosystem and a control tundra ecosystem representing natural conditions, respectively, are presented. The analyses compare datasets covering over 3 years of continuous measurements in combination with ancillary data to analyze the driver of the interannual variability.

5.2 RESULTS ON SEASONAL CONTRIBUTION

The growing season is dominating the annual cycle with both highest flux rates and cumulative budgets (Table 8). Net CO_2 uptake by the ecosystem (negative flux rates) only occurs around peak growing season when vegetation uptake outweighs respirational losses, while during the remaining parts of the year

net CO_2 emissions (positive flux rates) dominate (Figure 26 a). Highest CH_4 emission rates during the growing season are triggered by increased production rates linked to high soil temperatures, and efficient plant-mediated transport rates through a higher abundance of aerenchymatous plants

Table 8: Mean flux rates and cumulative flux budgets (both as mean ± sd) for each season (with mean length [days]) at the control site.

	CO_2		CH_4	
Season	mean [µmol m^{-2} s^{-1}]	cum. [gC m^{-2}]	mean [nmol m^{-2} s^{-1}]	cum. [gC m^{-2}]
Spring [38]	0.12 ± 0.31	5 ± 3	2.32 ± 5.01	0.1 ± 0.0
Growing [126]	-0.66 ± 2.65	-87 ± 19	40.04 ± 26.67	5.3 ± 0.7
Fall [71]	0.42 ± 0.49	30 ± 9	15.6 ± 12.62	1.2 ± 0.4
Winter [134]	0.05 ± 0.35	7 ± 0.6	2.86 ± 7.43	0.4 ± 0.0

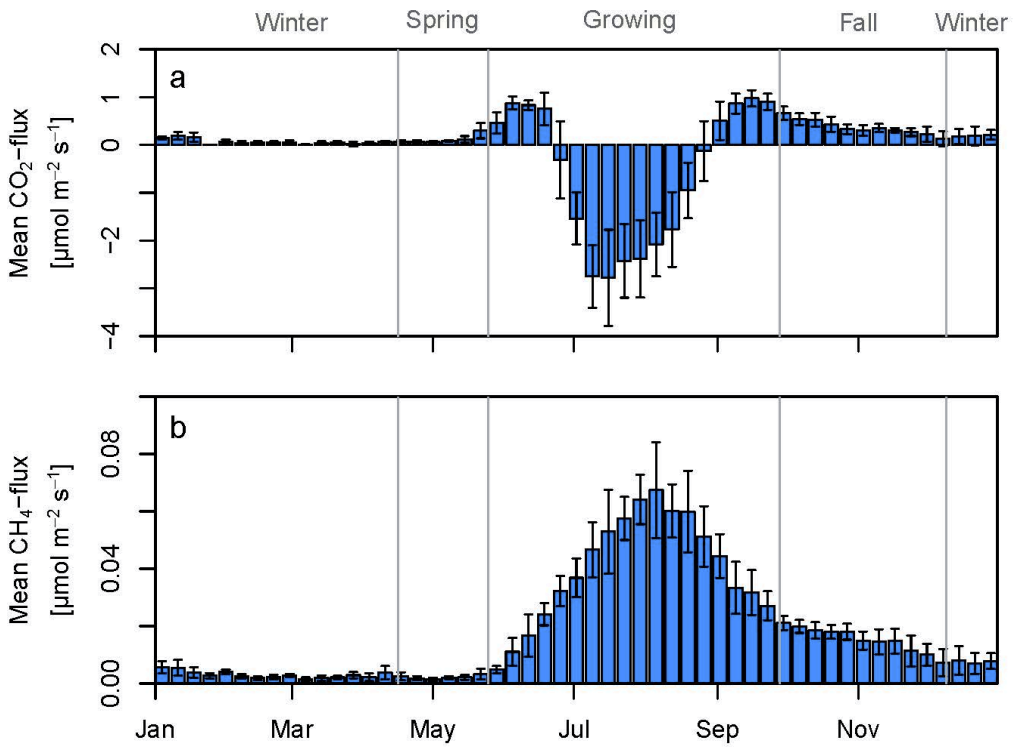

Figure 26: Averaged annual cycle as weekly means (colored bars) and standard deviation (error bars) for CO_2 (a) and CH_4 (b) at the control site.

In fall, during the zero-curtain period, flux rates remain at comparably high levels, with substantial net emissions for both CO_2 and CH_4 (Figure 26 and Table

8). Accordingly, this period adds major contributions to the net annual flux budgets, respiring ~ 35 % of the summertime CO_2 uptake, and adding another ~ 23 % to the growing season budget of CH_4. Emissions continue further into the winter (Figure 26 and Table 8) but average flux rates are minor compared to fall. Still, because of the length of this season with on average 134 days, these small wintertime emissions sum up to a notable wintertime contribution to the annual budget. In total, all non-growing seasons combined systematically impact the annual budget, emitting 50 % of the growing season CO_2 uptake and adding 32 % to the growing season budget CH_4 emissions.

5.3 RESULTS ON DRAINAGE IMPACT ON ANNUAL CARBON BUDGETS

5.3.1 Cumulative CO_2 and CH_4 fluxes

Including interpolated sections, our dataset covers continuous eddy-covariance observations with 4 years of CO_2 fluxes and 3 years of CH_4 fluxes (Figure 27). Cumulative budgets demonstrate that, in each data year, drainage has systematically altered the carbon fluxes of this Arctic floodplain ecosystem. The mean annual CO_2 budget (Figure 27 a) at the drained site sums up to 6 ± 19 gC m^{-2} averaged for the data years 2013–2016, while at the control site this multi-year average amounts to -44 ± 15 gC m^{-2}. The mean reductions of the annual sink strength following the drainage disturbance is 51 ± 11 gC m^{-2}, with annual differences ranging between 38 gC m^{-2} in 2014 and 66 gC m^{-2} in 2015. Partitioning of the net CO_2 fluxes during the growing season (Figure 28) reveals that minor increases in GPP following drainage are outweighed by dominating higher respiration losses. Accordingly, the drained site shows the tendency towards reduced net uptake.

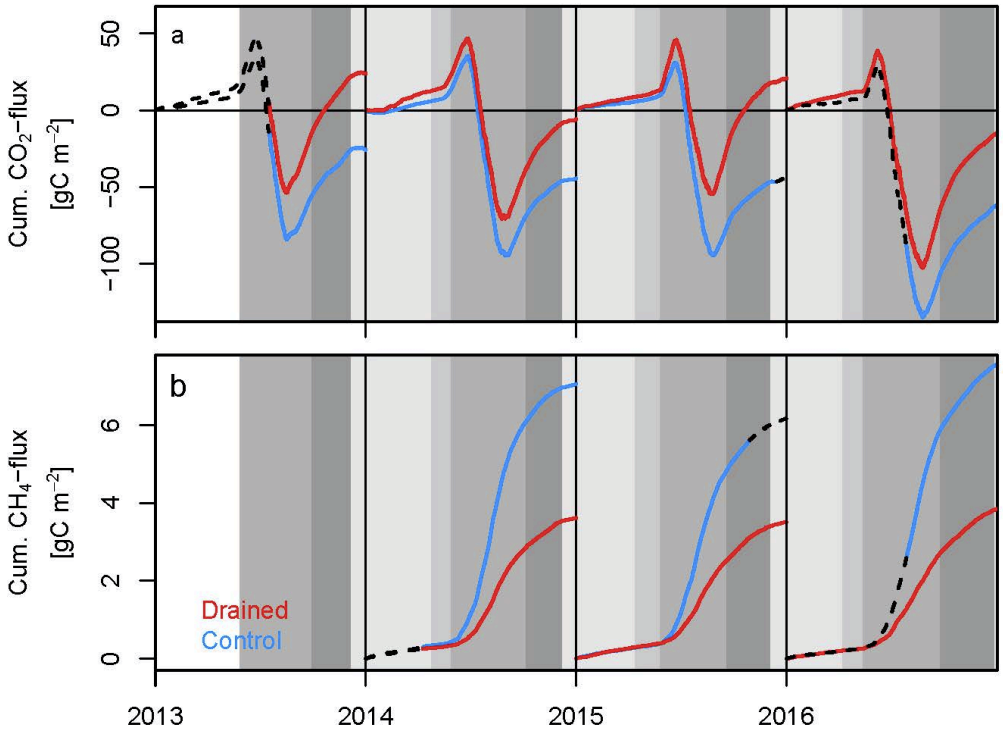

Figure 27: Cumulative budget for CO_2 (a) and CH_4 (b) from drained (red) and control (blue) ecosystems were calculated separately for each data year. Long gaps (black dashed lines) were filled using mean annual cycle trends. Background color shading indicates the seasons from winter (lightgrey) to fall (darkgrey).

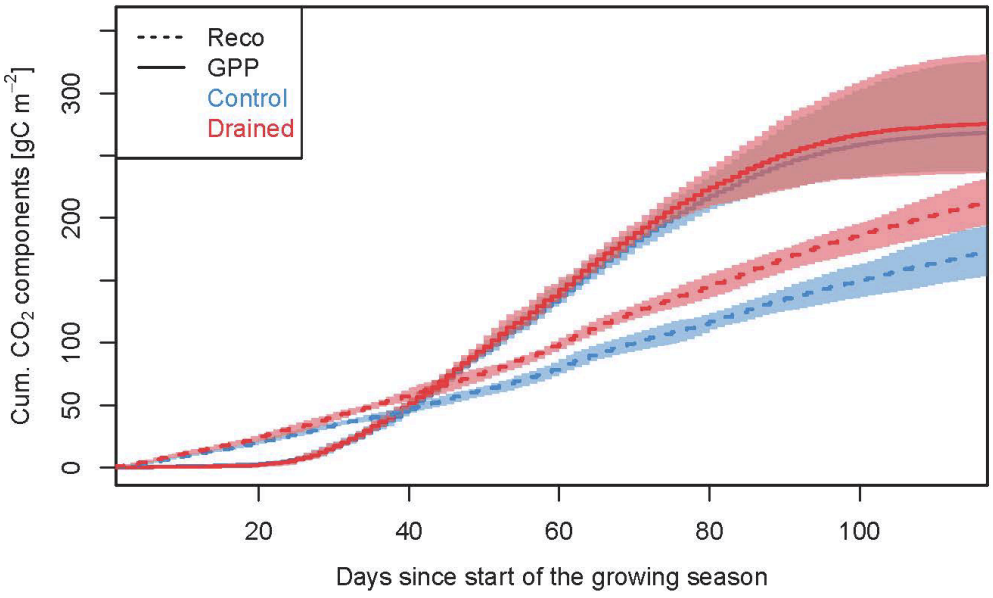

Figure 28: Cumulative CO_2 flux components as photosynthetic uptake (GPP, continuous lines) and respiration losses (Reco, dashed lines) at the drained (red) and control (blue) ecosystem. Lines give the mean values and the shaded area represents the range from minimum to maximum. Data are restricted to the growing season

CH_4 flux rates at the control site continuously exceed emissions at the drained site representing drier and therefore more aerobic conditions (Figure 27 b). Cumulative annual CH_4 budgets are 3.7 ± 0.2 gC m^{-2} (drained) and 7.0 ± 0.7 gC m^{-2} (control), for the period 2014–2016. Absolute annual budget differences between drained and control ecosystems average at 3.3 gC m^{-2}, and sum up to a maximum of 3.7 gC m^{-2} in 2016.

5.3.2 Total carbon budget and global warming potential

Focusing on the two data years 2014 and 2015 where large data gaps are absent at both sites, systematic differences between drained and control site have been determined (Figure 29). For CO_2, the net emissions at the drained site (8 gC m^{-2}) and the strong negative budget at the control site (-45 gC m^{-2}) add up to a net drainage impact of 52 gC m^{-2}, i.e. this tundra site is a moderately higher source for atmospheric CO_2 (Figure 29). In contrast CH_4 emissions at the drained site (4 gC m^{-2}) are systematically lower than those at the control site (7 gC m^{-2}), yielding a net reduction in the source strength for atmospheric CH_4 of -3 gC m^{-2} (Figure 29) following drainage. At both sites, the shifts in the total carbon mass budget are dominated by the CO_2 fluxes, thus the drainage triggers a net loss of carbon (49 gC m^{-2}) to the atmosphere. The global warming potential metrics are used to converted CH_4 fluxes into $CO_{2,\,eq.}$ by a conversion factor of 34 for a 100-year integration timeframe. Based on these metrics, the pronounced additional source of CO_2 as a consequence of the drainage is to a large part balanced by reductions in CH_4 emissions, but overall the changes in the CO_2 budget still dominate the total $CO_{2,\,eq.}$ budget. Taken together, the drainage disturbance increases the source of $CO_{2,\,eq.}$ to the atmosphere by ~ 14 gC m^{-2} (Figure 29). Assuming that similar drainage effects could result from ice-wedge degradation under Arctic warming, our results therefore demonstrate a positive effect of hydrological disturbance with climate change. Considering integration timeframes longer than 100 years, the global warming potential of CH_4 would decrease, therefore through a lower relative influence of CH_4 emissions the combined $CO_{2,\,eq.}$ budgets would be higher than shown in Figure 29. Summarizing, the $CO_{2,\,eq.}$ budget at the drained site always constitutes a small source for atmospheric carbon, while at the control site, where CO_2 uptake dominate over

CH_4 emissions for longer timeframes, we see a negative effect with Arctic warming in the long term.

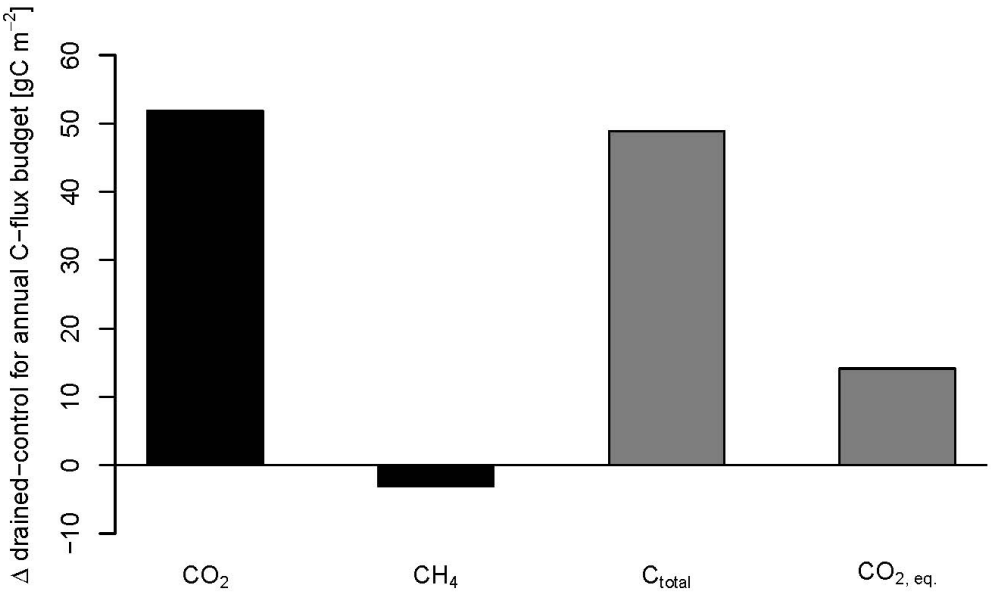

Figure 29: Carbon dioxide, methane, total carbon (C_{total} as sum of CO_2 and CH_4) and $CO_{2,\ eq.}$ by accounting for the global warming potential budget for CH_4 under a 100-year time horizon with inclusion of climate-carbon feedbacks (IPCC, 2013) average annually for the data years 2014 and 2015 as differences between drained and control site.

5.4 RESULTS ON INTERANNUAL VARIABILITY AND CONTROLLING FACTORS

5.4.1 Interannual variability of CO_2 and CH_4 fluxes

By calculating the cumulative budgets per season, we can attribute variability in net annual flux budgets to specific parts of the year (Figure 30). Our results demonstrate that flux rates in spring (Figure 30 a and f), fall (Figure 30 d and i) and winter (Figure 30 e and j) follow a uniform seasonal pattern in all data years, resulting in similar seasonal CO_2 and CH_4 budgets, independent of the prevailing environmental conditions such as e.g. snow depth, or mean wintertime temperatures. Year-to-year variability is therefore almost exclusively caused by pronounced shifts in carbon exchange processes during the growing season, where

major differences in both absolute fluxes rates and temporal patterns have been observed (Figure 30 c and h). The pronounced interannual variability during the growing season is not driven by the length of the season, which ranges between 116 days in 2015 to 134 days in 2016.

For CO_2, during the growing season a pronounced year-to-year variability is observed at both sites (Figure 30 c). In contrast, CH_4 emission rates at the drained site and in each data year are uniform, and variability can only be observed at the control site (Figure 30 h). During the growing season, the interannual variability of carbon fluxes for both, CO_2 and CH_4, is strongly pronounced in the period starting at day 61 towards the end of the growing season.

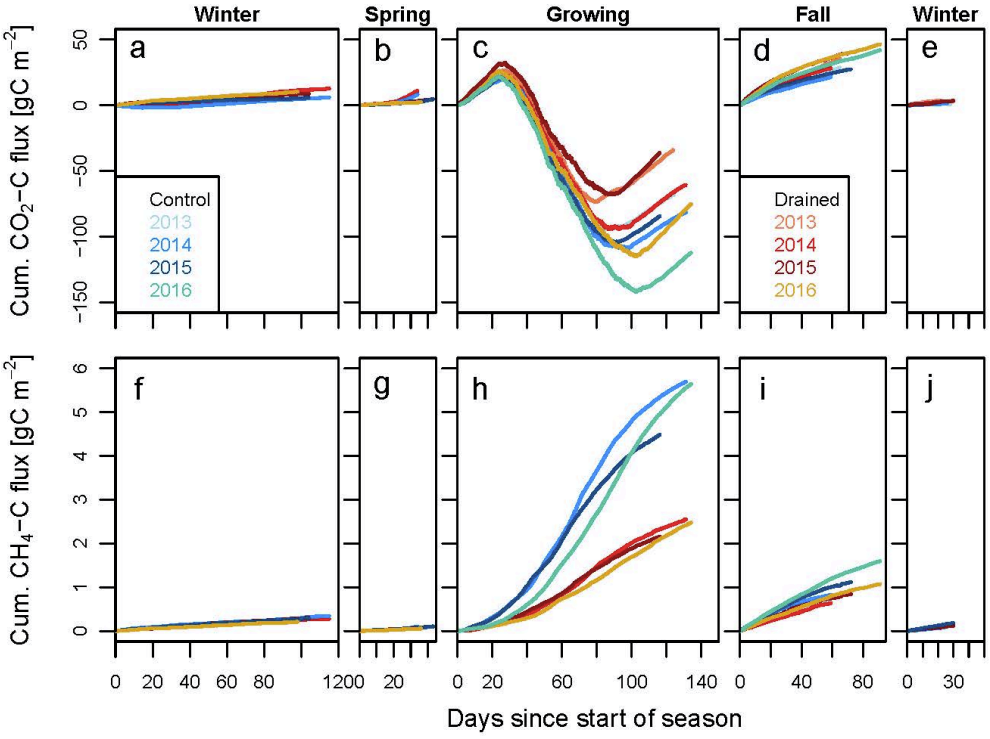

Figure 30: Cumulative CO_2 (a-e) and CH_4 (f-j) budgets Time series were separated into the four different seasons (see Sect. 2.9) and budgets were reset to zero at the beginning of each season.

5.4.2 Dominating drivers of growing season CO_2 fluxes

In the first part of the growing season (first 60 days) flux time series are rather uniform in all data years (Figure 30 c). In contrast, the year-to-year variability is very pronounced in the second part of the growing season (day 61 to end of growing season, Figure 30 c). By linking the cumulative budgets during both parts

of the growing season to mean air temperatures in the respective periods, contrasting dependencies are found accordingly. In the first part of the growing season, where no variability in CO_2 exchange was observed between data years, our findings show no correlation at all with the interannual variability in mean air temperatures (Figure 31 a). In contrast, during the second part of the growing season there is a direct linear relationship between mean air temperature and the cumulative CO_2 budget, suggesting that warmer conditions delay the senescence of the vegetation, therefore allowing high photosynthetic activity and accordingly more CO_2 uptake for a prolonged time during the growing season (Figure 31 b).

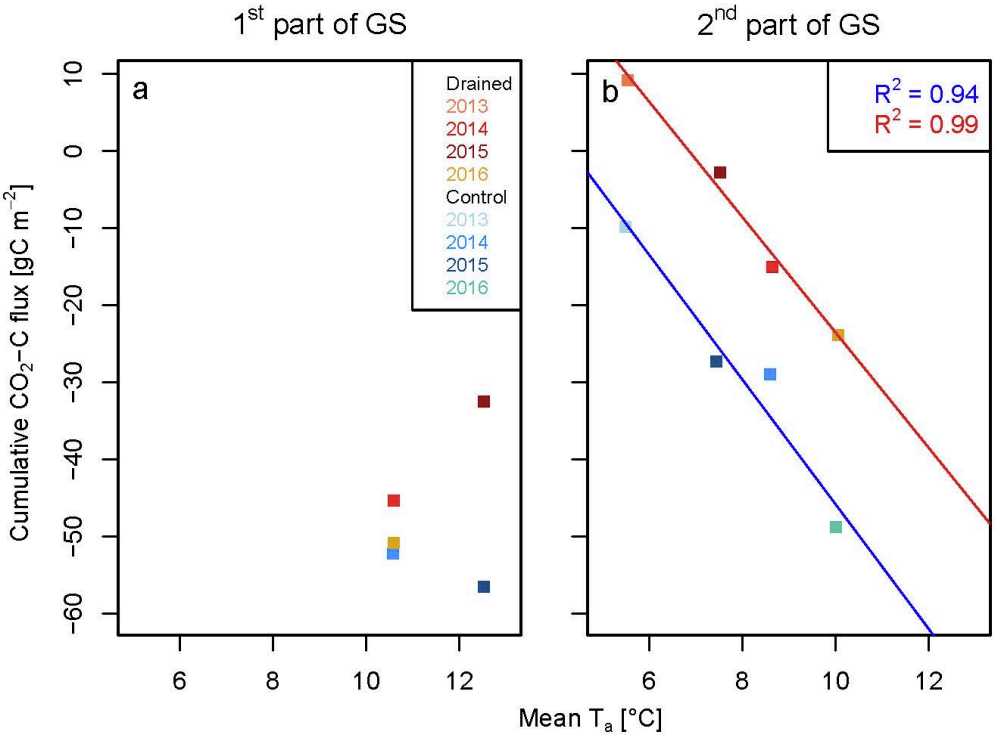

Figure 31: Cumulative CO_2 flux in relation to mean air temperature measured in 2 m height separated into first part of growing season (up to 60 days) and second part of growing season (day 60 to end of season). Lines are based on the standard least squares regression.

5.4.3 Dominating drivers of growing season CH_4 fluxes

Methane emission rates at the drained site are uniform within all data years, therefore only data from the control site with pronounced interannual variability are used for the analysis. Furthermore the data year 2016 was excluded since data are only available for the second part of the growing season (Figure 27 b). Methane emissions time series at the control site display similar characteristics as

observed for the CO_2 fluxes (see Section 5.4.2), i.e. we found uniform flux rates during the first part of the growing season (up to 60 days with ca. 2 gC m^{-2}) and a pronounced year-to year variability during the second part of the growing season (day 60 to end of the season). Emission rates during the second part of the growing season are higher in 2014 (3.6 gC m^{-2}) compared to 2015 (2.4 gC m^{-2}) with differences triggered mostly by soil temperature conditions (Figure 32) while soil moisture measurements indicate uniform conditions close to saturation in both data years. In the growing season 2014 the tendency towards higher than average soil temperatures is observed leading to increased CH_4 emissions. In contrast, during the second part of the growing season in 2015, soil temperatures are below mean resulting in reduced CH_4 emissions.

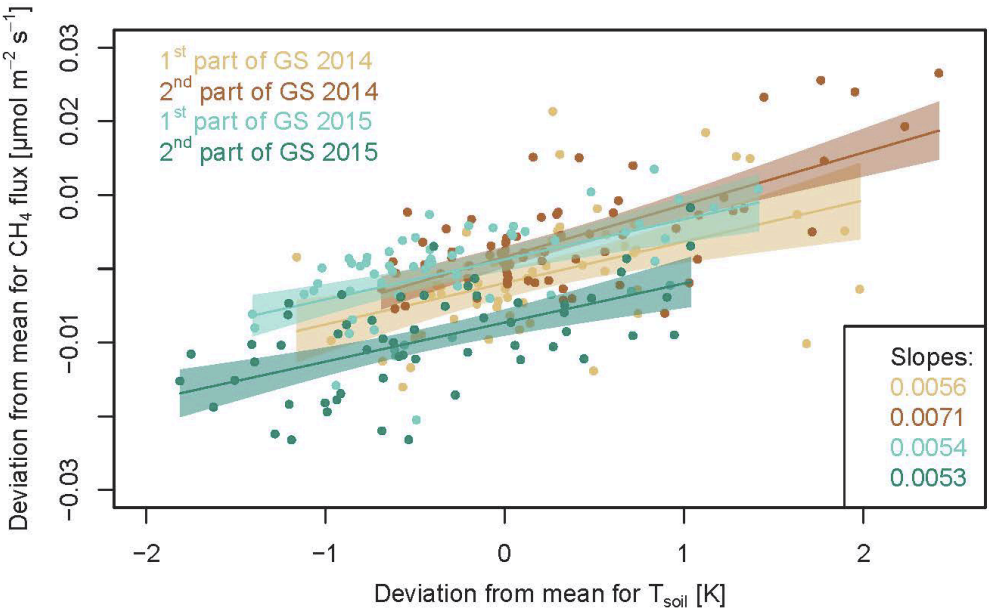

Figure 32: Deviations from mean annual cycle with daily means for CH_4 fluxes and soil temperatures (T_{soil}) in 0.08 m depth. Data are restricted to the growing season and are separated into 2 parts following Sect. 5.4.2 and Figure 31. Lines are based on the standard least squares regression with confidence intervals as shaded area.

5.5 Discussion

5.5.1 Seasonal contribution

The mean average annual CO_2 uptake of 44 gC m^{-2} at the control site corresponds with the lower range of the previously reported net uptake results for

Arctic ecosystems (Aurela et al., 2004; Aurela et al., 2007; Kutzbach et al., 2007). However, our findings differ systematically from the observations by other studies (-71 gC m^{-2} for a polygonal tundra in northern Siberia by Kutzbach et al., 2007; 14 gC m^{-2} for a moist acidic tundra in Alaska by Oechel et al., 2014) covering similar environmental conditions (e.g. mean annual air temperature or ecosystem type) as our site near Chersky. Following the growing season that typically features a pronounced CO_2 uptake (Euskirchen et al., 2016) peaking around July (Jammet et al., 2017), the fall is associated with major CO_2 losses (Kwon et al., 2016b; Laurila et al., 2001; Mikhailov et al., 2013) that result in non-negligible contributions of the fall season to the annual budget, in agreement with previous studies (Christiansen et al., 2012a; Kutzbach et al., 2007; Lüers et al., 2014; Oechel et al., 2014). Our findings confirm reports that observed cold season emissions amounted to up to 40 % of the annual budget (including spring, Kutzbach et al., 2007), while for some studies fall and winter emission even outbalanced the growing season uptake (Lüers et al., 2014; Oechel et al., 2014) Differences in the wintertime flux budgets between sites, but also between data years at single sites, can largely be attributed to interannual variability in the cold season soil temperatures, which in turn are strongly controlled by snow cover dynamics (Morgner et al., 2010; Yu et al., 2016) and latent heat effects associated with soil moisture levels. Sustained warmer conditions in soils commonly lead to higher CO2 emission rates (Webb et al., 2016).

Mean annual CH_4 emissions of 7 gC m^{-2} at the control site are lower than previously reported year-round rates within Northern wetland ecosystems. For example, Jammet et al. (2017) observed much higher mean emission rates during all seasons for a thawed fen of a subarctic peatland, while Rinne et al. (2007) observed about twice the mean annual CH_4 budget from a boreal fen. On the other hand, our contributions of winter emissions, which amount to around 6 % of the total annual emissions, are comparable with values reported by Rinne et al. (2007) and remaining differences are mainly associated with lower year-round temperatures at our site that reduce microbial activity (Lloyd and Taylor, 1994). Annual CH_4 budgets are comparable to Tagesson et al. (2012) with a similar ecosystem type even while differences in many other aspects (e.g., measurement

technique, observation period and active layer thickness) are present. Regarding the analysis of seasonal contributions, in agreement with previous studies (Jammet et al., 2017), growing season CH_4 emissions peak around August, but substantial CH_4 emissions were also observed during fall (Mastepanov et al., 2013; Wille et al., 2008). However, our datasets do not include any significant CH_4 outburst events during the freeze-up period (Mastepanov et al., 2008; Tagesson et al., 2012). Adding over 20 % to the growing season emissions, the zero curtain period in fall represents the second most important season for CH_4 emissions (Sturtevant et al., 2012). In total, cold-season emissions account for about 30 % of the annual CH_4 budget, which is a substantial fraction, but less than reported by Zona et al. (2016) that reported a strong dependency of emission rates on the duration and depth of the unfrozen soil.

Summarizing, our datasets emphasize the elevated importance of high-quality year-round observations to produce reliable carbon flux budgets for Arctic ecosystems. Neglecting fluxes outside the growing season, i.e. following previous suggestions that flux exchange between Arctic ecosystems and the atmosphere is negligible once the soil starts freezing up and a closed snow cover has developed, would lead to an overestimation of the CO_2 sink by about 50 %, and an underestimation of the CH_4 source by about 30 %, in case of our observation sites near Chersky. Accordingly, land-surface modeling schemes that are exclusively trained on growing season datasets for permafrost ecosystems must produce a biased representation of the current role of the Arctic for the global carbon budget, and also future projections on permafrost carbon-climate feedbacks would be subject to very high uncertainties.

5.5.2 Drainage impact

Observed differences in net CO_2 budgets between drained and control ecosystems reflect a reduction in CO_2 sink strength following drainage. The bulk of these annual budget differences can be attributed to higher CO_2 emissions at the drained site during the growing season (see Sect. 3.2.2), but more subtle flux shifts also continue further into the non-growing season as also observed with a chamber system by Kwon et al. (2016b). Partitioning net emissions into the flux

components GPP and Reco reveals that the restructuring of the ecosystem following sustained drainage (Göckede et al., 2016) leads to higher CO_2 emissions, mainly caused by a combination of factors dominated by higher soil temperatures in the upper part of the active layer (Kwon et al., 2016b) resulting in increasing respiration rates (Lloyd and Taylor, 1994).

Reduced CH_4 emissions are commonly observed under drier and more aerobic conditions (Kim, 2015; Sachs et al., 2008; Sturtevant et al., 2012; Turetsky et al., 2008; Zhang et al., 2012; Zona et al., 2009), thus the substantial reduction in CH_4 emissions by about 50% found for our study site agrees with previously reported results. Kwon et al. (2016a) found that a combination of changes in the soil temperature (lower temperatures in the anoxic layer and higher temperatures in the oxic layers), microbial communities (reduced abundance of methanogens) and plant communities (reduced abundance of aerenchymatous plant species, therefore reducing the efficiency of plant-mediated transport) explain changes in CH_4 emission under the influence of a decadal drainage. In an earlier study, Merbold et al. (2009) observed a significant decrease in CH_4 emission rates immediately following the drainage disturbance but these growing season CH_4 budgets measured by the chamber technique are associated with high uncertainties.

The net carbon budget in $CO_{2,\,eq.}$ metrics is strongly influenced by the CH_4 signal and therefore turns the drained ecosystems into a net source for $CO_{2,\,eq.}$. Positive $CO_{2,\,eq.}$ budgets triggered by substantial CH_4 emissions were reported also by previous studies (Rinne et al., 2007; Wille et al., 2008). However, regarding the net impact of the decadal drainage disturbance, which causes pronounced shifts in exchange fluxes of both CO_2 (Kittler et al., 2016; Kwon et al., 2016b) and CH_4 (Kwon et al., 2016a), the shifts in the CO_2 budget were found to be most important. As a consequence, the $CO_{2,\,eq.}$ budget of the drained ecosystem in comparison to control site is positive, a pattern also found by Kim (2015). The absolute number in this combined budget, however, depend strongly on the integration timeframe and the corresponding GWP value for CH_4 (IPCC, 2013). Linked to the atmospheric lifetime of CH_4, this value is high for short timescales, and continuously declines with increasing length of the integration

period. Accordingly, the dominance of the CO_2 signal for net drainage effect on the $CO_{2,\,eq.}$ budget will even grow when considering timeframes of >100 years.

The focus of this study was placed on the vertical carbon exchange but for a full carbon budget the lateral transport needs to be taken into consideration (Chapin III et al., 2006). While the spring flooding is affecting both sites similarly, the drainage is expected to be subject to higher lateral export of carbon, since the ditch system installed in 2004 forms a connection to the close-by river. Through this pathway, groundwater can more easily leave the ecosystem, and therefore also forms a major transportation pathway for dissolved and particular carbon. Most studies focusing on river systems report a pronounced seasonality in lateral carbon export patterns (Finlay et al., 2006; Holmes et al., 2012; Tank et al., 2012), and also differences in carbon enrichment along stream has been observed (Crawford et al., 2014). We therefore hypothesize that at the drained site lateral export through the ditch system constitutes a substantial net carbon loss, and needs to be taken into account for a full carbon balance assessment. Consequently, consideration of lateral export in the total carbon budget and the $CO_{2,\,eq.}$ budget of the drained site can be expected to further increase the net carbon emissions found for the vertical exchange processes alone, i.e. the ecosystem would act as an even stronger net source for carbon.

5.5.3 Interannual variability

The interannual variability in net budgets for both CO_2 and CH_4 was found to result mainly from variations during the growing season, comparable to the snow free period discussed by Aurela et al. (2004). In contrast to the results shown by Mastepanov et al. (2013), for our study sites we could even further narrow down the key period that dominates year-to-year variability in carbon fluxes to the second part of the growing season for CO_2 and CH_4.

A clear relationship with air temperature was found to explain the variability in late growing season CO_2 fluxes. In contrast to Parmentier et al. (2011), highest late growing season uptake is clearly associated with highest mean air temperatures. Since we defined the end of the growing season by the fractional snow cover from MODIS data, the length of the growing season (Lund et al.,

2012) will not reflect the temperature conditions in the late growing season and can therefore not be used as an indicator at our site. At the same time, prevailing temperature conditions in the first part of the growing season did not significantly affect the CO_2 flux patterns during that time. This finding implies that carbon cycle processes during the development stage of the vegetation at our site are not limited by cold temperatures. Instead, the uniform patterns in CO_2 fluxes we observed suggest that, once thaw depths have progressed enough to support growth of vascular plants, a fixed 'program' is started that is only marginally influenced by environmental conditions, which were found to vary strongly between data years 2014-2016. In contrast, favorable conditions during the late growing season, i.e. higher than normal air temperatures and sufficient water supplies, appear to extend the active vegetation period when photosynthetic uptake exceeds the respiration losses, leading to significant increases in net growing season CO_2 uptake by the ecosystem. This variation in temperature influence on carbon cycle processes between early and later growing season implies that a bulk growing season averaging of environmental conditions on the one hand and carbon budgets on the other can only yield weak causal relationships, and a sub-seasonal differentiation can significantly improve our capability to identify key drivers of interannual variability.

The patterns in interannual variability of CH_4 budgets are even more complex than those for CO_2, since we observed strongly deviating results between drainage and control sites. Interannual variability is only observed at the control site, while the cumulative flux budgets over the course of the year are rather uniform in the drainage area. Since meteorological forcing is uniform between both treatments, this observation accordingly must be triggered by the belowground conditions. We assume that drainage has reduced soil water levels in the drainage area substantially that the ecosystem cannot benefit from favorable temperature conditions anymore. Within the control area, however, shifts in CH_4 emission are closely linked to soil temperatures with higher soil temperatures triggering higher emission rates (Lloyd and Taylor, 1994). Also in this case, we find an overlapping sensitivity of CH_4 emission rates to soil temperature conditions during the early part of the growing season in both analyzed data years, and also uniform net

emission rates. As for CO_2, the major part of the interannual variability can be attributed to the second half of the growing season. During that time, we also find different sensitivities to soil temperature conditions between data years, suggesting that the dependence of CH_4 emissions on soil temperatures is further modulated by soil moisture conditions.

5.6 CONCLUSIONS

Our results covering more than 3 years of continuous flux observations within a moist tussock tundra ecosystem demonstrate that under drained conditions CO_2 uptake and CH_4 emissions are reduced in comparison to control conditions. Based on the global warming potential metrics under relevant timeframes, as a net effect the drainage the pronounced additional source of CO_2 dominates over reduced CH_4 emissions causing an increased source of $CO_{2,\,eq.}$ to the atmosphere that indicates a positive effect on global warming. In the long term CO_2 is dominating the net budget of vertical carbon exchange and with higher CO_2 uptake, the control site has a potential negative feedback with Arctic warming, while the drained site is always a net source for carbon to the atmosphere. Year-round measurements highlight the importance of covering also the non-growing season with continuous observations. We found substantial emissions particularly during fall, and an overall contribution of non-growing season fluxes to the annual budget of 30 % for CH_4, while cold season emissions account for 50 % of CO_2 growing season budget. Consideration of cold-season contributions substantially changes the annual carbon budgets, and is therefore essential also for the calibration of land-surface models that aim at simulating the sink/source dynamics of Arctic ecosystems under climate change. Regarding interannual variability, we identified environmental conditions during the late growing season as the key factor to explain year-to-year shifts in carbon budgets within this permafrost ecosystem.

6 SUMMARY

This thesis focusing on "Long Term drainage effects on carbon fluxes of an Arctic permafrost ecosystem" is based on direct micrometeorological observations. As a result of the above described work on the data collection and processing, a continuous and high quality dataset on ecosystem–atmosphere exchange fluxes for CO_2 and CH_4 as well as an extensive suite of ancillary meteorological variables is used to investigate carbon cycle processes within the context of climate change in Arctic permafrost ecosystems. The overall aim of this thesis is to improve the understanding of spatiotemporal variability of ecosystem–atmosphere carbon fluxes in Arctic permafrost ecosystem and findings are used to answer the proposed research questions:

1. *Is there a significant difference in flux signals between the drained and the control site?*

   The decadal drainage disturbance has significant effects on biotic and abiotic site conditions as well as on the carbon cycle dynamics. For CO_2, the net sink strength of the drained ecosystem is systematically reduced in comparison to the control ecosystem. Differences in CO_2 fluxes between the drained and control ecosystems are mainly caused by increased respiration rates under drained conditions that are triggered by higher near-surface temperatures. Over the growing seasons the CO_2 uptake is reduced by 20–40 gC m^{-2} yr^{-1} under drained conditions, with 70 % of these differences attributed to conditions in the high-summer period, when the effect of reduced water availability is most pronounced. Differences in CO_2 exchange patterns between drained and control ecosystem continue further into the non-growing season with a reduced sink strength following the drainage disturbance of 38–66 gC m^{-2} on an annual scale. A negative CO_2 budget at the control site indicates that this ecosystem acts as a net sink for atmospheric CO_2. In contrast net emissions of CO_2 are observed at

the drained site and this ecosystem represents a net source for atmospheric CO_2.

Methane flux rates at the control site, representing wetter and therefore more anaerobic conditions, constantly exceed emission rates at the drained site. Differences in the annual CH_4 budget between the drained and control ecosystems sum up to half the efflux at the drained site with an average annual difference of 3.3 gC m^{-2}. Accounting for the global warming potential under relevant time frames, reduced CO_2 uptake dominates reduced CH_4 emissions as a net effect of the drainage, resulting in a positive $CO_{2,\,eq.}$ budget that indicates a positive effect on global warming.

2. *Is there a significant difference between the recent datasets of both areas compared to the historic datasets?*

   In comparison to the strong reduction in CO_2 fluxes directly after the installation of the drainage disturbance in 2005, a higher carbon turnover and a seasonal amplitude that is comparable to the control site is observed in recent CO_2 flux data at the drained site. This indicates that the drained ecosystem has recovered from the intermediate disturbance impact and appears to have adapted to significantly different hydrologic conditions.

   At the control ecosystem, the comparison of recent and historic CO_2 flux data over the growing season indicates that this tundra ecosystem is now a stronger net sink than a decade ago. In the recent CO_2 flux data higher net emissions after the snowmelt are outweighed by a strongly intensified uptake around peak growing season. The observed long-term shifts are most likely linked to a trend towards higher plant biomass over the growing season.

3. *What is the contribution of the non-growing seasons to net carbon budgets of permafrost ecosystems, and which processes influence the winter season fluxes?*

   For the quantifications of reliable annual budgets, the quality of eddy-covariance flux measurements during the winter season is investigated with regards to instrument heating. The actively controlled sonic

anemometer heating affects temperature measurements and the resulting sensible heat flux. However, no direct effect on the vertical wind speed and the resulting friction velocity was observed. The self-heating of the open-path gas analyzer causes a systematic CO_2 uptake of 92 gC m^{-2}, mostly generated during both summer and winter seasons. By accounting for both heating effects, high quality CO_2 fluxes during the winter season indicate similar flux rates and budgets independent of the prevailing environmental conditions such as e.g. snow depth, or mean winter temperatures.

The control ecosystem shows a mean annual uptake of 44 gC m^{-2} for CO_2 and a mean annual release of 7 gC m^{-2} for CH_4. With year-round measurements the importance of the non-growing season to the annual budgets of CO_2 and CH_4 is demonstrated. Substantial contributions are observed during the zero-curtain period, representing the re-freezing of the active layer. In total, t non-growing season emissions account for 50 % of the growing-season CO_2 uptake and 30 % of the annual CH_4 budget.

4. *How is intra- and interannual variability linked to the environmental drivers that dominate the turbulent carbon dioxide and methane fluxes? Have these drivers changed due to the disturbance regime?*

   A seasonal classification based on environmental site conditions and phenology is applied for a detailed analysis of the intra- and interannual variability by normalizing fluxes by each season and sub-season. Similar exchange patterns and budgets are observed for CO_2 and CH_4 in all data years during the non-growing season. During the growing season, the interannual variability found in net budgets for both CO_2 and CH_4 are mainly linked to year-to-year variability in temperature conditions.

   A linear relationship with mean air temperature is identified to explain higher CO_2 uptake under warmer conditions. Primarily, the variability in CH_4 is driven by soil moisture conditions, with similar flux rates and budgets at the drained site in all data years, while the control ecosystem with soil moisture conditions close to saturation indicates a pronounced

year-to-year variability. Differences in the CH_4 flux rates at the control site are triggered by soil temperatures with increased emissions under warmer conditions.

With this thesis and the presented results important research fields are addressed. The long-term manipulation experiment with parallel observations over a disturbed tundra ecosystem (i.e., drained) and a control tundra ecosystem can give valuable insights into carbon cycle processes. These results improve the understanding of the sustainability of the permafrost carbon pool under future climate conditions (Kaufman et al., 2009; Kirschbaum, 1995; Serreze et al., 2000) and contributes to crucial data gaps and unclear results from long-term manipulation experiments (Christiansen et al., 2012b; Lamb et al., 2011; Lupascu et al., 2014; Mack et al., 2004; Sistla et al., 2013). Furthermore, new insights into the temporal variability after a drainage disturbance in contrast to a large spatial scale water table manipulation experiment in Alaska (Sturtevant et al., 2012; Zona et al., 2012; Zona et al., 2009) are provided. Building on previous studies (Goodrich et al., 2016; Järvi et al., 2009), the first general recommendation to avoid heating biases under cold climatic conditions is derived from winter season measurements that quantify direct and indirect instrument heating effects on turbulent CO_2 flux measurements. Accounting for these heating biases, high quality winter CO_2 observations contribute to ongoing research on processes and driving mechanisms of fluxes to determine winter season budgets that, because of large data lacks, are not sufficiently investigated and vary over a wide range (Lüers et al., 2014; Oechel et al., 2014). Furthermore, considerable uncertainties in the estimations of annual carbon budgets exist since only very few studies focus on eddy-covariance CH_4 measurements and observations during the non-growing season (Oechel et al., 2014; Zona et al., 2016). With year-round measurements of combined CO_2 and CH_4 fluxes existing knowledge gaps are addressed to give new insights into the intra- and interannual variability of carbon processes that are crucial to understand the variability of the carbon cycle and estimate reliable net budgets of vertical carbon exchange.

Having addressed the overall aim of this thesis by answering the posed research questions, there are still existing unexplored issues that should be part of

further work. With longer CO_2 and CH_4 flux observations at both sites a more detailed analysis of the interannual variability and the dominating environmental drivers will be possible since the dataset used here was limited by longer data gaps. In parallel to the eddy-covariance systems representing meso-scale observations, CO_2 and CH_4 fluxes were measured by manual chambers within the footprints for both towers. These observations reflect variabilities on the smallest (micro-) scales that can be upscaled to meso-scale observations and compared to the eddy-covariance data. Further, the high quality eddy-covariance flux dataset can be linked to products focusing on larger spatial resolution (macro-scale) as process-based models or inverse modelling. Integrating all observational components into a comprehensive framework will allow characterizing landscape scale permafrost fluxes and reducing associated uncertainties.

References

ACIA: Impacts of a Warming Arctic: Arctic Climate Impacts Assessment, Cambridge, 2004.

Amiro, B.: Estimating annual carbon dioxide eddy fluxes using open-path analysers for cold forest sites, Agr Forest Meteorol, 150, 1366-1372, 2010.

Arneth, A., Kurbatova, J., Kolle, O., Shibistova, O. B., Lloyd, J., Vygodskaya, N. N., and Schulze, E. D.: Comparative ecosystem-atmosphere exchange of energy and mass in a European Russian and a central Siberian bog II. Interseasonal and interannual variability of CO2 fluxes, Tellus B, 54, 514-530, 2002.

Aubinet, M., Joly, L., Loustau, D., De Ligne, A., Chopin, H., Cousin, J., Chauvin, N., Decarpenterie, T., and Gross, P.: Dimensioning IRGA gas sampling systems: laboratory and field experiments, Atmos Meas Tech, 9, 1361-1367, 2016.

Aubinet, M., Vesala, T., and Papale, D.: Eddy Covariance - A practical guide to measurement and data analysis, Springer, Dordrecht; Heidelberg; London; New York, 2012.

Aurela, M., Laurila, T., and Tuovinen, J.-P.: The timing of snow melt controls the annual CO_2 balance in a subarctic fen, Geophys Res Lett, 31, 826–837, 2004.

Aurela, M., Riutta, T., Laurila, T., Tuovinen, J.-P., Vesala, T., Tuittila, E. S., Rinne, J., Haapanala, S., and Laine, J.: CO_2 exchange of a sedge fen in southern Finland - the impact of a drought period, Tellus B, 59, 826-837, 2007.

Baldocchi, D.: Measuring fluxes of trace gases and energy between ecosystems and the atmosphere – the state and future of the eddy covariance method, Glob Change Biol, 20, 3600-3609, 2014.

Bate, G. C. and Smith, V. R.: Photosynthesis and Respiration in the Sub-Antarctic Tussock Grass Poa-Cookii, New Phytol, 95, 533-543, 1983.

Beer, C.: Soil science - The Arctic carbon count, Nature Geosci, 1, 569-570, 2008.

Belshe, E. F., Schuur, E. A. G., and Bolker, B. M.: Tundra ecosystems observed to be CO2 sources due to differential amplification of the carbon cycle, Ecol Lett, 16, 1307-1315, 2013.

Billings, W. D., Luken, J. O., Mortensen, D. A., and Peterson, K. M.: Arctic Tundra - a Source or Sink for Atmospheric Carbon-Dioxide in a Changing Environment, Oecologia, 53, 7-11, 1982.

Boike, J., Kattenstroth, B., Abramova, K., Bornemann, N., Chetverova, A., Fedorova, I., Frob, K., Grigoriev, M., Gruber, M., Kutzbach, L., Langer, M., Minke, M., Muster, S., Piel, K., Pfeiffer, E. M., Stoof, G., Westermann, S., Wischnewski, K., Wille, C., and Hubberten, H. W.: Baseline characteristics of climate, permafrost and land cover from a new permafrost observatory in the Lena River Delta, Siberia (1998-2011), Biogeosciences, 10, 2105-2128, 2013.

Bowling, D. R., Bethers-Marchetti, S., Lunch, C. K., Grote, E. E., and Belnap, J.: Carbon, water, and energy fluxes in a semiarid cold desert grassland during and following multiyear drought, J Geophys Res-Biogeo, 115, G04026, 2010.

Bret-Harte, M. S., Mack, M. C., Shaver, G. R., Huebner, D. C., Johnston, M., Mojica, C. A., Pizano, C., and Reiskind, J. A.: The response of Arctic vegetation and soils following an unusually severe tundra fire, Philos T R Soc B, 368, 2013.

Burba, G. G. and Anderson, D. J.: A brief practical guide to eddy covariance flux measurements, Li-COR Inc., Lincoln, 2010a.

Burba, G. G. and Anderson, D. J.: Part II. Eddy covariance workflow: Surface heat exchange and open-path gas fluxes from older analyzers. In: A Brief Guide to Eddy Covariance Flux Measurements, Principles and Workflow Examples for Scientific and Industrial Applications, Li-COR Inc., Lincon, 2010b.

Burba, G. G., Anderson, D. J., Xu, L., and McDermitt, D. K.: Additional term in the Webb–Pearman–Leuning correction due to surface heating from an open-path gas analyzer, Eos Transactions AGU, 2006a.

Burba, G. G., Anderson, D. J., Xu, L., and McDermitt, D. K.: Correcting apparent off-season CO_2 uptake due to surface heating of a an open path gas analyzer: process report of an ongoing study, Proceedings of 27th Annual Conference on Agricultural and Forest meteorology, San Diego, CA, 13, 2006b.

Burba, G. G., McDermitt, D. K., Grelle, A., Anderson, D. J., and Xu, L.: Addressing the influence of instrument surface heat exchange on the measurements of CO_2 flux from open-path gas analyzers, Glob Change Biol, 14, 1854-1876, 2008.

Carslaw, D. C.: The openair manual—open-source tools for analysing air pollution data. In: Manual for version 1.1-4, King`s Collage, London, 2015.

Chapin III, F. S., Woodwell, G. M., Randerson, J. T., Rastetter, E. B., Lovett, G. M., Baldocchi, D. D., Clark, D. A., Harmon, M. E., Schimel, D. S., Valentini, R., Wirth, C., Aber, J. D., Cole, J. J., Goulden, M. L., Harden, J. W., Heimann, M., Howarth, R. W., Matson, P. A., McGuire, A. D., Melillo, J. M., Mooney, H. A., Neff, J. C., Houghton, R. A., Pace, M. L., Ryan, M. G., Running, S. W., Sala, O. E., Schlesinger, W. H., and Schulze, E. D.: Reconciling Carbon-cycle Concepts, Terminology, and Methods, Ecosystems, 9, 1041-1050, 2006.

Chivers, M. R., Turetsky, M. R., Waddington, J. M., Harden, J. W., and McGuire, A. D.: Effects of Experimental Water Table and Temperature Manipulations on Ecosystem CO2 Fluxes in an Alaskan Rich Fen, Ecosystems, 12, 1329-1342, 2009.

Christensen, T. R.: Climate science: Understand Arctic methane variability, Nature, 509, 279-281, 2014.

Christensen, T. R., Friborg, T., Sommerkorn, M., Kaplan, J., Illeris, L., Soegaard, H., Nordstroem, C., and Jonasson, S.: Trace gas exchange in a high-Arctic valley: 1. Variations in CO_2 and CH_4 Flux between tundra vegetation types, Global Biogeochem Cy, 14, 701-7013, 2000.

Christiansen, C. T., Schmidt, N. M., and Michelsen, A.: High Arctic Dry Heath CO2 Exchange During the Early Cold Season, Ecosystems, 15, 1083-1092, 2012a.

Christiansen, C. T., Svendsen, S. H., Schmidt, N. M., and Michelsen, A.: High arctic heath soil respiration and biogeochemical dynamics during summer and autumn freeze-in - effects of long-term enhanced water and nutrient supply, Glob Change Biol, 18, 3224-3236, 2012b.

Clement, R. J., Burba, G. G., Grelle, A., Anderson, D. J., and Moncrieff, J. B.: Improved trace gas flux estimation through IRGA sampling optimization, Agr Forest Meteorol, 149, 623-638, 2009.

Corradi, C., Kolle, O., Walter, K., Zimov, S. A., and Schulze, E. D.: Carbon dioxide and methane exchange of a north-east Siberian tussock tundra, Glob Change Biol, 11, 1910-1925, 2005.

Coyne, P. I. and Kelley, J. J.: Carbon-Dioxide Partial Pressures in Arctic Surface Waters, Limnol Oceanogr, 19, 928-938, 1974.

Crawford, J. T., Lottig, N. R., Stanley, E. H., Walker, J. F., Hanson, P. C., Finlay, J. C., and Striegl, R. G.: CO2 and CH4 emissions from streams in a lake-rich landscape: Patterns, controls, and regional significance, Global Biogeochem Cy, 28, 197-210, 2014.

Curry, J. A., Schramm, J. L., and Ebert, E. E.: Sea-Ice Albedo Climate Feedback Mechanism, J Climate, 8, 240-247, 1995.

DeConto, R. M., Galeotti, S., Pagani, M., Tracy, D., Schaefer, K., Zhang, T. J., Pollard, D., and Beerling, D. J.: Past extreme warming events linked to massive carbon release from thawing permafrost (vol 484, pg 87, 2012), Nature, 490, 292-292, 2012.

Denman, K. L. and Brasseur, G.: Couplings Between Changes in the Climate System and Biogeochemistry, Climate Change 2007: The Physical Science Basis, 2007. 499-587, 2007.

Dunn, G.: Statistical Evaluation of Measurement Errors, Arnold, London, 2004.

Dutta, K., Schuur, E. A. G., Neff, J. C., and Zimov, S. A.: Potential carbon release from permafrost soils of Northeastern Siberia, Glob Change Biol, 12, 2336-2351, 2006.

Emmerton, C. A., St. Louis, V. L., Lehnherr, I., Humphreys, E. R., Rydz, E., and Kosolofski, H. R.: The net exchange of methane with high Arctic landscapes during the summer growing season, Biogeosciences, 11, 3095-3106, 2014.

Eugster, W. and Merbold, L.: Eddy covariance for quantifying trace gas fluxes from soils, SOIL, 1, 187-205, 2015.

Euskirchen, E. S., Bret-Harte, M. S., Scott, G. J., Edgar, C., and Shaver, G. R.: Seasonal patterns of carbon dioxide and water fluxes in three representative tundra ecosystems in northern Alaska, Ecosphere, 3, 2012.

Euskirchen, E. S., Bret-Harte, M. S., Shaver, G. R., Edgar, C. W., and Romanovsky, V. E.: Long-Term Release of Carbon Dioxide from Arctic Tundra

Ecosystems in Alaska, Ecosystems, doi: 10.1007/s10021-016-0085-9, 2016. 1-15, 2016.

Finlay, J., Neff, J., Zimov, S., Davydova, A., and Davydov, S.: Snowmelt dominance of dissolved organic carbon in high-latitude watersheds: Implications for characterization and flux of river DOC, Geophys Res Lett, 33, 2006.

Flanagan, L. B. and Syed, K. H.: Stimulation of both photosynthesis and respiration in response to warmer and drier conditions in a boreal peatland ecosystem, Glob Change Biol, 17, 2271-2287, 2011.

Foken, T.: Micrometeorology, Springer, Heidelberg, 2017.

Foken, T., Göckede, M., Mauder, M., Mahrt, L., Amiro, B. D., and Munger, J. W.: Postfield data quality control In: Handbook of Micrometeorology: A Guide for Surface Flux Measurement and Analysis, Lee, X., Massman, W., and Law, B. (Eds.), Kluwer Academic Publishers, Dordrecht, 2004.

Foken, T., Leuning, R., Oncley, S. P., Mauder, M., and Aubinet, M.: Corrections and data quality. In: Eddy Covariance - A practical guide to measurement and data analysis, Aubinet, M., Vesala, T., and Papale, D. (Eds.), Springer, Dordrecht; Heidelberg; London; New York, 2012.

Foken, T. and Wichura, B.: Tools for quality assessment of surface-based flux measurements, Agr Forest Meteorol, 78, 83-105, 1996.

Forkel, M., Carvalhais, N., Verbesselt, J., Mahecha, M. D., Neigh, C. S. R., and Reichstein, M.: Trend Change Detection in NDVI Time Series: Effects of Inter-Annual Variability and Methodology, Remote Sens-Basel, 5, 2113-2144, 2013.

Fratini, G. and Mauder, M.: Towards a consistent eddy-covariance processing: an intercomparison of EddyPro and TK3, Atmos Meas Tech, 7, 2273-2281, 2014.

Friedlingstein, P., Cox, P., Betts, R., Bopp, L., Von Bloh, W., Brovkin, V., Cadule, P., Doney, S., Eby, M., Fung, I., Bala, G., John, J., Jones, C., Joos, F., Kato, T., Kawamiya, M., Knorr, W., Lindsay, K., Matthews, H. D., Raddatz, T., Rayner, P., Reick, C., Roeckner, E., Schnitzler, K. G., Schnur, R., Strassmann, K., Weaver, A. J., Yoshikawa, C., and Zeng, N.: Climate-carbon cycle feedback analysis: Results from the C(4)MIP model intercomparison, J Climate, 19, 3337-3353, 2006.

Göckede, M., Foken, T., Aubinet, M., Aurela, M., Banza, J., Bernhofer, C., Bonnefond, J. M., Brunet, Y., Carrara, A., Clement, R., Dellwik, E., Elbers, J., Eugster, W., Fuhrer, J., Granier, A., Grünwald, T., Heinesch, B., Janssens, I. A., Knohl, A., Koeble, R., Laurila, T., Longdoz, B., Manca, G., Marek, M., Markkanen, T., Mateus, J., Matteucci, G., Mauder, M., Migliavacca, M., Minerbi, S., Moncrieff, J., Montagnani, L., Moors, E., Ourcival, J. M., Papale, D., Pereira, J., Pilegaard, K., Pita, G., Rambal, S., Rebmann, C., Rodrigues, A., Rotenberg, E., Sanz, M. J., Sedlak, P., Seufert, G., Siebicke, L., Soussana, J. F., Valentini, R., Vesala, T., Verbeeck, H., and Yakir, D.: Quality control of CarboEurope flux data – Part 1: Coupling footprint analyses with flux data quality assessment to evaluate sites in forest ecosystems, Biogeosciences, 5, 433-450, 2008.

Göckede, M., Kittler, F., Kwon, M. J., Burjack, I., Heimann, M., Kolle, O., Zimov, N., and Zimov, S.: Shifts in permafrost ecosystem structure following a decade-long drainage increase energy transfer to the atmosphere, but reduce thaw depth, The Cryosphere Discuss., 2016, 1-38, 2016.

Goodrich, J. P., Oechel, W. C., Gioli, B., Moreaux, V., Murphy, P. C., Burba, G., and Zona, D.: Impact of different eddy covariance sensors, site set-up, and maintenance on the annual balance of CO2 and CH4 in the harsh Arctic environment, Agr Forest Meteorol, 228–229, 239-251, 2016.

Gorham, E.: Northern Peatlands - Role in the Carbon-Cycle and Probable Responses to Climatic Warming, Ecol Appl, 1, 182-195, 1991.

Grelle, A. and Burba, G.: Fine-wire thermometer to correct CO2 fluxes by open-path analyzers for artificial density fluctuations, Agr Forest Meteorol, 147, 48-57, 2007.

Grogan, P., Michelsen, A., Ambus, P., and Jonasson, S.: Freeze-thaw regime effects on carbon and nitrogen dynamics in sub-arctic heath tundra mesocosms, Soil Biol Biochem, 36, 641-654, 2004.

Grøndahl, L., Friborg, T., and Soegaard, H.: Temperature and snow-melt controls on interannual variability in carbon exchange in the high Arctic, Theor Appl Climatol, 88, 111-125, 2007.

Harazono, Y., Mano, M., Miyata, A., Zulueta, R. C., and Oechel, W. C.: Inter-annual carbon dioxide uptake of a wet sedge tundra ecosystem in the Arctic, Tellus B, 55, 215-231, 2003.

Haslwanter, A., Hammerle, A., and Wohlfahrt, G.: Open-path vs. closed-path eddy covariance measurements of the net ecosystem carbon dioxide and water vapour exchange: A long-term perspective, Agr Forest Meteorol, 149, 291-302, 2009.

Helbig, M., Wischnewski, K., Gosselin, G. H., Biraud, S. C., Bogoev, I., Chan, W. S., Euskirchen, E. S., Glenn, A. J., Marsh, P. M., Quinton, W. L., and Sonnentag, O.: Addressing a systematic bias in carbon dioxide flux measurements with the EC150 and the IRGASON open-path gas analyzers, Agr Forest Meteorol, 228, 349-359, 2016.

Holmes, R. M., McClelland, J. W., Peterson, B. J., Tank, S. E., Bulygina, E., Eglinton, T. I., Gordeev, V. V., Gurtovaya, T. Y., Raymond, P. A., Repeta, D. J., Staples, R., Striegl, R. G., Zhulidov, A. V., and Zimov, S. A.: Seasonal and Annual Fluxes of Nutrients and Organic Matter from Large Rivers to the Arctic Ocean and Surrounding Seas, Estuaries and Coasts, 35, 369-382, 2012.

Huemmrich, K. F., Kinoshita, G., Gamon, J. A., Houston, S., Kwon, H., and Oechel, W. C.: Tundra carbon balance under varying temperature and moisture regimes, J Geophys Res-Biogeo, 115, 2010.

Hugelius, G., Strauss, J., Zubrzycki, S., Harden, J. W., Schuur, E. A. G., Ping, C. L., Schirrmeister, L., Grosse, G., Michaelson, G. J., Koven, C. D., O'Donnell, J. A., Elberling, B., Mishra, U., Camill, P., Yu, Z., Palmtag, J., and Kuhry, P.:

Estimated stocks of circumpolar permafrost carbon with quantified uncertainty ranges and identified data gaps, Biogeosciences, 11, 6573-6593, 2014.

IPCC: Climate Change 2013: The Physical Science Basis. Contribution of Working Group I to the Fifth Assessment Report of the Intergovernmental Panel on Climate Change, Cambridge University Press, Cambridge, United Kingdom and New York, NY, USA, 2013.

Jammet, M., Dengel, S., Kettner, E., Parmentier, F. J. W., Wik, M., Crill, P., and Friborg, T.: Year-round CH4 and CO2 flux dynamics in two contrasting freshwater ecosystems of the subarctic, Biogeosciences Discuss., 2017, 1-49, 2017.

Järvi, L., Mammarella, I., Eugster, W., Ibrom, A., Siivola, E., Dellwik, E., Keronen, P., Burba, G., and Vesala, T.: Comparison of net CO_2 fluxes measured with open- and closed-path infrared gas analyzers in an urban complex environment, Boreal Environ Res, 14, 499-514, 2009.

Jorgenson, M. T., Shur, Y. L., and Pullman, E. R.: Abrupt increase in permafrost degradation in Arctic Alaska, Geophys Res Lett, 33, 2006.

Kappen, L.: Plant Activity under Snow and Ice, with Particular Reference to Lichens, Arctic, 46, 297-302, 1993.

Kaufman, D. S., Schneider, D. P., McKay, N. P., Ammann, C. M., Bradley, R. S., Briffa, K. R., Miller, G. H., Otto-Bliesner, B. L., Overpeck, J. T., Vinther, B. M., and Arctic Lakes 2k Project, M.: Recent warming reverses long-term arctic cooling, Science, 325, 1236-1239, 2009.

Kelley, J. J., Weaver, D. F., and Smith, B. P.: Variation of Carbon Dioxide under Snow in Arctic, Ecology, 49, 358-361, 1968.

Khvorostyanov, D. V., Ciais, P., Krinner, G., Zimov, S. A., Corradi, C., and Guggenberger, G.: Vulnerability of permafrost carbon to global warming. Part II: sensitivity of permafrost carbon stock to global warming, Tellus B, 60, 265-275, 2008a.

Khvorostyanov, D. V., Krinner, G., Ciais, P., Heimann, M., and Zimov, S. A.: Vulnerability of permafrost carbon to global warming. Part I: model description and role of heat generated by organic matter decomposition, Tellus B, 60, 250-264, 2008b.

Kim, Y.: Effect of thaw depth on fluxes of CO2 and CH4 in manipulated Arctic coastal tundra of Barrow, Alaska, Sci Total Environ, 505, 385-389, 2015.

Kirschbaum, M. U. F.: The Temperature-Dependence of Soil Organic-Matter Decomposition, and the Effect of Global Warming on Soil Organic-C Storage, Soil Biol Biochem, 27, 753-760, 1995.

Kittler, F., Burjack, I., Corradi, C. A. R., Heimann, M., Kolle, O., Merbold, L., Zimov, N., Zimov, S., and Göckede, M.: Impacts of a decadal drainage disturbance on surface–atmosphere fluxes of carbon dioxide in a permafrost ecosystem, Biogeosciences, 13, 5315-5332, 2016.

Kolle, O. and Rebmann, C.: EddySoft; Documentation of a Software Package to Acquire and Process Eddy Covariance Data, Jena, 2007.

Koven, C. D., Ringeval, B., Friedlingstein, P., Ciais, P., Cadule, P., Khvorostyanov, D., Krinner, G., and Tarnocai, C.: Permafrost carbon-climate feedbacks accelerate global warming, P Natl Acad Sci USA, 108, 14769-14774, 2011.

Kutzbach, L., Wille, C., and Pfeiffer, E. M.: The exchange of carbon dioxide between wet arctic tundra and the atmosphere at the Lena River Delta, Northern Siberia, Biogeosciences, 4, 869-890, 2007.

Kwon, M. J., Beulig, F., Ilie, I., Wildner, M., Küsel, K., Merbold, L., Mahecha, M. D., Zimov, N., Zimov, S. A., Heimann, M., Schuur, E. A. G., Kostka, J. E., Kolle, O., Hilke, I., and Göckede, M.: Plants, microorganisms, and soil temperatures contribute to a decrease in methane fluxes on a drained Arctic floodplain, Glob Change Biol, doi: 10.1111/gcb.13558, 2016a. 2016a.

Kwon, M. J., Heimann, M., Kolle, O., Luus, K. A., Schuur, E. A. G., Zimov, N., Zimov, S. A., and Göckede, M.: Drainage reduces CO_2 uptake and increases CO_2 efflux by a Siberian floodplain due to shifts in vegetation community and soil thermal characteristics, Biogeosciences, 13, 4219-4235, 2016b.

Lafleur, P. M. and Humphreys, E. R.: Spring warming and carbon dioxide exchange over low Arctic tundra in central Canada, Glob Change Biol, 14, 740-756, 2007.

Lamb, E. G., Han, S., Lanoil, B. D., Henry, G. H. R., Brummell, M. E., Banerjee, S., and Siciliano, S. D.: A High Arctic soil ecosystem resists long-term environmental manipulations, Glob Change Biol, 17, 3187-3194, 2011.

Laurila, T., Soegaard, H., Lloyd, C. R., Aurela, M., Tuovinen, J. P., and Nordstroem, C.: Seasonal variations of net CO2 exchange in European Arctic ecosystems, Theor Appl Climatol, 70, 183-201, 2001.

Legendre, P. (Ed.): lmodel2: Model II Regression, 2014.

Liljedahl, A. K., Boike, J., Daanen, R. P., Fedorov, A. N., Frost, G. V., Grosse, G., Hinzman, L. D., Iijma, Y., Jorgenson, J. C., Matveyeva, N., Necsoiu, M., Raynolds, M. K., Romanovsky, V. E., Schulla, J., Tape, K. D., Walker, D. A., Wilson, C. J., Yabuki, H., and Zona, D.: Pan-Arctic ice-wedge degradation in warming permafrost and its influence on tundra hydrology, Nature Geosci, 9, 312–318, 2016.

Liu, H. P., Peters, G., and Foken, T.: New equations for sonic temperature variance and buoyancy heat flux with an omnidirectional sonic anemometer, Bound-Lay Meteorol, 100, 459-468, 2001.

Lloyd, J. and Taylor, J. A.: On the Temperature-Dependence of Soil Respiration, Funct Ecol, 8, 315-323, 1994.

Lüers, J., Westermann, S., Piel, K., and Boike, J.: Annual CO2 budget and seasonal CO2 exchange signals at a high Arctic permafrost site on Spitsbergen, Svalbard archipelago, Biogeosciences, 11, 6307-6322, 2014.

Lund, M., Falk, J. M., Friborg, T., Mbufong, H. N., Sigsgaard, C., Soegaard, H., and Tamstorf, M. P.: Trends in CO_2 exchange in a high Arctic tundra heath, 2000–2010, J Geophys Res-Biogeo, 117, G02001, 2012.

Lupascu, M., Welker, J. M., Seibt, U., Maseyk, K., Xu, X., and Czimczik, C. I.: High Arctic wetting reduces permafrost carbon feedbacks to climate warming, Nature Clim Change, 4, 51-55, 2014.

Mack, M. C., Schuur, E. A. G., Bret-Harte, M. S., Shaver, G. R., and Chapin, F. S.: Ecosystem carbon storage in arctic tundra reduced by long-term nutrient fertilization, Nature, 431, 440-443, 2004.

Mahecha, M. D., Reichstein, M., Carvalhais, N., Lasslop, G., Lange, H., Seneviratne, S. I., Vargas, R., Ammann, C., Arain, M. A., Cescatti, A., Janssens, I. A., Migliavacca, M., Montagnani, L., and Richardson, A. D.: Global Convergence in the Temperature Sensitivity of Respiration at Ecosystem Level, Science, 329, 838-840, 2010.

Makkonen, L. and Laakso, T.: Humidity Measurements in Cold and Humid Environments, Bound-Lay Meteorol, 116, 131-147, 2005.

Marushchak, M. E., Kiepe, I., Biasi, C., Elsakov, V., Friborg, T., Johansson, T., Soegaard, H., Virtanen, T., and Martikainen, P. J.: Carbon dioxide balance of subarctic tundra from plot to regional scales, Biogeosciences, 10, 437-452, 2013.

Massman, W. and Frank, J.: Three Issues Concerning Open- and Closed-Path Sensors: Self-heating, Pressure Effects, and Tube Wall Adsorption, AsiaFlux Workshop, Sapporo, Japan, 2009.

Mastepanov, M., Sigsgaard, C., Dlugokencky, E. J., Houweling, S., Strom, L., Tamstorf, M. P., and Christensen, T. R.: Large tundra methane burst during onset of freezing, Nature, 456, 628-630, 2008.

Mastepanov, M., Sigsgaard, C., Tagesson, T., Ström, L., Tamstorf, M. P., Lund, M., and Christensen, T. R.: Revisiting factors controlling methane emissions from high-Arctic tundra, Biogeosciences, 10, 5139-5158, 2013.

Mauder, M. and Foken, T.: Eddy-Covariance Software TK3, doi: 10.5281/zenodo.20349, 2015. 2015.

Mauder, M., Oncley, S. P., Vogt, R., Weidinger, T., Ribeiro, L., Bernhofer, C., Foken, T., Kohsiek, W., De Bruin, H. A. R., and Liu, H.: The energy balance experiment EBEX-2000. Part II: Intercomparison of eddy-covariance sensors and post-field data processing methods, Bound-Lay Meteorol, 123, 29-54, 2007.

McGuire, A. D., Anderson, L. G., Christensen, T. R., Dallimore, S., Guo, L. D., Hayes, D. J., Heimann, M., Lorenson, T. D., Macdonald, R. W., and Roulet, N.: Sensitivity of the carbon cycle in the Arctic to climate change, Ecol Monogr, 79, 523-555, 2009.

McGuire, A. D., Christensen, T. R., Hayes, D., Heroult, A., Euskirchen, E., Kimball, J. S., Koven, C., Lafleur, P., Miller, P. A., Oechel, W., Peylin, P., Williams, M., and Yi, Y.: An assessment of the carbon balance of Arctic tundra: comparisons among observations, process models, and atmospheric inversions, Biogeosciences, 9, 3185-3204, 2012.

Merbold, L., Kutsch, W. L., Corradi, C., Kolle, O., Rebmann, C., Stoy, P. C., Zimov, S. A., and Schulze, E. D.: Artificial drainage and associated carbon fluxes (CO_2/CH_4) in a tundra ecosystem, Glob Change Biol, 15, 2599-2614, 2009.

Metzger, S., Burba, G., Burns, S. P., Blanken, P. D., Li, J. H., Luo, H. Y., and Zulueta, R. C.: Optimization of an enclosed gas analyzer sampling system for measuring eddy covariance fluxes of H2O and CO2, Atmos Meas Tech, 9, 1341-1359, 2016.

Mikhailov, O. A., Zagirova, S. V., Miglovets, M. N., and Wille, C.: Carbon dioxide fluxes in the ecosystem of meso-oligotrophic peatland during the transition period from autumn to winter, Contemp Probl Ecol, 6, 143-148, 2013.

Monson, R. and Baldocchi, D.: Terrestrial Biosphere-Atmosphere Fluxes, Cambridge University Press, Cambridge, 2014.

Moore, C. J.: Frequency response corrections for eddy correlation systems, Bound-Lay Meteorol, 37, 17-35, 1986.

Moore, T. R., De Young, A., Bubier, J. L., Humphreys, E. R., Lafleur, P. M., and Roulet, N. T.: A Multi-Year Record of Methane Flux at the Mer Bleue Bog, Southern Canada, Ecosystems, 14, 646, 2011.

Morgner, E., Elberling, B., Strebel, D., and Cooper, E. J.: The importance of winter in annual ecosystem respiration in the High Arctic: effects of snow depth in two vegetation types, Polar Res, 29, 2010.

Munger, J. W., Loescher, H. W., and Luo, H.: Measurement, Tower, and Site Design Considerations. In: Eddy Covariance - A practical guide to measurement and data analysis, Aubinet, M., Vesala, T., and Papale, D. (Eds.), Springer Dordrecht; Heidelberg; London; New York, 2012.

Nordstroem, C., Soegaard, H., Christensen, T. R., Friborg, T., and Hansen, B. U.: Seasonal carbon dioxide balance and respiration of a high-arctic fen ecosystem in NE-Greenland, Theor Appl Climatol, 70, 149-166, 2001.

Nzotungicimpaye, C.-M. and Zickfeld, K.: The Contribution from Methane to the Permafrost Carbon Feedback, Current Climate Change Reports, doi: 10.1007/s40641-017-0054-1, 2017. 1-11, 2017.

Oechel, W. C., Laskowski, C. A., Burba, G., Gioli, B., and Kalhori, A. A. M.: Annual patterns and budget of CO_2 flux in an Arctic tussock tundra ecosystem, J Geophys Res-Biogeo, 119, 323-339, 2014.

Oechel, W. C., Vourlitis, G., and Hastings, S. J.: Cold season CO_2 emission from Arctic soils, Global Biogeochem Cy, 11, 163-172, 1997.

Oechel, W. C., Vourlitis, G. L., Hastings, S. J., Ault, R. P., and Bryant, P.: The effects of water table manipulation and elevated temperature on the net CO_2 flux of wet sedge tundra ecosystems, Glob Change Biol, 4, 77-90, 1998.

Olivas, P. C., Oberbauer, S. F., Tweedie, C. E., Oechel, W. C., and Kuchy, A.: Responses of CO_2 flux components of Alaskan Coastal Plain tundra to shifts in water table, J Geophys Res-Biogeo, 115, 2010.

Ono, K., Miyata, A., and Yamada, T.: Apparent downward CO_2 flux observed with open-path eddy covariance over a non-vegetated surface, Theor Appl Climatol, 92, 195-208, 2007.

Overland, J. E., Wang, M., Walsh, J. E., and Stroeve, J. C.: Future Arctic climate changes: Adaptation and mitigation time scales, Earth's Future, 2, 68-74, 2014.

Panikov, N. S., Flanagan, P. W., Oechel, W. C., Mastepanov, M. A., and Christensen, T. R.: Microbial activity in soils frozen to below -39 degrees C, Soil Biol Biochem, 38, 785–794, 2006.

Parmentier, F. J. W., van der Molen, M. K., van Huissteden, J., Karsanaev, S. A., Kononov, A. V., Suzdalov, D. A., Maximov, T. C., and Dolman, A. J.: Longer growing seasons do not increase net carbon uptake in the northeastern Siberian tundra, J Geophys Res, 116, 2156-2202, 2011.

Peterson, K. M., Billings, W. D., and Reynolds, D. N.: Influence of Water Table and Atmospheric CO_2 Concentration on the Carbon Balance of Arctic Tundra, Arctic Alpine Res, 16, 331-335, 1984.

Philipp, R. S., Mark, A. K. G., Sabine, B. R., Nanna, B., Bo, E., and Elisabeth, J. C.: High Arctic plant phenology is determined by snowmelt patterns but duration of phenological periods is fixed: an example of periodicity, Environ Res Lett, 11, 125006, 2016.

Pries, C. E. H., Schuur, E. A. G., and Crummer, K. G.: Thawing permafrost increases old soil and autotrophic respiration in tundra: Partitioning ecosystem respiration using delta C-13 and Delta C-14, Glob Change Biol, 19, 649-661, 2013.

R Core Team: R: A Language and Environment for Statistical Computing. R Foundation for Statistical Computing, Vienna, Austria, 2014.

Reichstein, M., Falge, E., Baldocchi, D., Papale, D., Aubinet, M., Berbigier, P., Bernhofer, C., Buchmann, N., Gilmanov, T., Granier, A., Grunwald, T., Havrankova, K., Ilvesniemi, H., Janous, D., Knohl, A., Laurila, T., Lohila, A., Loustau, D., Matteucci, G., Meyers, T., Miglietta, F., Ourcival, J. M., Pumpanen, J., Rambal, S., Rotenberg, E., Sanz, M., Tenhunen, J., Seufert, G., Vaccari, F., Vesala, T., Yakir, D., and Valentini, R.: On the separation of net ecosystem exchange into assimilation and ecosystem respiration: review and improved algorithm, Glob Change Biol, 11, 1424-1439, 2005.

Reverter, B. R., Carrara, A., Fernandez, A., Gimeno, C., Sanz, M. J., Serrano-Ortiz, P., Sanchez-Canete, E. P., Were, A., Domingo, F., Resco, V., Burba, G. G., and Kowalski, A. S.: Adjustment of annual NEE and ET for the open-path IRGA self-heating correction: Magnitude and approximation over a range of climate, Agr Forest Meteorol, 151, 1856-1861, 2011.

Rinne, J., Riutta, T., Pihlatie, M., Aurela, M., Haapanala, S., Tuovinen, J.-P., Tuittila, E.-S., and Vesala, T.: Annual cycle of methane emission from a boreal fen measured by the eddy covariance technique, Tellus B, 59, 449-457, 2007.

Rogiers, N., Conen, F., Furger, M., Stockli, R., and Eugster, W.: Impact of past and present land-management on the C-balance of a grassland in the Swiss Alps, Glob Change Biol, 14, 2613-2625, 2008.

Rohde, R., Muller, R. A., Jacobsen, R., Muller, E., Perlmutter, S., Rosenfeld, A., Wurtele, J., Groom, D., and Wickham, C.: A New Estimate of the Average Earth

Surface Land Temperature Spanning 1753 to 2011, Geoinfor Geostat: An Overview 1:1, doi: 10.4172/2327-4581.1000101, 2013. 2013.

Runkle, B. R. K., Sachs, T., Wille, C., Pfeiffer, E. M., and Kutzbach, L.: Bulk partitioning the growing season net ecosystem exchange of CO_2 in Siberian tundra reveals the seasonality of its carbon sequestration strength, Biogeosciences, 10, 1337-1349, 2013.

Sachs, T., Wille, C., Boike, J., and Kutzbach, L.: Environmental controls on ecosystem-scale CH_4 emission from polygonal tundra in the Lena River Delta, Siberia, Biogeosciences, 113, 2008.

Schaefer, K., Zhang, T., Bruhwiler, L., and Barrett, A. P.: Amount and timing of permafrost carbon release in response to climate warming, Tellus B, 63, 165-180, 2011.

Schirrmeister, L., Grosse, G., Wetterich, S., Overduin, P. P., Strauss, J., Schuur, E. A. G., and Hubberten, H.-W.: Fossil organic matter characteristics in permafrost deposits of the northeast Siberian Arctic, Journal of Geophysical Research: Biogeosciences, 116, 2011.

Schuur, E. A. G., Bockheim, J., Canadell, J. G., Euskirchen, E., Field, C. B., Goryachkin, S. V., Hagemann, S., Kuhry, P., Lafleur, P. M., Lee, H., Mazhitova, G., Nelson, F. E., Rinke, A., Romanovsky, V. E., Shiklomanov, N., Tarnocai, C., Venevsky, S., Vogel, J. G., and Zimov, S. A.: Vulnerability of permafrost carbon to climate change: Implications for the global carbon cycle, Bioscience, 58, 701-714, 2008.

Schuur, E. A. G., McGuire, A. D., Schadel, C., Grosse, G., Harden, J. W., Hayes, D. J., Hugelius, G., Koven, C. D., Kuhry, P., Lawrence, D. M., Natali, S. M., Olefeldt, D., Romanovsky, V. E., Schaefer, K., Turetsky, M. R., Treat, C. C., and Vonk, J. E.: Climate change and the permafrost carbon feedback, Nature, 520, 171-179, 2015.

Serreze, M. C., Walsh, J. E., Chapin III, F. S., Osterkamp, T., Dyurgerov, M., Romanovsky, V., Oechel, W. C., Morison, J., Zhang, T., and Barry, R. G.: Observational evidence of recent change in the northern high-latitude environment, Climatic Change, 46, 159-207, 2000.

Shaver, G. R., Billings, W. D., Chapin III, F. S., Giblin, A. E., Nadelhoffer, K. J., Oechel, W. C., and Rastetter, E. B.: Global Change and the Carbon Balance of Arctic Ecosystems, Bioscience, 42, 433-441, 1992.

Sistla, S. A., Moore, J. C., Simpson, R. T., Gough, L., Shaver, G. R., and Schimel, J. P.: Long-term warming restructures Arctic tundra without changing net soil carbon storage, Nature, 497, 615-618, 2013.

Skelly, B. T., Miller, D. R., and Meyer, T. H.: Triple-Hot-Film Anemometer Performance in Cases-99 and A Comparison With Sonic Anemometer Measurements, Bound-Lay Meteorol, 105, 275-304, 2002.

Strack, M., Kellner, E., and Waddington, J. M.: Effect of entrapped gas on peatland surface level fluctuations, Hydrol Process, 20, 3611-3622, 2006.

Stull, R. B.: An Introduction to Boundary Layer Meteorology, Kluwer Academic Publishers, Dordrecht, Bosten, London, 1988.

Sturtevant, C. S., Oechel, W. C., Zona, D., Kim, Y., and Emerson, C. E.: Soil moisture control over autumn season methane flux, Arctic Coastal Plain of Alaska, Biogeosciences, 9, 1423-1440, 2012.

SWIPA: Snow, Water, Ice and Permafrost in the Arctic (SWIPA): Climate Change and the Cryosphere, Arctic Monitoring and Assessment (AMAP), AMAP, Oslo, Norway, 2011.

Tagesson, T., Mölder, M., Mastepanov, M., Sigsgaard, C., Tamstorf, M. P., Lund, M., Falk, J. M., Lindroth, A., Christensen, T. R., and Ström, L.: Land-atmosphere exchange of methane from soil thawing to soil freezing in a high-Arctic wet tundra ecosystem, Glob Change Biol, 18, 1928-1940, 2012.

Tank, S. E., Raymond, P. A., Striegl, R. G., McClelland, J. W., Holmes, R. M., Fiske, G. J., and Peterson, B. J.: A land-to-ocean perspective on the magnitude, source and implication of DIC flux from major Arctic rivers to the Arctic Ocean, Global Biogeochem Cy, 26, 2012.

Titlyanova, A. A., Bulavko, G. I., Kudryashova, S. Y., Naumov, A. V., Smirnov, V. V., and Tanasienko, A. A.: The reserves and losses of organic carbon in the soils of Siberia, Eurasian Soil Sci, 31, 45-53, 1998.

Tolonen, K. and Turunen, J.: Accumulation rates of carbon in mires in Finland and implications for climate change, Holocene, 6, 171-178, 1996.

Turetsky, M. R., Kotowska, A., Bubier, J., Dise, N. B., Crill, P., Hornibrook, E. R. C., Minkkinen, K., Moore, T. R., Myers-Smith, I. H., Nykänen, H., Olefeldt, D., Rinne, J., Saarnio, S., Shurpali, N., Tuittila, E. S., Waddington, J. M., White, J. R., Wickland, K. P., and Wilmking, M.: A synthesis of methane emissions from 71 northern, temperate, and subtropical wetlands, Glob Change Biol, 20, 2183-2197, 2014.

Turetsky, M. R., Treat, C. C., Waldrop, M. P., Waddington, J. M., Harden, J. W., and McGuire, A. D.: Short-term response of methane fluxes and methanogen activity to water table and soil warming manipulations in an Alaskan peatland, Journal of Geophysical Research: Biogeosciences, 113, 2008.

Turunen, J., Tomppo, E., Tolonen, K., and Reinikainen, A.: Estimating carbon accumulation rates of undrained mires in Finland - application to boreal and subarctic regions, Holocene, 12, 69-80, 2002.

Ueyama, M., Hirata, R., Mano, M., Hamotani, K., Harazono, Y., Hirano, T., Miyata, A., Takagi, K., and Takahashi, Y.: Influences of various calculation options on heat, water and carbon fluxes determined by open- and closed-path eddy covariance methods, 2012, 64, 2012.

van der Molen, M. K., van Huissteden, J., Parmentier, F. J. W., Petrescu, A. M. R., Dolman, A. J., Maximov, T. C., Kononov, A. V., Karsanaev, S. V., and Suzdalov, D. A.: The growing season greenhouse gas balance of a continental tundra site in the Indigirka lowlands, NE Siberia, Biogeosciences, 4, 985-1003, 2007.

Webb, E. E., Schuur, E. A. G., Natali, S. M., Oken, K. L., Bracho, R., Krapek, J. P., Risk, D., and Nickerson, N. R.: Increased wintertime CO2 loss as a result of sustained tundra warming, Journal of Geophysical Research: Biogeosciences, 121, 249-265, 2016.

Webb, E. K., Pearman, G. I., and Leuning, R.: Correction of flux measurements for density effects due to heat and water vapour transfer, Q J Roy Meteor Soc, 106, 85-100, 1980.

Wille, C., Kutzbach, L., Sachs, T., Wagner, D., and Pfeiffer, E. M.: Methane emission from Siberian arctic polygonal tundra: eddy covariance measurements and modeling, Glob Change Biol, 14, 1395-1408, 2008.

Wohlfahrt, G., Fenstermaker, L. F., and Arnone, J. A.: Large annual net ecosystem CO2 uptake of a Mojave Desert ecosystem, Glob Change Biol, 14, 1475-1487, 2008.

Wyngaard, J. C.: Turbulence in the Atmosphere, Cambridge University Press, 2010.

Yu, Z., Wang, J., Liu, S., Piao, S., Ciais, P., Running, S. W., Poulter, B., Rentch, J. S., and Sun, P.: Decrease in winter respiration explains 25% of the annual northern forest carbon sink enhancement over the last 30 years, Global Ecology and Biogeography, 25, 586-595, 2016.

Zhang, T. J., Barrya, R. G., Knowlesa , K., Heginbottomb, J. A., and Brownc, J.: Statistics and characteristics of permafrost and ground-ice distribution in the Northern Hemisphere, Polar Geography, 23, 132-154, 1999.

Zhang, Y., Sachs, T., Li, C., and Boike, J.: Upscaling methane fluxes from closed chambers to eddy covariance based on a permafrost biogeochemistry integrated model, Glob Change Biol, 18, 1428-1440, 2012.

Zhuang, Q. L., Melillo, J. M., Kicklighter, D. W., Prinn, R. G., McGuire, A. D., Steudler, P. A., Felzer, B. S., and Hu, S.: Methane fluxes between terrestrial ecosystems and the atmosphere at northern high latitudes during the past century: A retrospective analysis with a process-based biogeochemistry model, Global Biogeochem Cy, 18, 2004.

Zimov, N. S., Zimov, S. A., Zimova, A. E., Zimova, G. M., Chuprynin, V. I., and Chapin, F. S.: Carbon storage in permafrost and soils of the mammoth tundra-steppe biome: Role in the global carbon budget, Geophys Res Lett, 36, 2009.

Zimov, S. A., Davidov, S. P., Voropaev, Y. V., F., P. S., Semiletov, I. P., Chapin, M. C., and Chapin III, F. S.: Siberian CO_2 efflux in winter as a CO_2 source and cause of seasonality in atmospheric CO_2, Climatic Change, 33, 111-120, 1996.

Zimov, S. A., Daviodov, S. P., Voropaev, Y. V., and Prosiannikov, S. F.: Planetary Maximum CO_2 and Ecosystems of the North, Department of Civil Engineering, Oregon State University, Corvallis, Oregon1993, 21-34.

Zona, D., Gioli, B., Commane, R., Lindaas, J., Wofsy, S. C., Miller, C. E., Dinardo, S. J., Dengel, S., Sweeney, C., Karion, A., Chang, R. Y. W., Henderson, J. M., Murphy, P. C., Goodrich, J. P., Moreaux, V., Liljedahl, A., Watts, J. D.,

Kimball, J. S., Lipson, D. A., and Oechel, W. C.: Cold season emissions dominate the Arctic tundra methane budget, P Natl Acad Sci USA, 113, 40-45, 2016.

Zona, D., Lipson, D. A., Paw, K. T., Oberbauer, S. F., Olivas, P., Gioli, B., and Oechel, W. C.: Increased CO_2 loss from vegetated drained lake tundra ecosystems due to flooding, Global Biogeochem Cy, 26, 2012.

Zona, D., Oechel, W. C., Kochendorfer, J., U, K. T. P., Salyuk, A. N., Olivas, P. C., Oberbauer, S. F., and Lipson, D. A.: Methane fluxes during the initiation of a large-scale water table manipulation experiment in the Alaskan Arctic tundra, Global Biogeochem Cy, 23, 2009.

Zona, D., Oechel, W. C., Peterson, K. M., Clements, R. J., Paw U, K. T., and Ustin, S. L.: Characterization of the carbon fluxes of a vegetated drained lake basin chronosequence on the Alaskan Arctic Coastal Plain, Glob Change Biol, 16, 1870-1882, 2010.

Zubrzycki, S., Kutzbach, L., Grosse, G., Desyatkin, A., and Pfeiffer, E. M.: Organic carbon and total nitrogen stocks in soils of the Lena River Delta, Biogeosciences, 10, 3507-3524, 2013.

Acknowledgement

First, I want to thank my supervisors Prof. Dr. Sabine Attinger, Prof. Dr. Werner Eugster, Prof. Dr. Thomas Foken, Dr. Mathias Göckede and Prof. Dr. Martin Heimann, for their advice and support during my PhD project.

I am grateful for the two individual research stays with Prof. Dr Werner Eugster and Dr. Ivan Mammarella that I enjoyed a lot scientifically and personally.

Special thanks to our Russian partners, the Zimov family with Sergey, Galya, Nikita and Nastya. They hosted me during all field trips and without them this work in such a remote and harsh environment would not have been possible.

I would like to thank the people in the IPAS group Ina Burjack, Sandra Bölck, Karel Castro-Morale, Sonja Kaiser, Min-Jung Kwon and Friedemann Reum for their feedback, motivation and cooperation. Furthermore within the Institute and especially in the Biogeochemical Systems department there was always a warm and friendly atmosphere that I appreciated a lot.

I am also grateful that Mathias Mauder did not give up on me during my countless request and questions regarding the processing software TK.

Financial support has been provided by the European Commission (FP7-ENV-2011, Grant Agreement No. 282700), the German Ministry of Education and Research (CarboPerm-Project, BMBF Grant No. 03G0836G) and the Max-Planck Society.

Last but not least I want to thank my friends and family for the never ending support and motivation but also for providing welcome diversion.

Erklärung

Ich erkläre, dass ich die vorliegende Arbeit selbstständig und unter Verwendung der angegebene Hilfsmittel, persönlicher Mitteilungen und Quellen angefertigt habe.

Jena, den

Fanny Kittler